Technical Information Exchange

LOAN COPY

FOR USE OF G E EMPLOYEES ONLY

GENERAL ELECTRIC

TECHNICAL INFORMATION SERIES

Title Page

AUTHOR	SUBJECT	NO.
J. Hogan D. Podgurski N. Stultz	TC 300 SOLAR COLLECTOR	78-SDS016
		DATE 31 Dec 1978
TITLE Development of a 3 x Solar Collector and other Collector Development Activities		G E CLASS 2
		GOVT. CLASS Unclass
REPRODUCIBLE COPY FILED AT		NO. PAGES

SUMMARY

The design, development, analysis and performance of the TC 300 solar collector are detailed herein. This collector uses the GE evacuated shroud as the solar receiver. The intended operating temperature range of the collector is 350°F to 500°F. The collector is mounted east-west and requires seasonal elevation adjustments. The concentration ratio is 2.9. Daily efficiency of the collector itself is approximately 40% at a fluid inlet temperature of 400°F. A feasibity model of a 30 x solar collector was built and tested.

KEY WORDS

Concentration ratio, solar energy, evacuated shroud, thermal resistance, insulation efficiency, compound parabolic concentrator, serpentine, solar collector.

INFORMATION PREPARED FOR Division IR&D Program

TESTS MADE BY J. Hogan

AUTHOR J. Hogan, D. Podgurski, N. Stultz

COMPONENT Advanced Energy Programs, Space Division

APPROVED K. L. Hanson

TIS DISTRIBUTION LIST

		No. of Copies
R. Berg	Rm. 20B52 - Bldg. B	1
J. Bledsoe	Rm. 7554 - Bldg. 7	1
J. Hogan	Rm. 29B12 - Bldg. B	2
J. Nichols	Rm. 7554 - Bldg. 7	1
N. Stultz	Rm. 20B56 - Bldg. B	1
K. Hanson	Rm 29B12 - Bldg. B	10 + Master co
J. Hatman	Rm. 20B38 - Bldg. B	1
R. Hodge	Rm. 20B56 - Bldg. B	1
R. Karcher	Rm. M3041 - VFSC	1
W. Terrill	Rm. 7246 - Bldg. 7	1

General Electric Co.
Technical Information Exchange
Building 5, Room 221
P. O. Box 43
Schenectady, New York 12301
Attn: Pat Kmoroske

5 Copies Plus
6 Title Pages

Documents Library Rm. L1343 - VFSC

10 Copies Plus
1 Unbound Copy

Table of Contents

Section		Pages
1	Introduction	1-1
2	Collector Hardware Description	2-1
	2.1 Overall Configuration	2-1
	2.2 Shrouds	2-3
	2.3 Serpentine	2-3
	2.4 Refector	2-7
	2.5 Support Structure	2-7
3	Collector Analysis	3-1
4	Serpentine Design	4-1
	4.1 Serpentine Thermal Resistance	4-1
	4.2 Insulation Thickness	4-6
5	TC 300 Thermal Receiver	5-1
	5.1 Glass Shroud Evaluation at 2.9 Concentration	5-1
	5.2 Test Results of Shrouds Exposed to 2.9 Concentration	5-1
6	Structural Design	6-1
	6.1 Structural Design	6-1
	6.2 Structural Foam Design	6-1
	6.3 Sheet Metal Structural Design	6-4
	6.4 Fluid	6-7
7	Performance Test Results	7-1
	7-1 Introduction	7-1
	7-2 Test Loop and Instrumentation	7-1
	7-3 Test Results	7-3
	7-4 Summary of Test Results	7-11
	7-5 Discussion	7-12
8	Fabrication and Test of a Tracking Parabolic Trough	8-1

Table of Contents (Continued)

Section		Pages
9	Flow Through Evacuated Shroud	9-1
	Reference	12-1
	Appendices	
	a. Structural Analysis of Foam Module	A-1
	b. TC-300 Structural Analysis Sheet Metal Design	B-1
	c. TC-300 Fluid Loop Stress Analysis	C-1
	d. Flow-Through Evacuated Shroud	D-1

SECTION 1

INTRODUCTION

Vacuum tube solar collectors which have been developed for heating only systems, heating and cooling systems, and process hot water systems provide optimum performance at approximately 250°F with maximum operating temperature in the 300-350°F range. It now appears that a collector designed for higher temperature operation is required for a large portion of industrial process heat applications. Analyses of potential applications indicate that a collector designed to operate in the temperature range of 350-500°F would cover a wide range of process heat applications, including process steam. A study and preliminary breadboard tests were inititated to determine the best approach for a collector concept that would operate satisfactorily in this temperature range. They indicated that maximum use could be made of existing TC-100 collector technology with an appropriate increase in concentration ratio.

This collector technology described in reference 1, is built around the GE evacuated shroud and finned serpentine fluid loop. Increasing the concentration ratio lowers the thermal losses (thermal losses are inversely proportional to the concentration ratio) and thereby increases efficiency at higher temperatures. Intimately related to the increase in concentration ratio are; an increase in stagnation temperature, a decrease in collector field of view - the angle, measured from the normal to the aperture plane, over which radiation passing through the aperture will

strike the absorber; an increase in the amount of energy that is reflected or refracted into the absorber. As the TC-100 components are taken to higher temperatures and concentration ratios, several hardware limitations arise. Some of the specific considerations are listed below:

1. The capability of the serpentine to operate in the 350-500°F range as well as withstand stagnation temperatures of 900°F.
2. The capability of the serpentine to transfer a high heat flux without introducing high thermal resistance between the absorber and working fluid.
3. The ability of shroud to withstand high heat transfer rates and high stagnation temperatures without glass breakage.
4. The ability of selective coating to withstand stagnation temperature without degradation.
5. The effect of increased concentration ratio on optical efficiency.
6. The relationship between increased concentration and tracking requirements.

The above considerations have each been addressed analytically and experimentally. The results have led to the design of a 2.9 concentration ratio collector with an operating range of 350°F to 500°F and with a daily collector efficiency at 400°F of 40%. The collector is designated the TC-300. This report describes the collector theory, design and hardware; describes development pro-

grams (and results) aimed at extending the TC-100 technology to this temperature range; and presents detailed performance test data for the TC-300 collector.

This collector development activity was integrated with parallel efforts which involved the application of the TC-300 collector to a solar process steam system and a plan to supply shrouds and serpentines to another collector manufacturer. In addition, the program interfaced with other collector development, fabrication and test activities underway at the Valley Forge facility.

This report also describes the build and test of a tracking parabolic trough - another avenue to high temperature solar collection. Performance comparisons between the tracking trough and TC-300 are made.

The final section of this report describes the invention of a flow throug evacuated shroud for use with the TC-300 collector. The benefit of this shroud lies in the reduction of piping heat loss and fluid loop cost.

SECTION 2

COLLECTOR HARDWARE DESCRIPTION

Figure 2-1 shows the major physical characteristics of the TC-300 collector final design. All of the major collector components will be discussed in this section.

2.1 OVERALL CONFIGURATION. The load carrying structure for each collector is composed of the reflector substrate (aluminum), four bulkheads (aluminized steel), four longitudinal rails (aluminum), and the mounting pipe (steel) to which the collector is attached. Six GE evacuated tube collector shrouds act as receivers of the solar energy. Each shroud is positioned in a separate compound parabolic cusp. The reflective surface of each cusp uses a metalized protective coating. The fluid loop which extracts useful heat from the receivers is made up of a finned serpentine tube connected to the inlet-outlet headers. The tubing used is ¼ inch diameter stainless steel. Aluminum fins are clamped to the tube. These fins also make thermal contact with the inner glass surface of the shrouds and thereby transfer heat from the shroud to a coolant flowing in the serpentine tube. The inlet-outlet headers are comprised of 3/4 inch diameter stainless steel tubes and are integral to each collector module. When joined in the field, these headers provide parallel fluid flow through each collector. The collectors are designed to provide a 2.9:1 concentration ratio. The collector is mounted east-west with four seasonal adjustments used to keep the sun's rays within the acceptance angle of the reflector cusp. (Analytical studies have shown that four

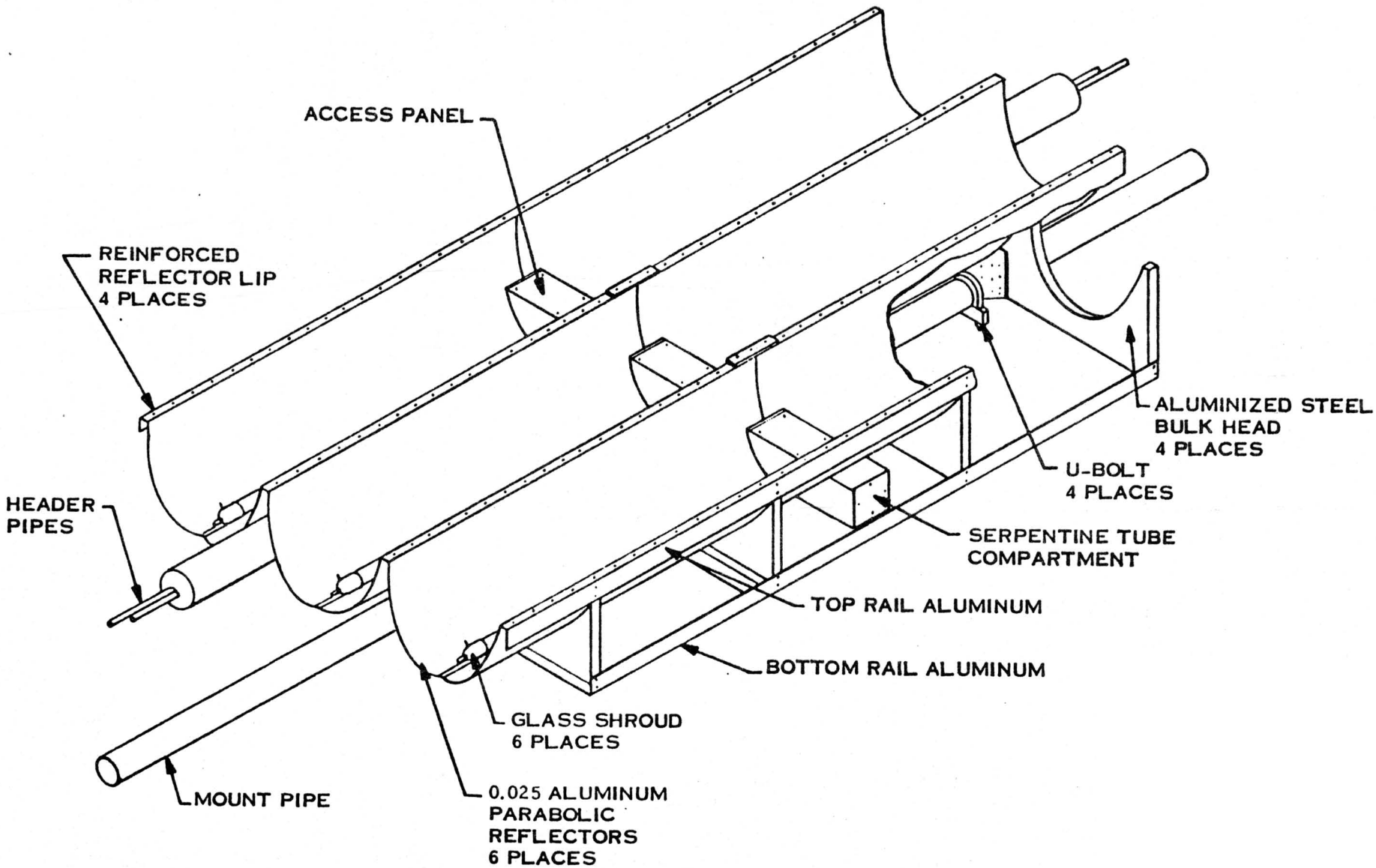

Figure 2-1 **TC-300 Collector (1/10 Scale)**

adjustments provide within 1 or 2% of the energy provided by daily adjustments on an annual bases.)

2.2 SHROUDS. Figure 2-2 shows the GE evacuated glass shroud. Two concentric glass tubes are used, with the outer one being transparent. The outer surface of the inner tube has an optically selective coating, and acts as the solar absorber. Standard fluorescent lamp tubing is used. The region between the inner and outer tubes is evacuated, to essentially eliminate conduction and convestion losses from the inner tube. The emissivity of the optical coating is a relatively linear function of temperature, ranging from 0.04 at 200°F to 0.06 at 400°F. Testing of these shrouds at the 2.9:1 concentration ratio has been conducted at a stagnation temperature of approximately 900°F, with no increase in emissivity. An insulation plug is inserted in the open end of each shroud to prevent convection currents from thermally connecting the inner tube with ambient air.

2.3 SERPENTINE. The serpentine configuration is illustrated in Figure 2-3 which shows the piping network for two adjuacent collectors. All piping, with the exception of junction tubing, is integral with each collector module. As can be inferred from the diagram, all collectors in the field are fed in parallel. The headers are sized to ensure uniform fluid flow through all collectors. All tubing connections are brazed joints. Eight collectors are fed from each 3/4 inch diameter tube run. The header, which is held at the center (and expands from that point), will expand a total of approximately 3 inches at an operating tempera-

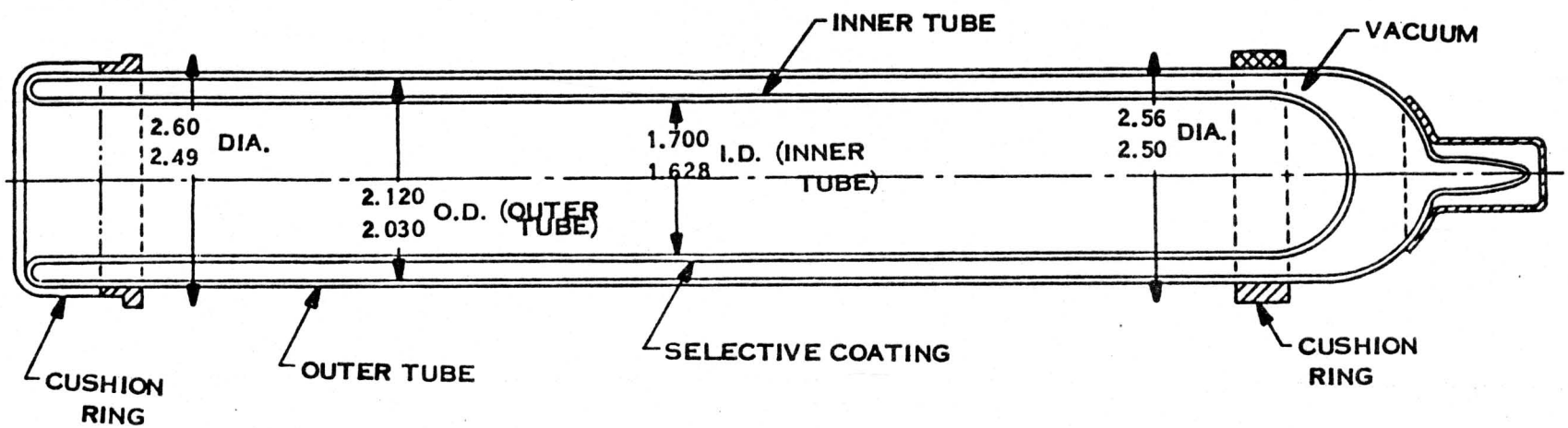

Figure 2-2 Evacuated Shroud

ture of 400°f. The 1/4 inch to 3/4 inch "T" farthest from the center on each side will move about 1.5 inches. This expansion is accommodated by a 1/4 inch flexible tube between the individual header "T" and the point where the serpentine tube is fixed relative to the collector structure. Header tubes are nested in a single run of commercial pipe insulation as shown in Figure 2-1. Nesting pipes in this fashion significantly reduces piping heat loss and insulation cost.

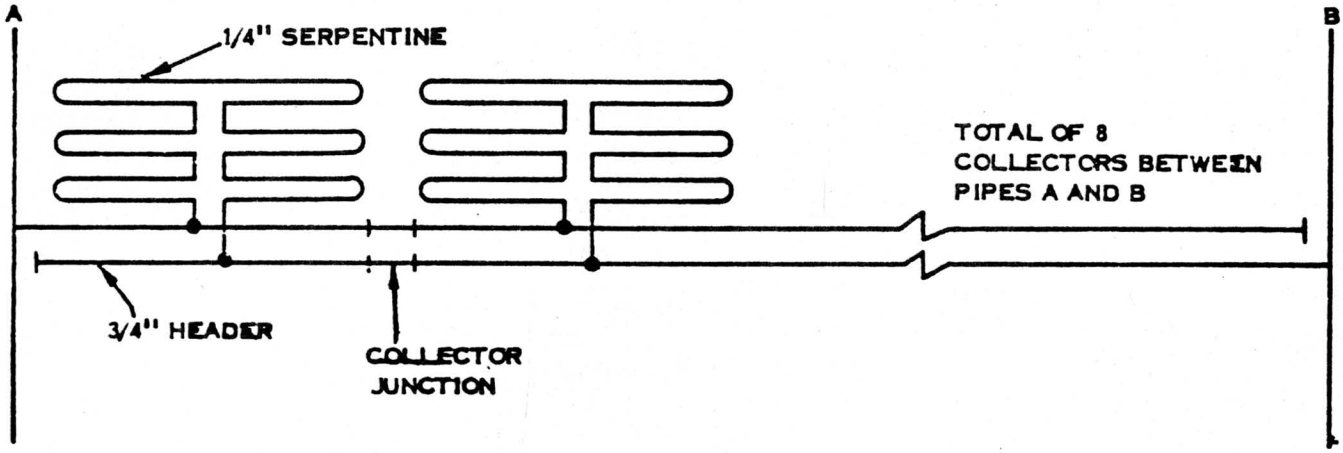

Figure 2-3

Heat is delivered from the evacuated shroud to the coolant via the aluminum fins mentioned previously. These fins conform to, and make contact with, the inner shroud (tube) surface. The clamping mechanism which holds the fins to the serpentine tube is shown in Figure 2-4. The clamp material is Inconel X750. A stainless steel spring is used to insure thermal contact between the aluminum fin and the glass shroud. The thermal resistance of the assembly shown in Figure 2-4 has been determined in a series of bench tests. Resistance from the absorber to the 1/4 inch serpentine tube is 0.35 hr. ft. °F/Btu. This resistance does not increase on exposure to stagnation temperature (900°F).

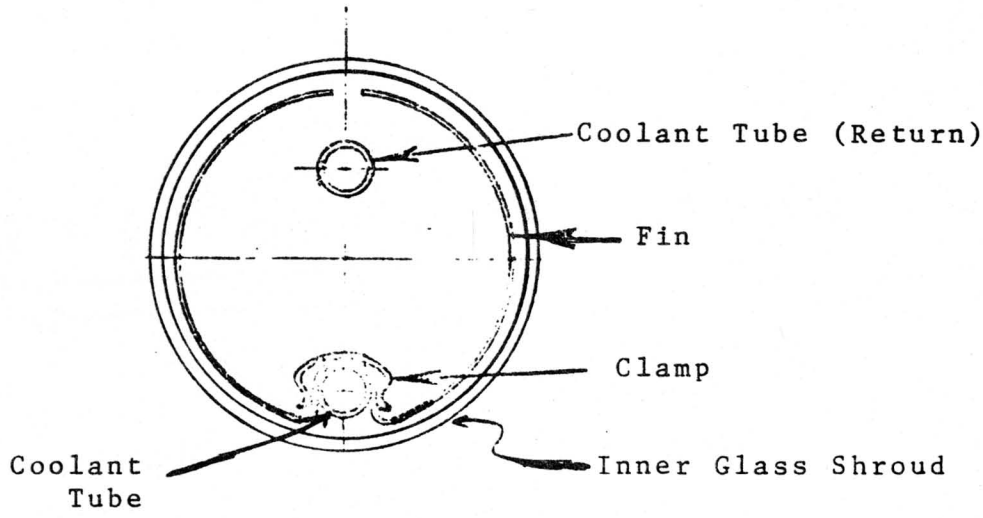

Figure 2-4. Serpentine-Shroud Interface

2.4 REFLECTOR.

Two reflector options may be used in the TC-300 collector. One is the GE patented Alglas coating applied to .025 inch #5457 bright rolled aluminum. The second option is a metalized UV stable polyester film laminated to either steel (.018 inch thick) or aluminum (.025 inch thick). Both have an effective reflectivity of roughly 84%.

2.5 SUPPORT STRUCTURE.

The major structural elements include the reflector panels, the four bulkheads, and the mounting pipe (Figure 2-1). The collector is sized to sustain a load of 40 pounds per square foot, normal to the aperture. Because of the large moment of inertia of each cusp, longitudinal bending stresses in the reflective substrate are negligible. The load on each reflector is transmitted through the bulkheads to the mounting pipe. Each bulkhead is therefore subject to a bending stress. The maximum bending moment occurs beneath the center cusp. A doubler is located at that point in order to reduce this stress. The doubler also provides the flange which allows the bulkhead to be clamped to the mounting pipe. Clamping is achieved with a U-bolt assembly. Torsional stiffness of the collector is provided by the mounting pipe.

SECTION 3

COLLECTOR ANALYSIS

This section derives the system equation for the efficiency of the TC-300 versus fluid temperature. Such a model is required to make cost effective design decisions. Efficiency can generally be increased with an increase in hardware costs. Since solar systems must be designed to maximize the ratio of delivered energy to life cycle costs not all increases in efficiency are cost effective. Likewise, neither are all cost reductions. Hardware decisions should be based on whether they increase the BTU per dollar. Therefore, an efficiency model based on the properties of hardware components (reflector, absorber, insulation, heat transfer surfaces, etc.) is required.

The general characteristics of a compound parabolic concentrator will be discussed prior to the derivation of the TC-300 system equation. The concentration ratio of a solar collector is defined as the ratio of the aperture area to the absorber area. Concentration of solar energy is necessary when high temperatures are required since absorber losses depend on temperature and area. Intimately related to concentration is the acceptance angle, the solid angle over which radiation is accepted without moving all or part of the reflector. In general, high concentrations imply small acceptance angles. As shown in reference 2, the maximum possible concentration for a given acceptance half angle Θc is $1/\sin \Theta c$ for a two-dimensional concentrator. Concentrators which

achieve this limit are termed ideal. A compound parabolic concentrator as shown in Figure 3-1(from reference 1) is such a concentration. The geometry of the reflector is such that sections AD and AF of the concentrator are convolutes of sections AC and AB of the absorber. For the rest of the concentrator it is required that at any point P of the reflector the reflector normal bisect the angle between the line PT (tangent to absorber at T) and the ray incident on P at angle Θc. Figure 3-1 shows the major penalty associated with ideal concentration - a large ratio of reflector area to aperture area. This may be partially off set by truncation; i.e., the upper regions of the reflector represent a small fraction of the aperture and may be removed with a small effect on concentration, but with a large material savings. The TC-300 cusp has the shape of an ideal concentration ratio of 4.1, but is truncated to an actual 2.9 CR. The ratio of reflector area to aperture area is 2 to 1. Acceptance half angle is 13°. The cusps are oriented east-west. Four seasonal adjustments in elevation to maintain the sun's rays within the acceptance angle are sufficient to provide within 99% of the energy collected with daily adjustment of the elevation angle.

The derivation of the system equation now begins with the heat balance on the absorber surface. It is assumed in what follows, that the collector is oriented such that the sun's beam radiation falls within the collectors acceptance angle. For this case

$$Q_I = Q_U + Q_L \qquad (1)$$

where

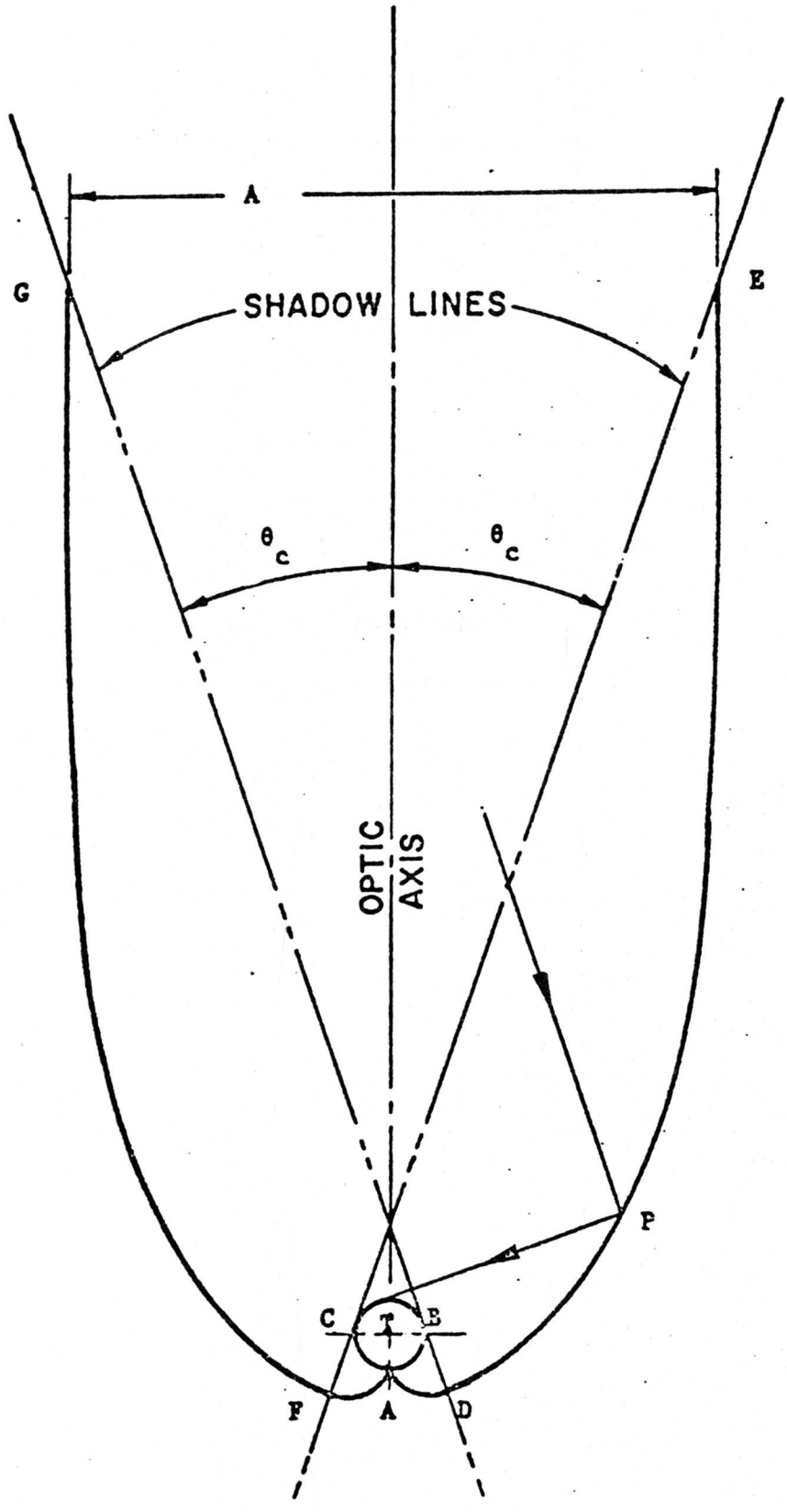

Figure 3-1. Ideal Cylindrical Concentrator with Circular Absorber Shape

Q_I is the energy incident on the absorbing surface

Q_U is the energy delivered by the absorber to the collector coolant (useful energy)

Q_L is the heat lost by the absorber to the surroundings

Q_I is given by

$$Q_I = (K_1 q_B + K_2 q_D) A_1 \qquad (2)$$

where

K_1 is the optical efficiency with which beam radiation is delivered from the aperture to the absorber

K_2 is the optical efficiency with which diffuse radiation is delivered from the aperture to the absorber

q_B is the beam radiation incident on the aperture

q_D is the diffuse radiation incident on the aperture

A_1 is the aperture area

K_1 is given by

$$K_1 = \left[(\alpha\tau)_D I + \rho^N (\alpha\tau)_R (1-I)\right] \qquad (3)$$

where

ρ is the reflectivity

N is the average number of reflections solar radiation incident on the reflector.

$(\alpha\tau)$ is the effective absorptance and transmittance of the receiver assembly.

I is the fraction of radiation which strikes the absorber directly.

I is expressed as the ratio of the planform area of the absorber to the aperature area.

An effective $(\alpha\tau)$ is used since radiation entering the aperture in different locations impinges on the receiver at different angles. Both τ (transmittance) and α (absorptance) are functions of incidence angle. Detailed beam tracing (analytical or experimental) could be used to directly calculate K_1. To date an effective $(\alpha\tau)$ has been employed. Subscripts D and R are used to indicate that the effective absorptance-transmittance product may be different for direct and reflected radiation.

K_2 is empirically given by

$$K_2 = \frac{I\ (\alpha\tau) + \rho^N (\alpha\tau)(1-I)}{CR_{UT}} \qquad (4)$$

where

CR_{UT} is the untruncated concentration ratio. For the evacuated tube design the heat lost from the collector can be written as

$$Q_L = q_r A_2 + Q_{IF} + Q_{IT} \qquad (5)$$

where

q_r is the heat reradiated by the absorber per unit area

A_2 is the absorber surface area

Q_{IF} is the heat lost from the fins inside the inner tube through the insulation of the header region

Q_{IT} is the heat lost from the serpentine in the header region and from inlet and outlet header pipes.

These various heat loss terms can be expressed as follows:

$$q_r = \epsilon\sigma(T_{abs}^4 - T_\infty^4) \qquad (6)$$

$$Q_{IF} = \frac{(T_f - T_\infty)N}{R_I} \qquad (7)$$

$$Q_{IT} = \frac{(T_f - T_\infty)}{(R_T/\ell)} \qquad (8)$$

where

ϵ is the emissivity

σ is the Stephan-Boltzmann constant

T_{abs} is the absorber temperature

T_f is the fluid temperature

R_I is the insulation resistance per shroud

R_T is the insulation resistance per unit length of exposed coolant

ℓ is the length of header tube (includes pieces of serpentine outside shroud)

N is the number of shrouds

Expressions for R_I and R_T may be directly derived. For the present, however, it will be more convenient to work in terms of thermal resistors. Equation 1 can now be written as

$$\left[(\tau\alpha)_D\, I + \rho^N (\tau\alpha)_R (1 - I)\right]\left(q_B + \frac{q_D}{CR}\right) =$$

$$\frac{Q_u}{A_1} + \frac{\epsilon\sigma(T_{abs}^4 - T_\infty^4)}{CR} + \frac{(T_f - T_\infty)N}{R_I A_1} + \frac{(T_f - T_\infty)}{(R_T/\ell)A_1} \qquad (9)$$

The term $(q_B + q_D/CR)$ represents the energy in the aperture and will be denoted as q_A. For convenience use K to denote $\left[(\tau\alpha)_D I + \rho^N (\tau\alpha)_R (1 - I)\right]$. K is the optical efficiency of the collector.

Note that radiation losses occur at the absorber temperature while insulation losses occur at the fluid temperature. These two temperatures may be related by the thermal resistance of the glass-fin-tube assembly. Denoting this thermal resistance per unit length of shroud by R_w yields:

$$T_{abs} - T_f = \frac{R_w Q_u}{NL} \qquad (10)$$

where L is the shroud length and other quantities have been identified previously.

equation 10 will be used to eliminate T_{abs} from equation 9. Some complexity arises by virtue of the fact that T_{abs} is raised to the fourth power. However, since the temperature difference between T_{abs} and T_f is small compared to T_{abs} the binomial theorem can be used to yield:

$$T_{abs}^4 = (T_f + \frac{R_w Q_u}{NL})^4 \approx T_f^4 + 4T_f^3 \frac{R_w Q_u}{NL} \qquad (11)$$

Equations 10 and 11 can be used to transform equation 9 to

$$K_{q_A} = \frac{Q_u}{A_1} + \frac{\epsilon\sigma(T_f^4 - T_\infty^4)}{CR} + \frac{4\epsilon\sigma T_f^3 R_w Q_u A_2}{A_1 NL} + \frac{(T_f - T_\infty)N}{R_I A_1} + \frac{(T_f - T_\infty)}{(R_T/\ell)A_1} \qquad (12)$$

Equation 12 is now divided by K_{q_A}. In two of the terms on the right hand side the term $Q_u/q_A A_1$ will appear. This term is the efficiency of the collector and will be denoted as η. Note also that A is given by π DNL for circular absorbers. Here D is absorber diameter and L absorber length. Making use of the above, equation 12 can be transformed to:

$$\eta = \frac{K - \frac{(T_f^4 - T_\infty^4)}{CRq_s} - \frac{(T_f - T_\infty)}{CR\pi DLq_s}\left(\frac{1}{R_I}\right) - \frac{(T_f - T_\infty)}{(R_T/\ell)A_1 q_s}}{1 + 4\epsilon\sigma T_f^3 R_w \pi D} \qquad (13)$$

The numerator of equation 13 is the classical efficiency expression when the collector resistance (R_w) is ignored. The numerator reflects the efficiency gain which accrues from higher concentration ratios. The denominator contains the effect of the thermal resistance which occurs between absorber and working fluid. For R_w=0 the denominator is unity and the classical efficiency expression is

recovered. For $R_w \neq 0$ the second term in the denominator reflects the fact that the absorber is reradiating heat at a higher temperature than T_f.

Equation 13 was used to make several key design decisions as well as to predict collector efficiency. Hardware design decisions should be based on whether they increase the energy delivered per installed dollar (BTU/$). Increasing the BTU/$ is equivalent to increasing the efficiency per dollar of installed cost as shown below. The energy collected by a solar system is given by

$$q_c = \eta q_s A \tag{14}$$

where q_c is the energy collected over the systems life

q_s is the solar insolation available during the systems life

η is the average efficiency

A is the system aperture area

Dividing equation 14 by the total system cost, T, gives

$$\frac{q_c}{T} = \frac{\eta q_s A}{T} \tag{15}$$

T/A is the cost per square foot of the system. Designating this cost by c leaves

$$\frac{q_c}{T} = \left(\frac{\eta}{c}\right) q_s \tag{16}$$

q_c/T is the BTU/$ delivered by the system. Since q_s is beyond the control of the solar designer, maximizing the BTU/$ is equivalent to maximizing η/C. Thus design changes should be considered in light of whether the associated increase (decrease) in efficiency is greater than (less than) the associated increase (decrease) in system cost per square foot of aperture.

SECTION 4

SERPENTINE DESIGN

The serpentine design is an excellent example of the tradeoff between hardware dollars and efficiency. As mentioned above, the goal of this tradeoff is to increase the energy delivered per dollar of installed cost. In this section the term serpentine will be used to include the 1/4 inch U-tubes, the fins and clamps which thermally join these tubes to the shroud, the 3/4 inch headers, and all insulation. As hardware dollars are increased in the fin and clamp assembly the thermal resistance, R_w in equation 13, decreases and performance increases.At a certain level of fin and clamp cost the BTU's/$ are maximized. Likewise as hardware dollars are invested in insulation thickness the performance increases. A specific insulation thickness can be calculated which maximizes the BTU's/$.

4.1 SERPENTINE THERMAL RESISTANCE

The effect of serpentine thermal resistance on collector performance is included in equation 13. For convenience, this equation is written as

$$\eta = k\eta_o \qquad (17)$$

where η is the actual efficiency

η_o is the efficiency with no thermal resistance between fluid and absorber (ideal efficiency)

$$k = \frac{1}{1 + 4\epsilon T_f^3 R_w \pi D} \qquad (18)$$

Figure 4-1 plots k as a function of R_w for five temperature levels.

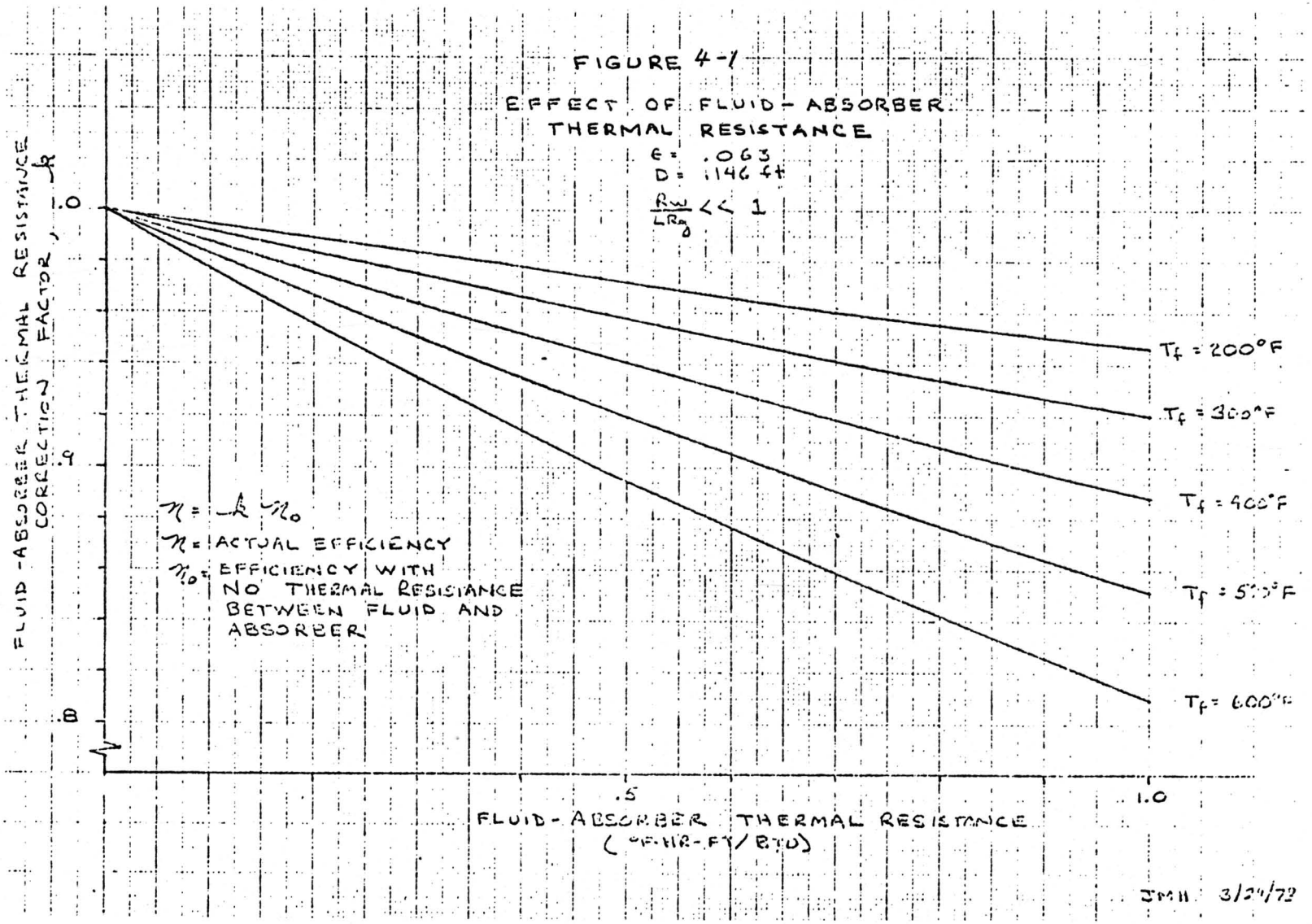

Figure 4-1. Effect of Fluid-Absorber Thermal Resistance

The higher the temperature, the more severe the effect of the thermal resistance.

The net thermal resistance is the sum of the thermal resistances of each component across which the useful heat must flow from the absorber to the fluid. These are the resistance of the inner glass shroud, R_g, the air gap and fin, R_f, and the fin-coolant tube juncture, R_c. R_g and R_f are given by

$$R_g = \frac{\ell n(r_o/r_i)}{2\pi k_g \ell} \tag{19}$$

$$Rf = \frac{1}{\sqrt{k_a k_f t/G}\,\ell \tanh(mL)} \tag{20}$$

where r_o = outer radius of inner tube

r_i = inner radius of inner tube

ℓ = length along serpentine (into the paper in Figure 2-4)

t = fin thickness

G = air gap thickness (assumed constant around circumference)

L = length of fin from weld (or clamp) to free end

k_g = glass thermal conductivity

k_f = fin thermal conductivity

k_a = air thermal conductivity

and

$$m^2 = \frac{k_a}{k_f t G} \tag{21}$$

The expression for R_f results from manipulation of the classical fin analysis for the case in which a fin receives heat by conduc-

tion across an air gap. R_c is not amenable to a concise analytical treatment and must be determined through experimentation.

Experience with the TC-100 copper serpentine/fin revealed a potential corrosion problem at temperatures exceeding 400°F, and in particular, at the stagnation temperature of 900°F. Since this is in the operating range of the 3X solar collector, it is judicious to select materials other than copper for the serpentine/fin. Additionally, due to the high concentration ratio of the 3X collector, it is necessary to use materials which can withstand stagnation temperatures up to 900°F. The two materials selected for the serpentine assembly are an aluminum fin and stainless steel tubing. Due to the different thermal expansion coefficients of these materials, it was necessary to design a mechanical clamp that has durability, low cost and ease of assembly. Both Inconel and A-286 alloy were considered for the clamps; Inconel was selected after initial testing. Figure 2-4 shows a typical clamp fin arrangement. Two distinct testing programs were undertaken. The first studied the thermal resistance of the clamp assembly alone. After this initial testing lead to clamp material choice, a second test program was initiated to study the thermal resistance of the entire heat extraction assembly (glass, air gap, fin, clamp, coolant tube). The results of these test programs are discussed in References 4 and 5. Figure 4-2 summarizes the final test results. Here the thermal resistance of the heat extraction assembly (inner glass to coolant tube) is shown versus various hardware configurations. The first assembly, copper-copper, is the current TC-100

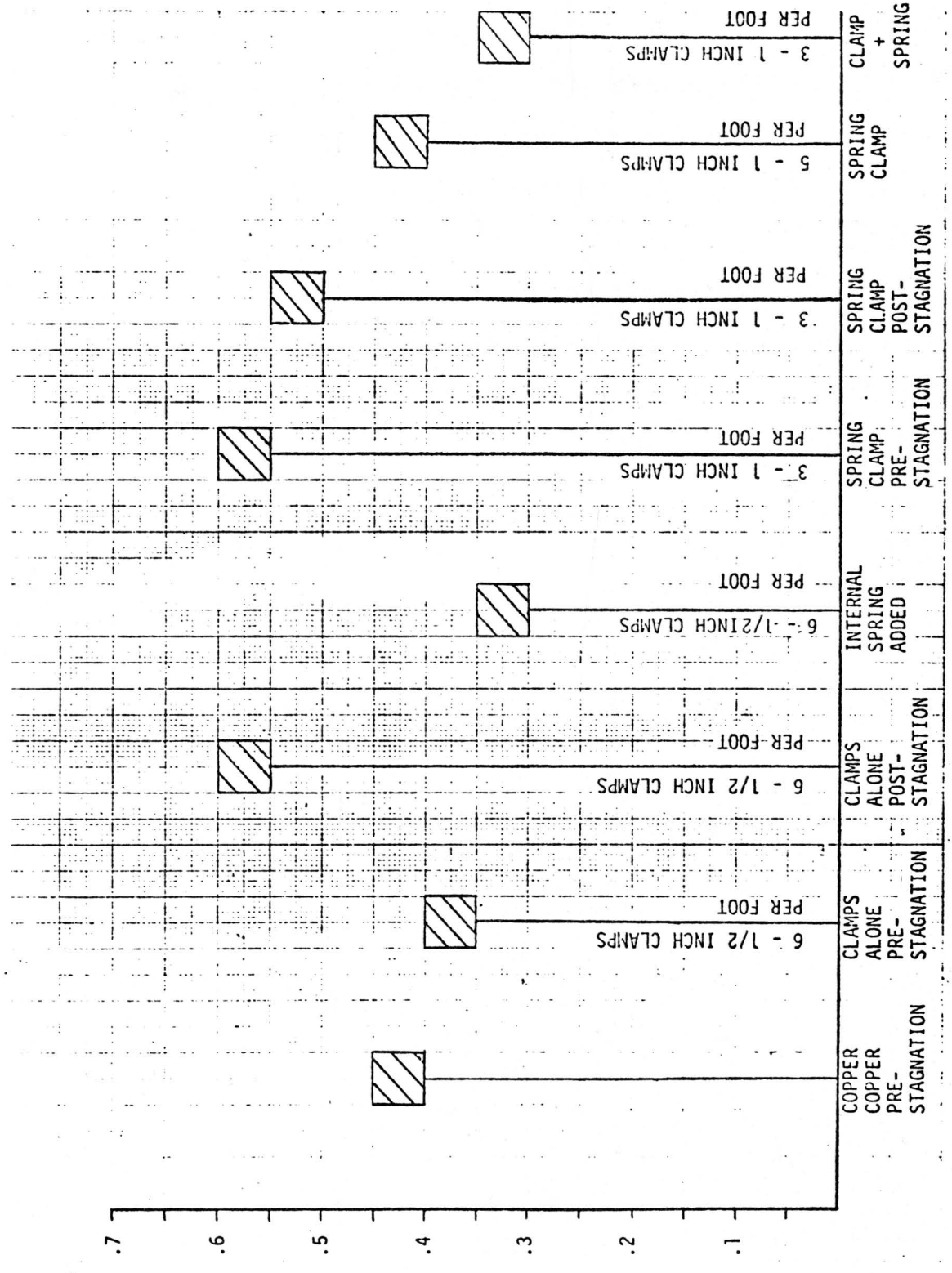

Figure 4-2 Clamped Fin Test Summary

design. Measurements of the clamped aluminum fin thermal resistance were made both before and after a two hour exposure to 1000°F (stagnation simulation). At this temperature the aluminum fin yielded and fell away from the shroud. An internal spring was therefore required to maintain the aluminum fin in thermal contact with the inner glass shroud. During this testing clamp length and clamp spacing were both varied. The cost associated with each option was determined along with the thermal resistance. The thermal resistance was used to calculate efficiency.. Serpentine cost was added to the remaining collector cost to determine total installed cost. Therefore, the energy delivered per unit of installed cost was known for each clamp length and spacing option. It was found that 1 inch clamps spaced three per foot were the most cost effective clamp arrangement tested.

4.2 INSULATION THICKNESS

A major source of heat loss in solar collectors are the losses associated with the header pipes which transfer the fluid to and from the collectors. In designing the TC-300 collector, the header pipes were analyzed to determine a cost efficient method of reducing the heat loss. Two basic methods were analyzed and compared for cost and efficiency. The two different configurations of insulation are shown in Figure 4-3.

A piece of insulation pliable enough to conform to the shape of the pipes is placed between them in the nested configuration to cut down on heat transfer between the two pipes. The heat loss

to the ambient air and the heat transfer from pipe A to B in the nested configuration were calculated. The nested pipes were modeled to be two semi-circles of insulation with a piece of insulation between the two halves. (See Figure 4-4).

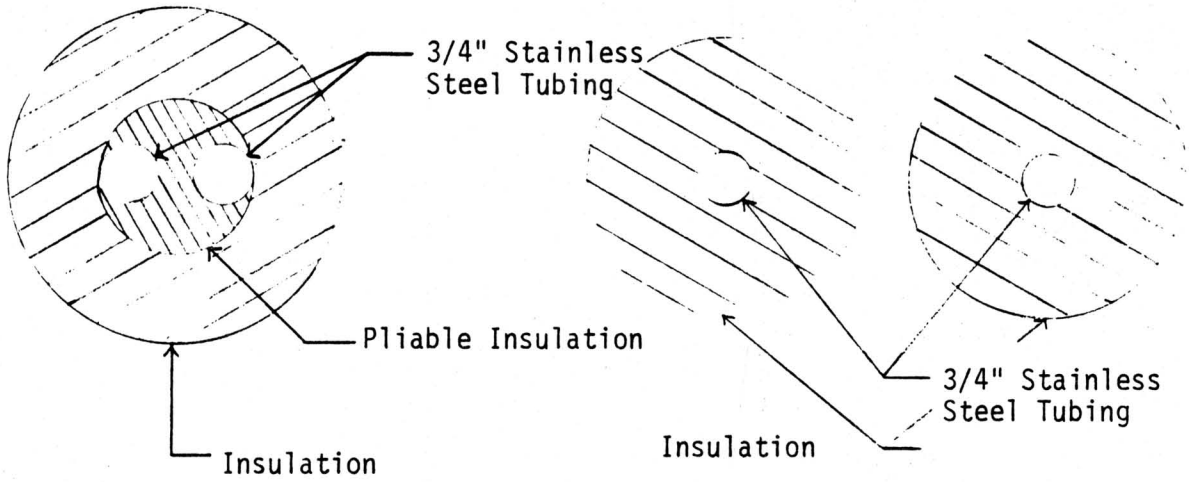

Figure 4-3. Insulation Configuration Candidates

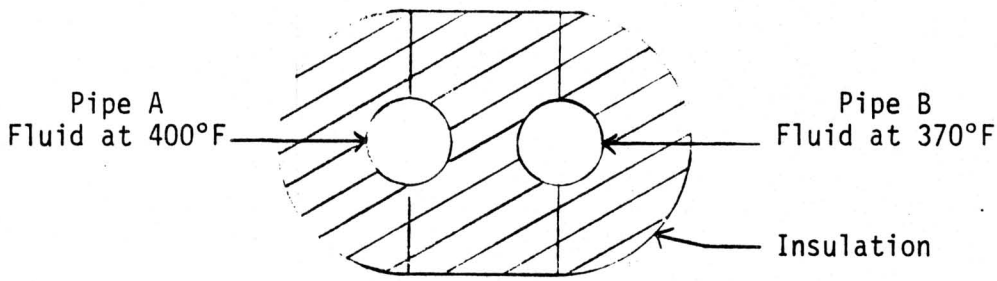

Figure 4-4. Insulation Model

The equation used to determine the heat loss from the semi-circle is:

$$q = \frac{(T_i - T_\infty)(\frac{1}{2})}{\frac{\ln(r_2/r_1)}{2\pi k \ell}} \qquad (22)$$

where:

T_i is the fluid temperature in Pipe A or Pipe B

T_∞ is the temperature of the ambient air

r_2 is the radius of the semi-circle including insulation

r_1 is the radius of the Pipe A or B

k is the conductivity of the insulation

ℓ is the length of one collector

The equation used to determine the heat loss from the middle section is:

$$q = \frac{KA\left(\frac{T_1 + T_2}{2}\right) - T_\infty}{\Delta x} \times 2 \qquad (23)$$

where:

K is the conductivity of the insulation

A is the area of the insulation

T_∞ is the temperature of the ambient air

Δx is the thickness of the insulation

ℓ is the length of the collector

$\frac{T_1 + T_2}{2}$ is the average of the two fluid temperatures in the pipes

The heat losses calculated from these equations were then added together to approximate the heat loss from the entire model. The heat loss from the separated pipes were calculated by using the following equation:

$$q = \frac{(T_i - T_\infty)}{\frac{\ell n (r_2/r_1)}{2\pi k \ell}} \qquad (24)$$

where the variables are defined as for Equation 22. Each design

has its own optimum insulation thickness i.e., the thickness that maximizes the delivered BTU/$. For the nested configuration this thickness is 2 1/2 inches (as shown below), for the separated heat pipes it is 3 inches. The resulting heat losses per 8.5 feet of header piping (the length of one collector) are:

Nested Pipes	Separated Pipes
220.15 Btu/hr.	329.8 Btu/hr.

Less insulation is used with the nested configuration (less cost). Thus nested header pipes are the superior design approach.

An insulation thickness must be chosen for the nested assembly. The thickness and thermal conductivity of the insulation determines the thermal resistance, R_T. Equation 13 shows the dependence of efficiency on R_T. The dependence of insulation cost on R_T was determined from vendor quotes. R_T was then increased until the energy delivered per dollar was maximized.

The remaining insulation term in equation 13 is R_I. It represents the thermal resistance between the fins in the inner shroud and ambient air. In the TC-100 this heat transfer path is controlled by blanket insulation in the serpentine box and by the tendency of the hot air in the inner tube to stagnate. (TC-100 collectors are installed north-south with the open end of the inner tube lower than the domed end.) Char patterns in the serpentine box insulation, however, indicate that convective currents do transfer heat from the fins to ambient air in the TC-100 design. Such convective currents can be expected to increase when the tubes

are mounted horizontally (as in the TC-300 east-west configuration). Analytically quantifying this heat loss would be extremely difficult and of limted accuracy. The decision was made to insert an insulation plug in the open end of each shroud. The thermal resistance across each plug is given by R_I (see equation 13). Since the heat loss without the plug cannot be quantified the increase in η is unknown. However, the associated cost is minimal. Engineering judgement indicates the BTU's/$ have been increased with this decision.

SECTION 5

TC-300 THERMAL RECEIVER

5.1 GLASS SHROUD EVALUATION AT 2.9 CONCENTRATION.

The evacuated shroud which acts as the receiver in the TC-300 design is the same as that used in the TC-100 collector. Extending the shroud to a higher concentration system imposes larger stress levels and therefore, the potential for glass breakage must be investigated. Three major failure modes are functions of the concentration ratio. All involve the occurrence of thermal stress; i.e., stress induced by differential thermal expansion of the glass.

A failure mode results from the transfer of heat from the absorbing surface of the inner tube (outer surface) to the inner surface. The transfer of heat across this tube induces a higher temperature on the outer surface than on the inner surface. This is a classical problem in stress analysis, see Reference 3. The stress is given by

$$\sigma = \frac{\alpha E \Delta T}{2(1-\nu)} \qquad (25)$$

where α is the coefficient of thermal expansion

E is Young's Modulus

ν is Poisans ratio

T is the temperature differential across the glass

The stress depends on the amount of heat transferred and therefore, on the concentration ratio (with increasing concentration ratio the amount of heat collected by shroud increases). At a concentration ratio of 1.0875 (TC-100) this stress is 360 psi. At 2.9 CR (TC-300) the stress is 1,200 psi. This stress is sufficiently large to require experimental monitoring of this failure mode.

Stagnation also imposes a thermal stress. At stagnation, the inner glass tube runs at a temperature significantly higher than the operating temperature. The outer shroud, however, remains fairly close to ambient temperature. This situation imposes a thermal stress on the DeWar seal which increases with stagnation temperature (and therefore with increasing concentration ratio). Testing was therefore required to determine the potential for TC-300 stagnation temperatures to induce glass breakage.

Thermal shock may also cause glass breakage. The term thermal shock refers to flowing a fluid through the serpentine which has a different temperature than the glass shroud. Thermal shock typically occurs when cold fluid begins to flow through a collector already exposed to solar insolation. The critical parameter is the temperature difference between coolant and shroud. The general shroud temperature increases with concentration ratio. Coolant temperature upon startup, however, is tied to the ambient temperature rather than concentration ratio. Thus thermal shock becomes more of a hazard as concentration ratio increases. Glass breakage

is a catastrophic failure which can be visually detected. The stability of the selective coating on the inner shroud is not as easily monitored. Changes in the emissivity or absorbtivity of this coating will affect the performance. The stability of such coatings depends in part on the temperature to which they are exposed and is therefore related to the concentration ratio. An experimental program was designed to insure the adequacy of the coating when used in the TC-300 configuration.

5.2 TEST RESULTS OF SHROUDS EXPOSED TO 2.9 CONCENTRATION.

The breakage potential of the TC-300 shrouds was monitored during performance and stagnation testing. Results are outlined below:

- The heat flux associated with 2.9 concentration did not shatter the shrouds during normal operation. At a concentration ratio of 13 (TC-400) the shrouds shattered as soon as the collector was focused.
- Shrouds can withstand a stagnation temperature of 900°F.
- Starting the TC-300 collector with the shrouds already up to temperature (~400°F) resulted in severe glass breakage. Such a procedure has been attempted twice (in each case after the glass successfully withstood stagnation). In one instance, three shrouds broke; in the other instance, two shrouds shattered. It is difficult to determine the exact coolant temperature which caused the failure since slugs of relatively cold fluid may occur in some of the test loop lines.

The results outlined above indicate that proper startup of the system is critical if glass breakage is to be avoided.

The stability of the selective coating was also experimentally monitored. Shrouds which had never experienced stagnation were allowed to achieve successively higher temperatures on separate days. At selected temperature plateaus the collector was covered and the temperature decay measured. The decay rate is a function of emissivity, ϵ. In fact the decay rate can be used to calculate emissivity through the equation

$$\epsilon \sigma (T_{abs}^4 - T_{amb}^4) \pi D = \frac{\mathcal{M}_g C_{pg}}{L} + \frac{\mathcal{M}_{cu} C_{pcu}}{L} \frac{dT_{abs}}{dt} \qquad (26)$$

where σ is the Stephen Boltzman constant

T_{abs} is the absorber temperature

T_{amb} is the ambient temperature

D is the absorber diameter

$\mathcal{M}$ is linear density

C_p is specific heat

L is absorber length

t is time

and subscripts g and cu represent glass and copper respectively. (A copper serpentine was used in this test.) The results of this test are shown in Table 5-1 and indicate no increase in emissivity on exposure to the higher stagnation temperatures characteristic of the TC-300.

Table 5-1. Effect of Stagnation Temperature on Emissivity

Highest Temperature To Which Shroud Had Been Subjected	ϵ At 400° F As Calculated From Equation 26
700° F	.0705
880° F	.0654
950° F	.0673

The stability of the coating may also be assessed by measuring performance before and after exposure to stagnation. Such tests are underway as of December, 1978. Initial results indicate no decrease in performance.

A third indication of the stability of the coating is the magnitude and repeatibility of the stagnation temperature attained at 2.9 concentration. Through a complete summer of stagnation testing a 900° F temperature was consistently attained on all clear days at solar noon. This corresponded to roughly 45 cycles to the full 900° F stagnation temperature.

SECTION 6

STRUCTURAL DESIGN

6.1 STRUCTURAL DESIGN.

The major fuctions of the TC-300 collector structure are

1. to maintain the reflector in its correct optical position relative to the absorber under anticipated wind loading;
2. to support piping and insulation;
3. to allow seasonal rotation in elevation of the collector.

Two separate structural approaches to the TC-300 have been investigated. One employed a structural polyurethane foam blown into a mold with the required optical shape. The second approach was a sheet metal design in which the parabolic shape is generated by a blanking and stamping operation. The latter approach proved to be the more cost effective and is discussed in detail below. A brief overview of the structural foam design is also given. This section also contains the structural analysis required for the fluid loop design.

6.2 STRUCTURAL FOAM DESIGN.

The structural foam concept is based on the polyurethane mold shown in Figure 6-1. Figure 6-2 shows the assembly of the mold with the reflector and hydraulic network. The layout of the la-

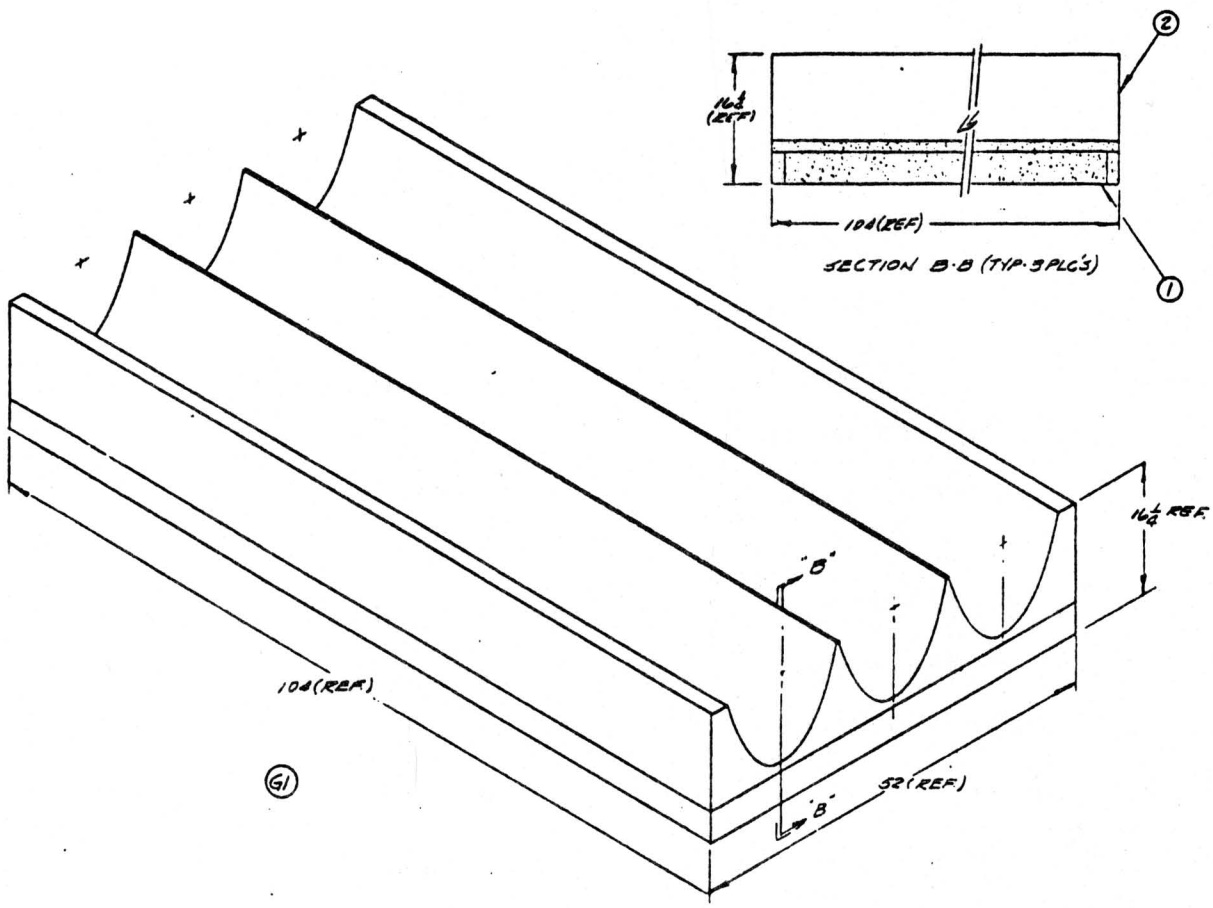

Figure 6-1. Structural Foam Reflector Substrate

TC-300
MANUFACTURING PROTOTYPE FABRICATION

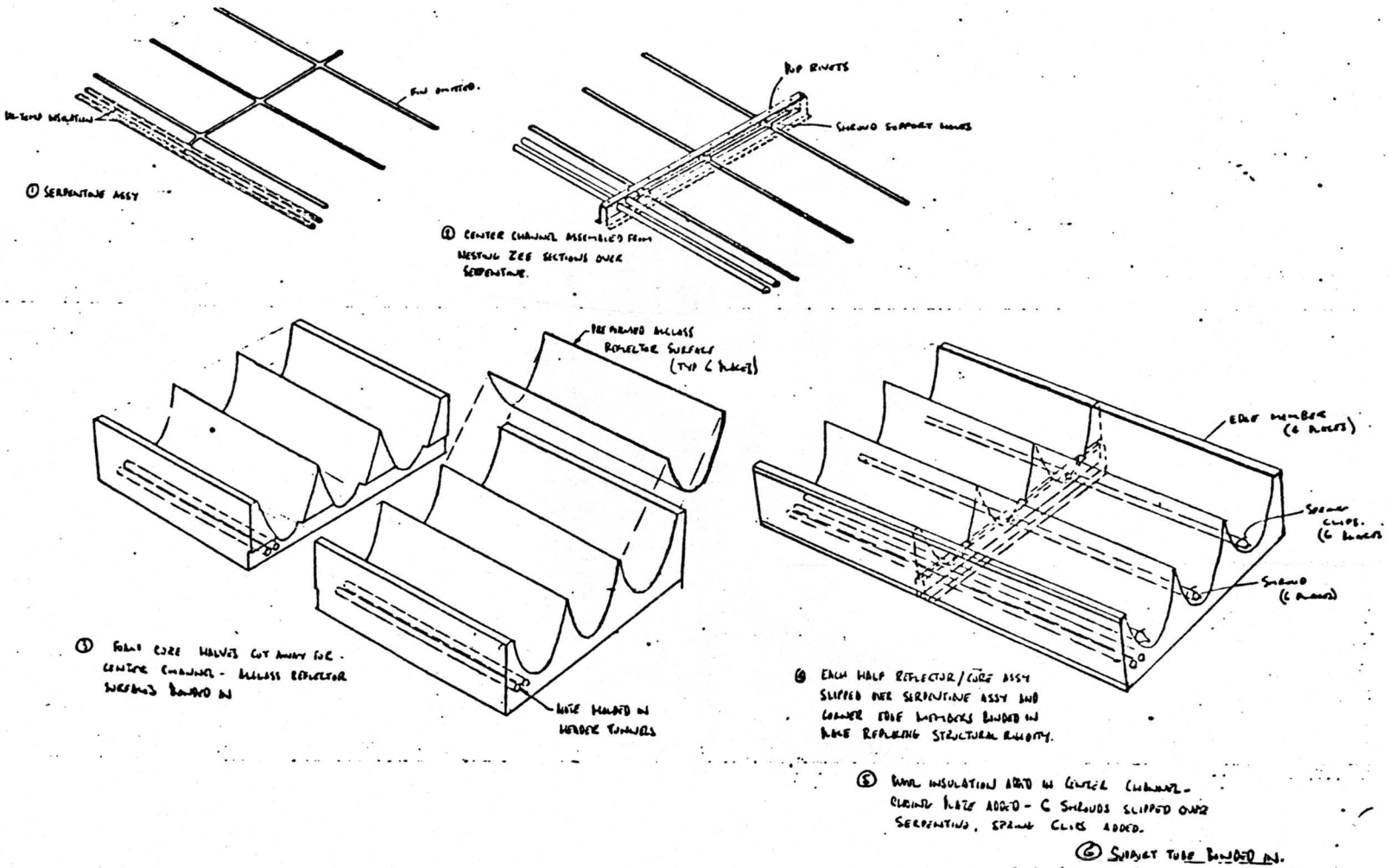

Figure 6-2. TC-300 Manufacturing Prototype Fabrication Structural Foam

test design appears in Figure 6-3. The appendix contains the structural analysis of the foam collector (Appendix A) and the product specification for the polyurethane foam (Appendix B). The collector is capable of withstanding a 100 mph wind and 20 psf snow loads.

Three polyurethane substrates (Figure 6-1) were molded in order to assess the producibility of this design. One complete collector assembly (Figure 6-3) was manufactured. A photograph of this assembly is shown in Figure 6-4. The cusp surface of all three polyurethane molds was irregular. Cusp dimensions varied by 1/8 inch over the length of the cusp. Both effects made bending the reflection to the polyurethane difficult. Delamination was noted on exposure to outdoor weathering. The TC-300 must be rotated seasonally. Mounting a number of collectors to a single rotable pipe was a very direct method of meeting this requirement. The structural foam design did not efficiently utilize this mounting pipe for either the bending or torsional stiffness it afforded. In a cost comparison between the foam and sheet metal collectors the latter was less costly and had less risk associated with its producibility.

6.3 SHEET METAL STRUCTURAL DESIGN.

The main structural components of the TC-300 sheet metal design are outlined in Section 2. A detailed stress analysis was performed on each component assuming a design wind loading of 40 lbs/ft.^{2}. Appendix B contains the design calculations.

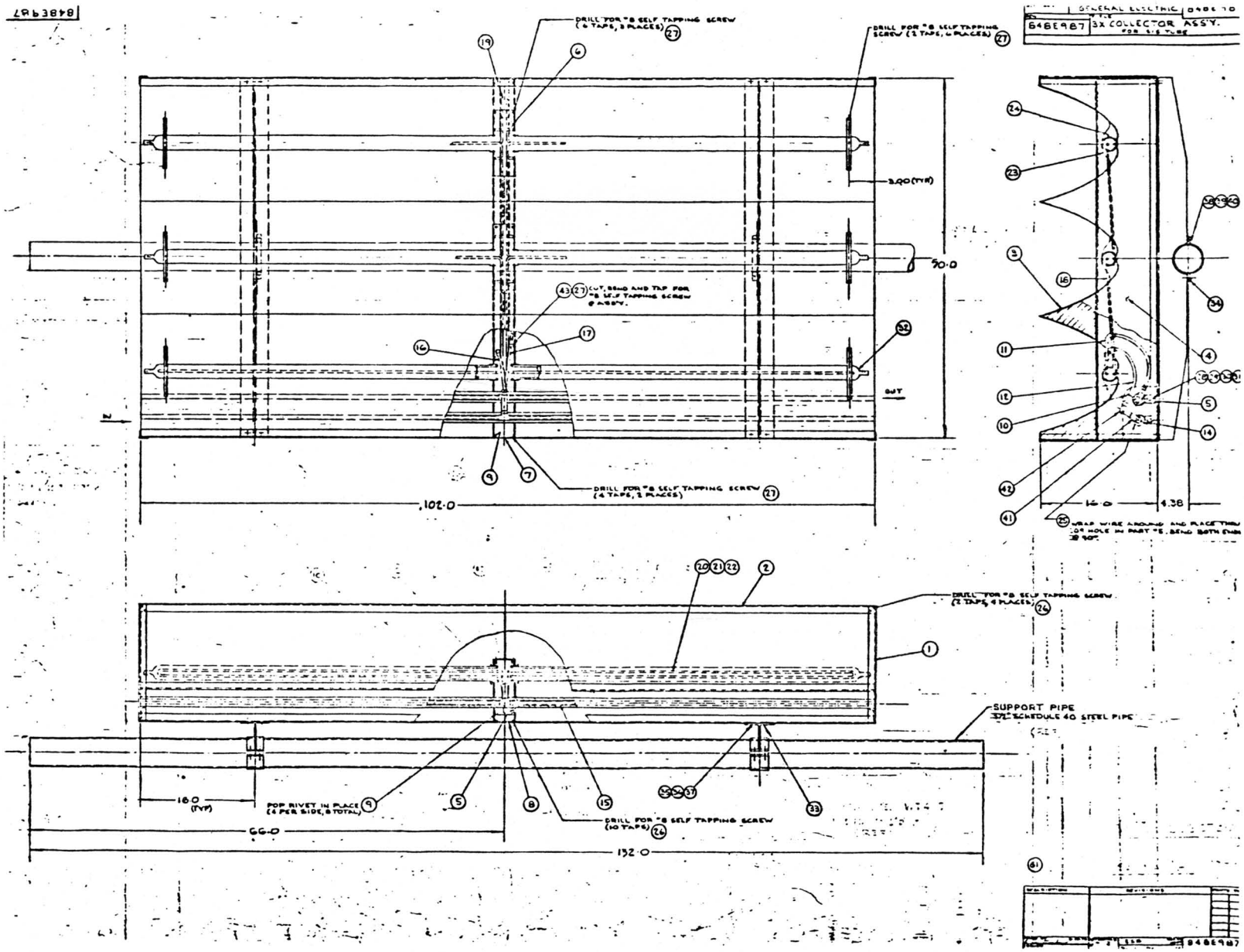

Figure 6-3. TC-300 Collector Module Assembly - Structural Foam

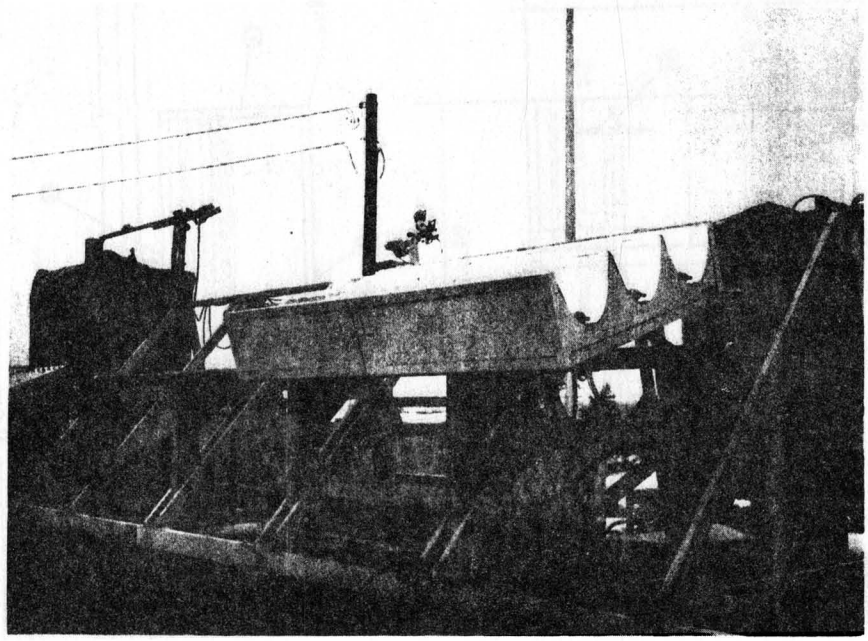

Figure 6-4. Structural Foam Collector

6.4 FLUID LOOP.

Two locations in the TC-300 fluid pipe loop were analyzed to determine alternating plus steady stress intensity due to pressure, temperature and component expansion. The areas analyzed were:

1. Header pipe welded branch connection.
2. Hairpin expansion tube.

The two loading conditions used in this analysis were the operating pressure and temperature and the occassional condition of pressure and temperature at stagnation.

Appendix C contains the design calculations for the fluid loop.

SECTION 7

PERFORMANCE TEST RESULTS

7.1 INTRODUCTION

The performance of the TC-300 collector was experimentally monitored on a high temperature (400°F) high pressure (500 psi) test loop specifically built during 1978 for the evaluation of this collector. Two collectors were placed in series on this loop - the structural foam collector shown in Figure 6-4 and the engineering prototype collector.

The engineering prototype collector had a more accurate reflector surface than the structural foam collector (because of bonding and delamination problems as discussed in Section 6.1). The engineering prototype was equipped with the clamped fin serpentine developed specifically for the TC-300. The structural foam collector had the standard TC-100 copper-copper serpentine. The data presented below was measured on the engineering prototype collector. Performance is based on the temperature differential directly across the collector - 1/4 inch serpentine inlet to 1/4 inch serpentine outlet. In other words, header losses are not included in the data discussed below.

7.2 TEST LOOP AND INSTRUMENTATION

Figure 7-1 shows the TC-300 unit with associated instrumentation. Temperature measurements T_1, T_2, T_3, T_4 were in fluid measurements. Pressure measurements P_1, P_2, P_3 and P_4 yielded the pressure drop across each collector and

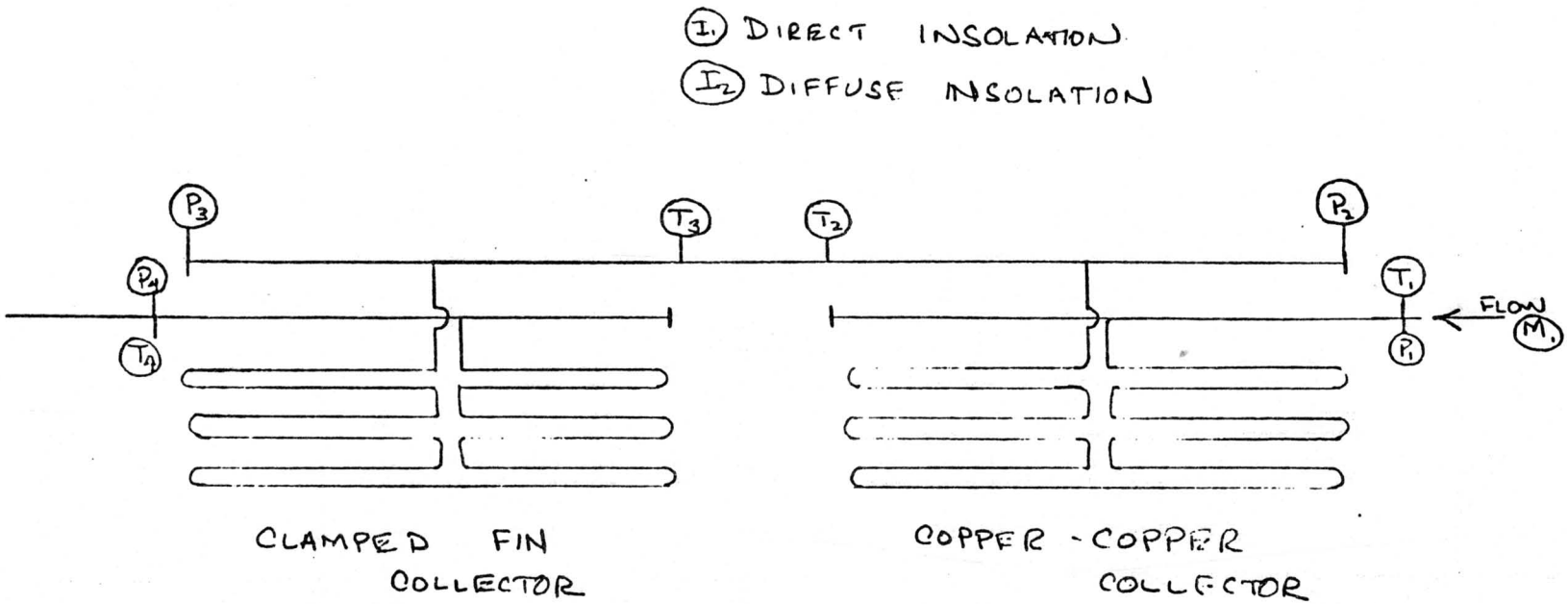

Figure 7-1. Test Instrumentation

measurement M_1 gave the flow rate. The direct (I_1) and total (I_2) insolation are measured on a plane parallel to the collector aperture. The collector tilt angle was adjusted and recorded. The test loop was set-up to vary flow rate, inlet temperature and tilt angle.

7.3 TEST RESULTS

All of the efficiency data collected on the TC-300 collector is displayed in Table 7-1 and figures 7-2 through 7-7. Table 7-1 is a compilation of all the tests performed on the TC-300 collector at the Building B test facility. Figures 7-2 through 7-4 plot the efficiency versus inlet temperature for the collector. Figure 7-2 is performance based on total insolation, Figure 7-3 is performance based on direct insolation, and Figure 7-4 is performance based on the energy in the aperture. Energy in the aperture is defined as the energy within the collector's field of view ($\pm$ 13°). All of the direct energy falls within this angle. Empirically, 25% of the diffuse is within this field of view, i.e.:

$$\frac{1}{CR_{untruncated}} \times \% \text{ Diffuse}$$

The efficiencies were all taken at solar noon. All of the results tabulated in Table 7-1 are shown on these performance curves with the exception of stagnation data.

TABLE 7-1

PERFORMANCE DATA SUMMARY

Strip Chart Number:	64	65	66	67	69	70	71	72	76	78
Date:	9/5/78	9/6/78	9/12/78	9/13/78	9/25/78	9/26/78	9/27/78	9/29/78	10/4/78	10/18/78
Time: (Local)	1300	1300	1300	1300	1300	1300	1300	1300	1300	1205
Shroud Lot Number:	Mixed	Mixed	Mixed	Mixed	Mixed	Mixed	Mixed	Mixed	Mixed	Mixed
Absorbtivity:	.901	.901	.901	.901	.901	.901	.901	.901	.901	.901
Emissivity:	.045	.045	.045	.045	.045	.045	.045	.045	.045	.045
Inlet Temperature - °F:	319.0	354.2	311.0	322.6	396.4	148.1	88.9	318.9	397.0	663.9*
Ambient Temperature - °F:	79.2	84.6	84.2	68.1	73.0	66.3	68.2	65.3	68.4	59.0
Insolation in Btu/hr-ft² - Total[1]:	313.75	305.75	250.08	303.91	327.90	332.82	311.91	330.36	313.14	301.76
Insolation in Btu/hr-ft² - Direct[2]:	269.03	227.62	80.96	229.58	283.94	305.45	263.99	301.93	263.21	264.77
% Diffuse[3]:	14.24	25.55	67.63	24.46	13.41	8.22	15.36	8.61	15.94	12.26
Flow in GPM:	.302	.292	.292	.296	.298	.313	.295	.314	.304	—
Tilt Angle in Degrees:	33	33	33	33	40	40	40	40	47	52
Wind Speed in MPH:	5.90	1.83	1.41	4.69	14.10	0.33	0.01	0.15	2.41	0.01
η using Total Insolation:	.4102	.3578	.2414	.3667	.3403	.4643	.4625	.3914	.3442	—
η using Direct Insolation:	.4777	.4798	.7414	.4854	.3930	.5059	.5465	.4283	.4095	—
η using Aperture Energy:	.46	.445	.49	.45	.38	.495	.52	.42	.39	—
Notes			Very Hazy and cloudy		Tilt changed to 40°				Tilt changed to 47°	Tilt changed to 52°

Strip Chart Number:	79	80	81	82	83	84	87	88	89	90	91	92	93	96
Date:	10/23/78	10/24/78	10/25/78	10/27/78	10/30/78	10/31/78	11/3/78	11/5/78	11/6/78	11/8/78	11/14/78	11/18/78	11/19/78	12/6/78
Time: (Local)	1315	1330	1220	1200	1205	1215	1200	1200	1200	1200	1200	1150	1230	1135
Shroud Lot Number:	Mixed	Mixed	Mixed	Mixed	Mixed	Mixed	8C7112	8C7112	8C7112	8C7112	8C7112	8C7112	8C7112	8C7112
Absorbtivity:	.901	.901	.901	.901	.901	.901	.90	.90	.90	.90	.90	.90	.90	.90
Emissivity:	.045	.045	.045	.045	.045	.045	.0424	.0424	.0424	.0424	.0424	.0424	.0424	.0424
Inlet Temperature - °F:	739.2*	825.5*	836.2*	832.5*	835.8*	840.7*	399.1	137.0	119.7	95.2	292.4	806.5*	811.7*	806.2*
Ambient Temperature - °F:	80.9	51.1	57.3	57.3	55.7	62.2	65.4	70.2	70.4	57.6	63.4	62.3	51.0	56.6
Insolation in Btu/hr-ft² - Total[1]:	309.14	332.52	318.37	85.21	312.83	322.06	306.83	330.67	272.53	319.90	304.83	333.44	301.45	322.98
Insolation in Btu/hr-ft² - Direct[2]:	229.97	297.24	267.51	16.04	254.22	265.56	257.73	**	197.11	287.85	266.73	253.82	**	276.12
% Diffuse[3]:	25.61	10.61	15.98	81.19	18.74	17.54	16.55	**	27.67	10.02	12.50	23.88	**	14.51
Flow in GPM:	—	—	—	—	—	—	.307	.328	.312	.304	.306	—	—	—
Tilt Angle in Degrees:	52	52	52	52	57	57	57	57	57	57	57	57	57	62
Wind Speed in MPH:	0.63	9.89	4.70	6.21	1.80	1.59	1.61	2.10	3.57	6.82	0.34	7.16	12.02	0.15
η using Total Insolation:	—	—	—	—	—	—	.3909	.4365	.4626	.4701	.4140	—	—	—
η using Direct Insolation:	—	—	—	—	—	—	.4684	***	.6396	.5224	.4731	—	—	—
η using Aperture Energy:	—	—	—	—	—	—	.45	***	.58			—	—	—
Notes	* Avg Stag Temp.	* Avg Stag Temp. Lenticulars were cleaned off in test	* Avg. Stag. Temp	* Avg Stag. Temp. Sunny and hazy cloudy	* Avg. Stag. Temp Tilt changed to 57° Local time set back 1 hr.	* Avg Stag. Temp.	* Avg. Stag Temp changed Shrouds to Batch # 8C7112	*** Could not be calculated ** Not Measured				* Avg Stag. Temp.	** Not Measured * Avg Stag Temp Clouds passed at Solar noon	* Avg Stag. Temp.

1 Measured by PSP Pyranometer
2 Measured by Pyrheliometer
3 Computed from total and direct Insolation readings

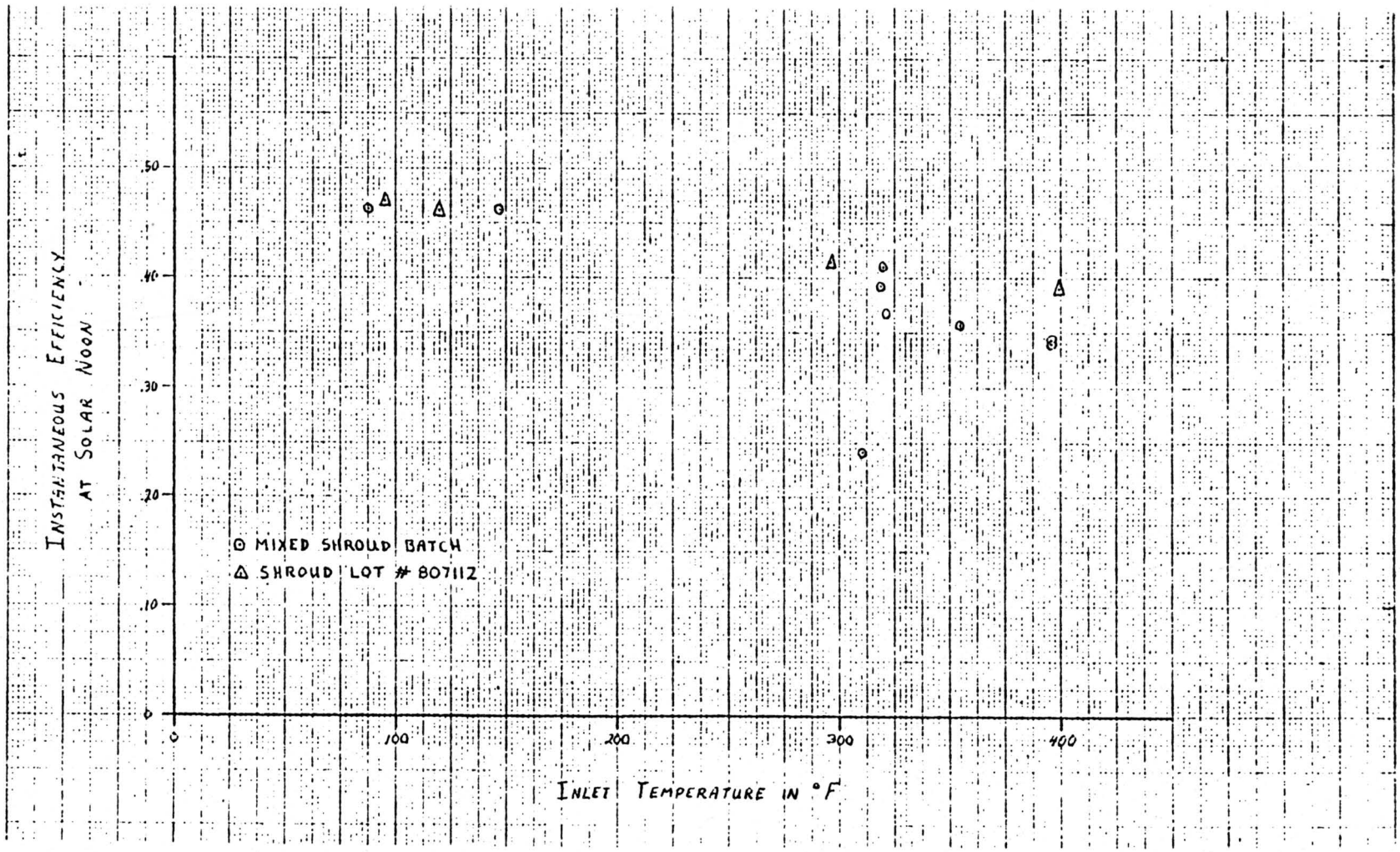

Figure 7-2. TC-300 Efficiency Based on Total Insolation

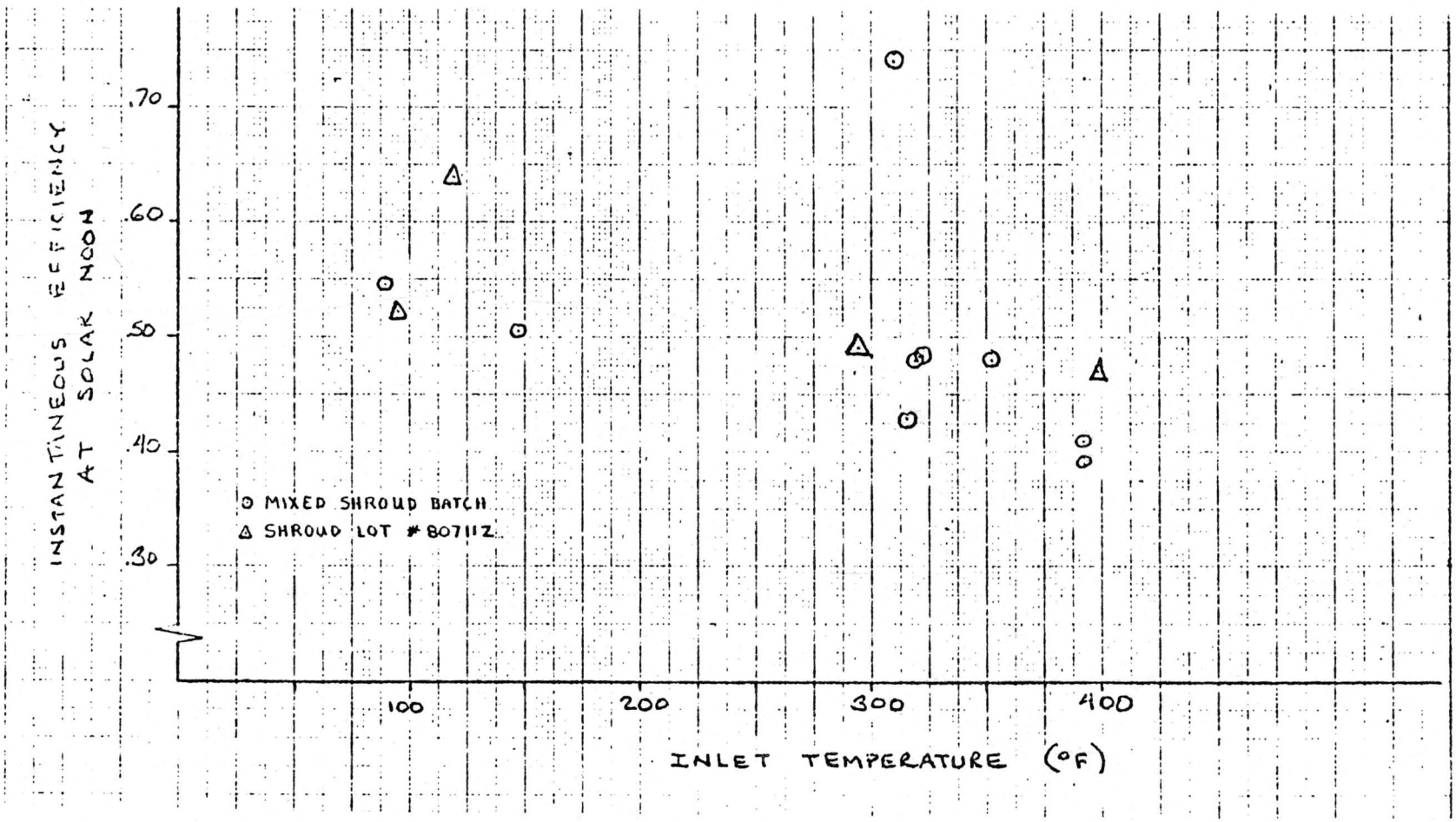

Figure 7-3. TC-300 Efficiency Based on Direct Insolation

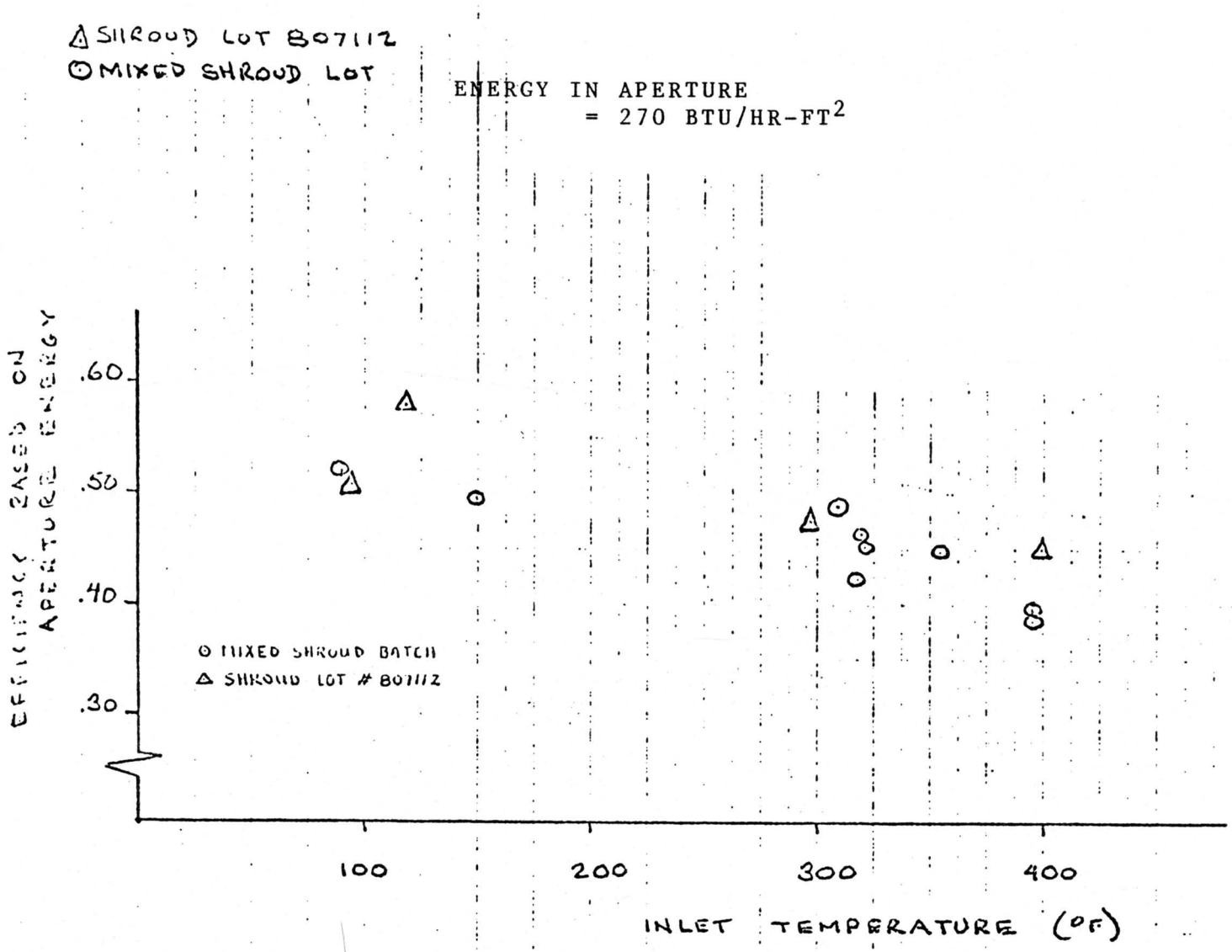

Figure 7-4. TC-300 Performance At Solar Noon

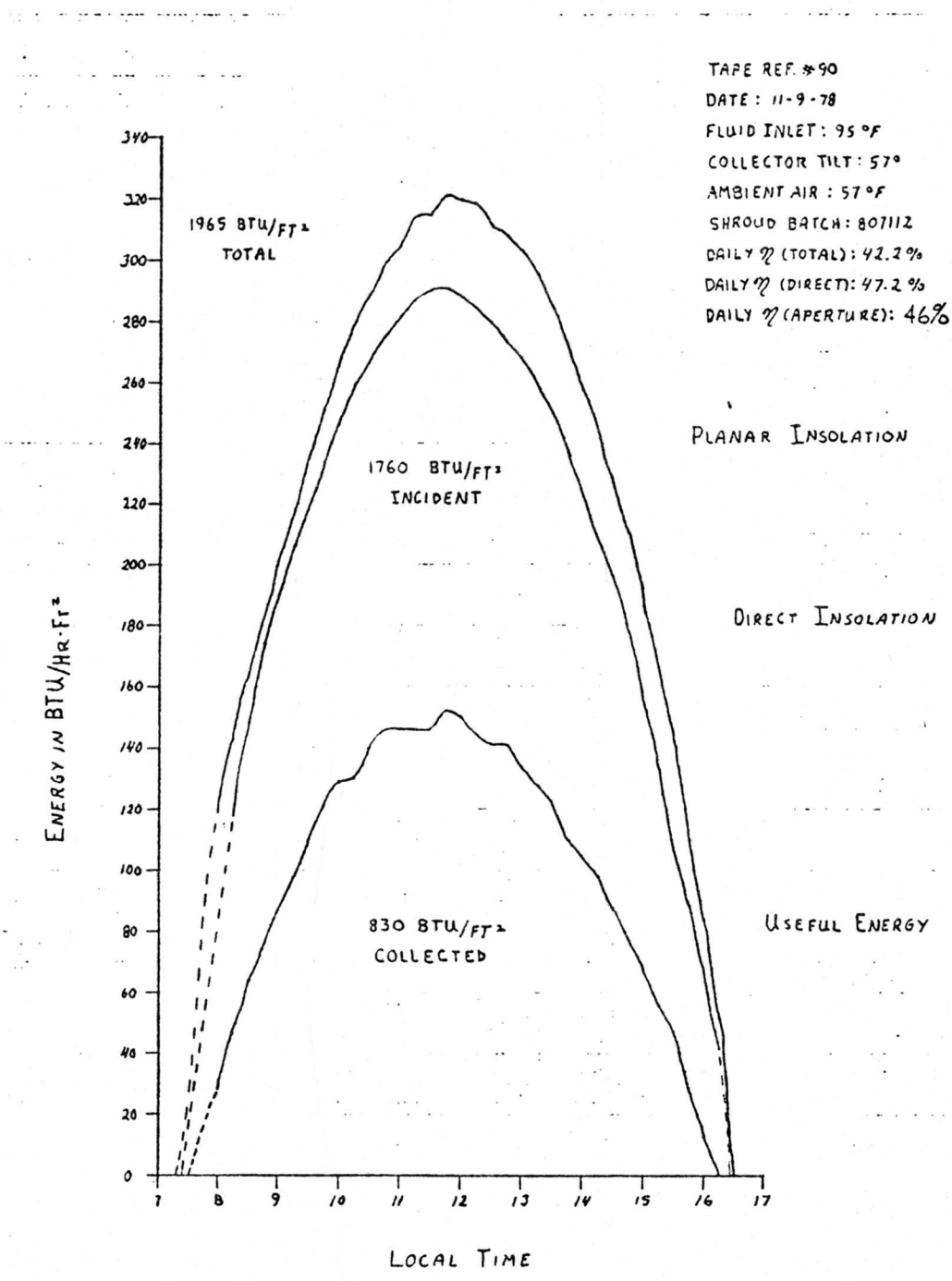

Figure 7-5. Daily Efficiency of the 3X Collector

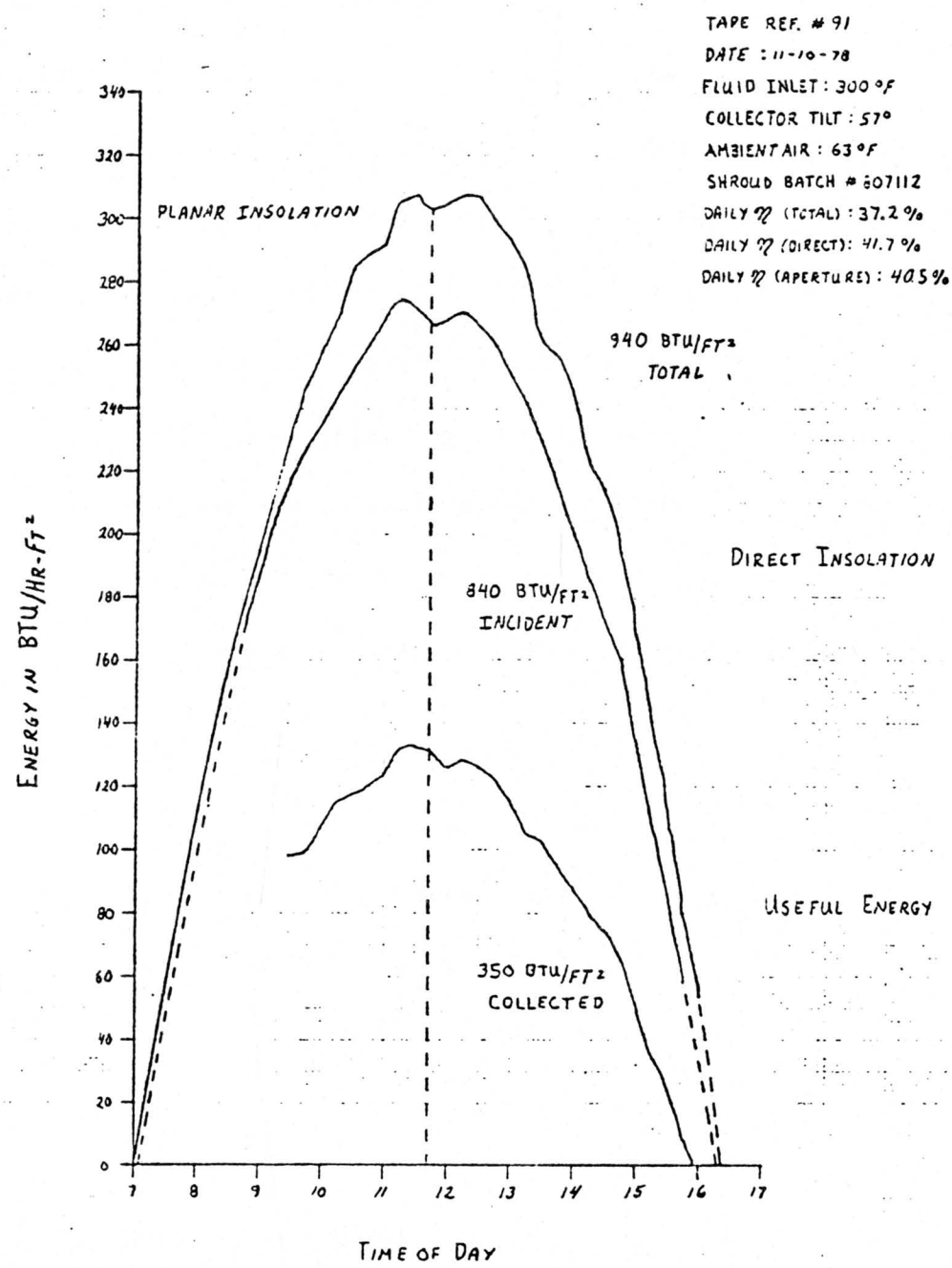

Figure 7-6. Daily Efficiency of the 3X Collector

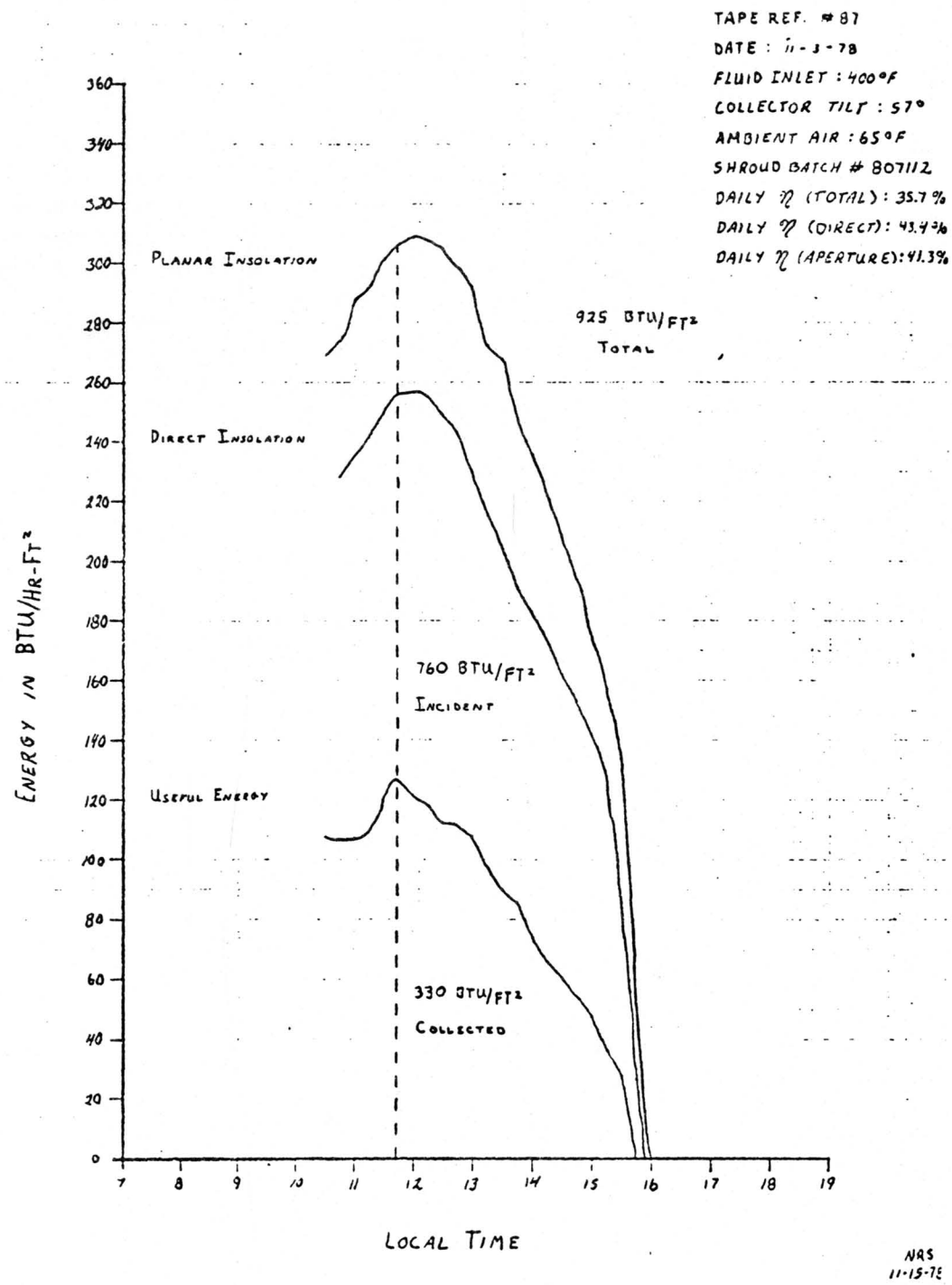

Figure 7-7. Daily Efficiency of the 3X Collector

Figures 7-5 through 7-7 plot energy as a function of time for planar insolation, direct insolation, and useful energy. The all day efficiency is computed from these curves. Figures 7-5, 7-6 and 7-7 have inlet temperatures of 95°F, 300°F, and 400°F respectively.

Figure 7-8 plots the instantaneous efficiency (based on total insolation) of both the TC-300 collector and the TC-100 eight shroud collector.

The pressure drop across the collector clamped fin serpentine was 6 psi at .25 gpm.

7.4 SUMMARY OF TEST RESULTS

- The TC-300 daily efficiency at solar noon (based on energy in the collector field of view) is 45% when the fluid inlet temperature is 400°F.
- The TC-300 daily efficiency is 41% at a fluid inlet temperature of 400°F.
- Increasing the concentration ratio from 1.0875 (TC-100 8 shroud collector) to 2.9 (TC-300 collector) decreases the optical efficiency from 60% to 48%. Thermal losses, however, are reduced by a factor of 3. The net result is that the efficiency of the TC-300 is less than that of the TC-100 8 shroud below an inlet temperature of 330°F and greater than the TC-100 8 shroud above this temperature.
- Without regular cleaning the reflectors collect enough dirt to lower the reflectivity and decrease performance .
- Shrouds did not shatter during normal operation or stagnation. Thermal shock, however, shattered several shrouds.

7.5 DISCUSSION OF TEST RESULTS

The goal for the TC-300 collector was a daily efficiency of 40% at an inlet temperature of 350°F. Such a goal justified the development of this new collector. The TC-100 has adequate performance up to this temperature level. Figure 7-7 shows that at an inlet temperature of 400°F, the daily efficiency using the energy in the aperture was 41.3%. Instantaneous efficiency at solar noon was 45%. This efficiency was closely maintained on either side of solar noon. This behavior is due to the fact that the TC-300 collector is oriented east-west. The sun is within the acceptance angle for the great majority of the day. Actual duration depends upon collector orientation. With four adjustments per year, the average collection time is 8.76 hours per day.

Figure 7-8 is a performance curve of the TC-300 collector versus the TC-100 8 shroud collector. The same shroud lot was used on each to eliminate the variables in shroud manufacture. This curve illustrates the lower optical efficiency of the TC-300 collector. The optical efficiency is the efficiency obtained as fluid temperature approaches ambient temperature. The TC-300 collector does not begin to be more efficient than the TC-100 8 shroud collector until an inlet temperature of 325°F. This curve also shows the differences in thermal losses experienced by each collector. The thermal loss is given by the difference between the optical efficiency and actual efficiency. As theory would indicate, the thermal losses on the TC-300 collector are approximately 1/3 lower than those associated with the TC-100

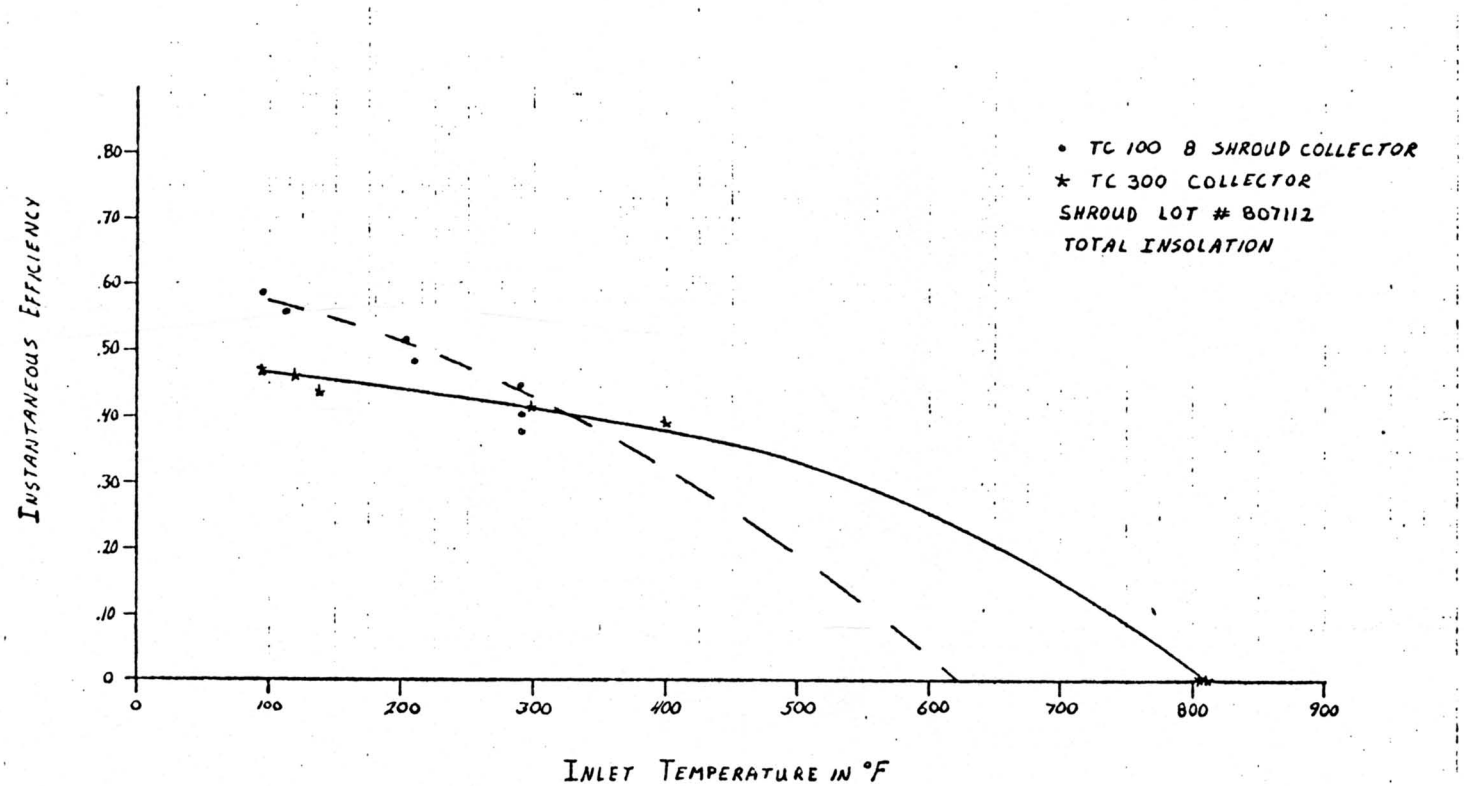

Figure 7-8. Efficiency vs. Inlet Temperature - TC-300 Collector & TC-100-B Shroud Collector

8 shroud collector.

Quantifying the difference in optical efficiency between the two collectors is a major result of this testing program. Any sensible product line utilizing the evacuated shroud must be built around the fact that as concentration ratio increases, the optical efficiency decreases along with the desirable decrease in thermal losses.

The optical efficiency model developed in Section 3 may lead to a better understanding of this phenomena. Optical efficiency, K, is given by:

$$K = (\alpha\tau)_D I + \rho^N (\alpha\tau)_R (1-I) \qquad (27)$$

See section 3 for the definition of each term. Both α and τ depend on the incidence angle between each beam of radiation and the absorber surface (α) or outer glass shroud (τ).

A detailed beam tracking computer program is required to accurately integrate this effect over all radiation striking the absorber. In the absence of such an in-house program, a qualitative assessment of equation 27 will be made in order to better understand the decrease in optical efficiency with increasing concentration ratio. The question becomes what terms in equation 27 explain a decrease in K with increasing CR. The term I certainly depends on CR. I is the fraction of radiation that strikes the absorber directly. It is .3 for the TC-101 (CR = 1.0875) and .1 for the TC-300 (CR = 2.9).

For ideal concentrators, an increase in concentration implies a deeper trough. This translates to an increase in the incidence angle between incoming radiation and the normal to the reflector surface. Bench tests indicate a decrease in reflectance as this angle increases. At 70°F the reflectance off Alglas is roughly 10% less than the value at normal incidence. N, the average number of reflections, also increases with increasing CR. As mentioned previously, α and τ depend on the incidence angle of radiation striking the absorber or outer shroud.

Figure 7-9 shows the results of a limited beam tracing program developed by the Chamberlain Manufacturing Corporation. The program does not integrate the incidence angle effect on α and τ over all radiation striking the receiver. However, the qualitative nature of this angle and its dependence on reflector location is shown by this figure. For the present, consider the TC-300 cusp as an extension of the TC-101 cusp. As reflector material is added, the additional radiation strikes the receiver at an increasingly greater angle until double reflections begin. Thus the effective $\alpha\tau$ will decrease with increasing concentration ratio.

Assume that the TC-101 has an effective $(\alpha\tau)$ of .73 ($\alpha \sim .85, \tau \sim .86$). These values are meant to include angle effects and assume an average incidence angle of 30°. Take ρ as .85 and N as 1. This results in an optical efficiency of .65.

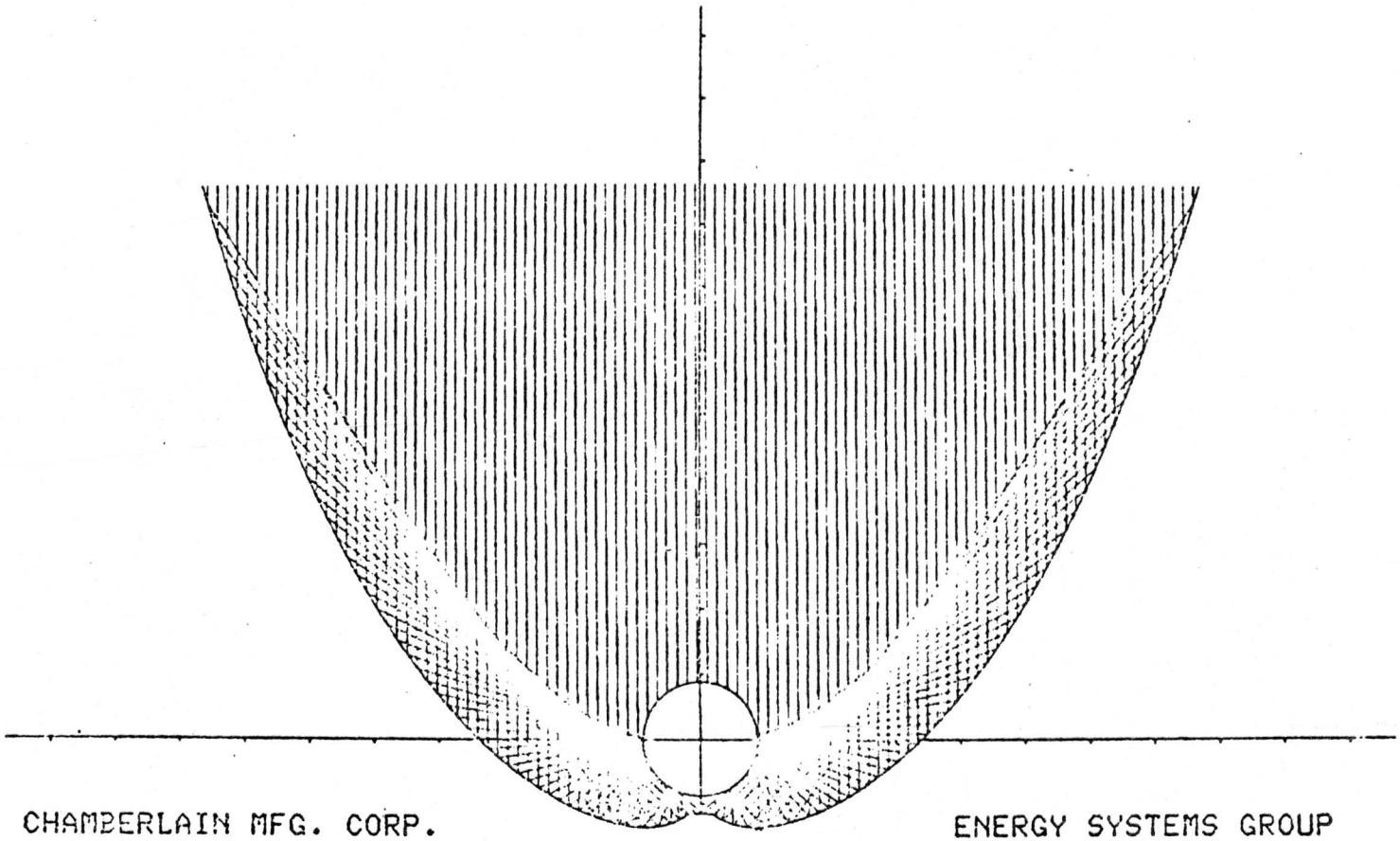

Figure 7-9. 3X Beam Tracing

For the TC-300, assume an N of 1.3, a ρ of .8 (decreased by 5% to account for increased incidence angle), and an effective $\alpha\tau$ of .69 (α = .82, τ = .84). This assumes half the radiation has a 30^{o} incidence angle and half a 45^{o} angle.

These assumptions result in an optical efficiency of .53. Without detailed beam tracing the analysis of optical efficiency remains qualitative and empirical. However, the above discussion shows that the observed decrease in optical efficiency may be explained by reasonable assumptions on the behavior of ρ, N, α, and τ, with increasing concentration ratio.

A prediction of instantaneous efficiency (with the above optical efficiency) is shown in Figure 7-10. Note that the general behavior of the thermal losses is accurately characterized by the system equation.

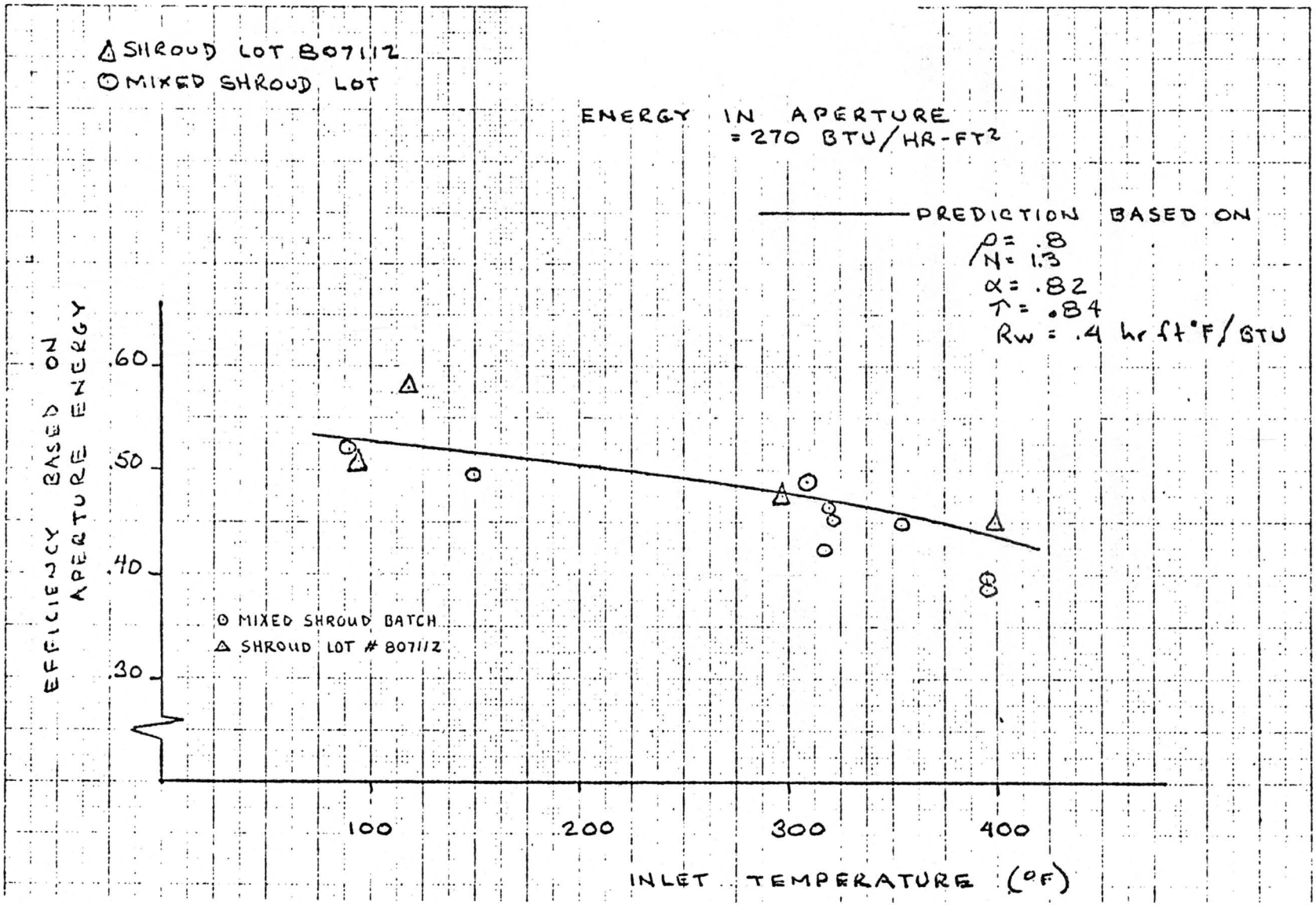

Figure 7-10. TC-300 Performance At Solar Noon

SECTION 8

FABRICATION AND TEST OF A TRACKING PARABOLIC TROUGH

The performance section shows the relationship of the TC-300 to a collector of lower concentration, the TC-100 (CR = 1.0875). At high temperatures the TC-300 shows its advantage. Another approach to high temperature performance is a focusing collector (either a dish or trough) which continuously tracks the sun. Two dimensional troughs appear more cost effective than dishes at present. A parabolic trough (aperture width 6 ft., length 10 ft.) was built and tested in order to assess the efficiency and producibility of the trough concept. An internal parabolic rib design was used with rib spacing of 5 ft. A bottom keel and two side members are connected to the ribs. The reflector assembly was Scotch Cal laminated to .032 inch thick aluminum. Reflector dimensions were 4 ft. by 5 ft. The reflectors were wrapped around and fastened to the frame, composed of the bottom keel, and side members. No preforming of the reflector substrate was required. A picture of the assembled collector appears in Figure 8-1. The collector was mounted to a pipe frame by a torque tube which ran through the center of gravity of the assembled trough. The receivers shown in Figure 24 are standard TC-100 shrouds.

The assembly shown in Figure 24 proved to be structurally sound and optically accurate. A strip of tape was mounted along the focal line of the trough

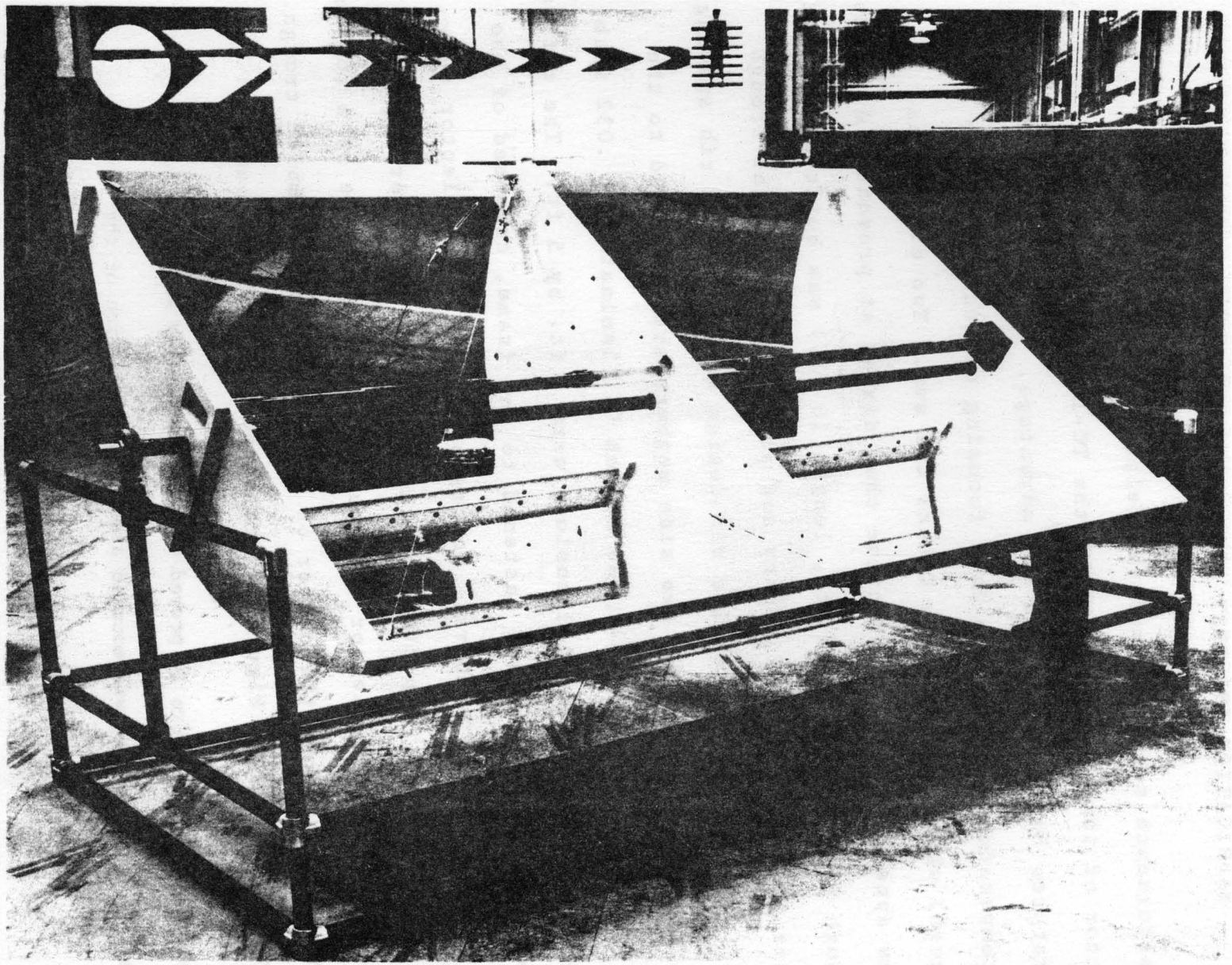

Figure 8-1. TC-400 (VF78-320B)

and allowed to clear when the collector was aimed at the sun. The resulting clear pattern is shown in the photograph of Figure 8-2. Beam width at the receiver is roughly 1/2 inch.

Performance testing was accomplished by manually tracking the sun and measuring the temperature increase through the receiver. The receiver was a length of TC-100 serpentine inserted in an unevacuated shroud. The fins of the serpentine were painted black. The resulting concentration ratio was 13. Efficiency based on direct insolation was 50% at an absorber temperature of 400^{o}F and an insolation level of 230 Btu/in.ft^{2}.

The performance was roughly 10% higher than the TC-300 at the same temperature. The advantages of the TC-300 lie in the fact that continuous tracking is not required and that a portion of the diffuse energy is available for collection. More experience with the reliability and cost of tracking is required to determine if these advantages outweigh the fact that the TC-300 has a lower performance than tracking parabolic troughs.

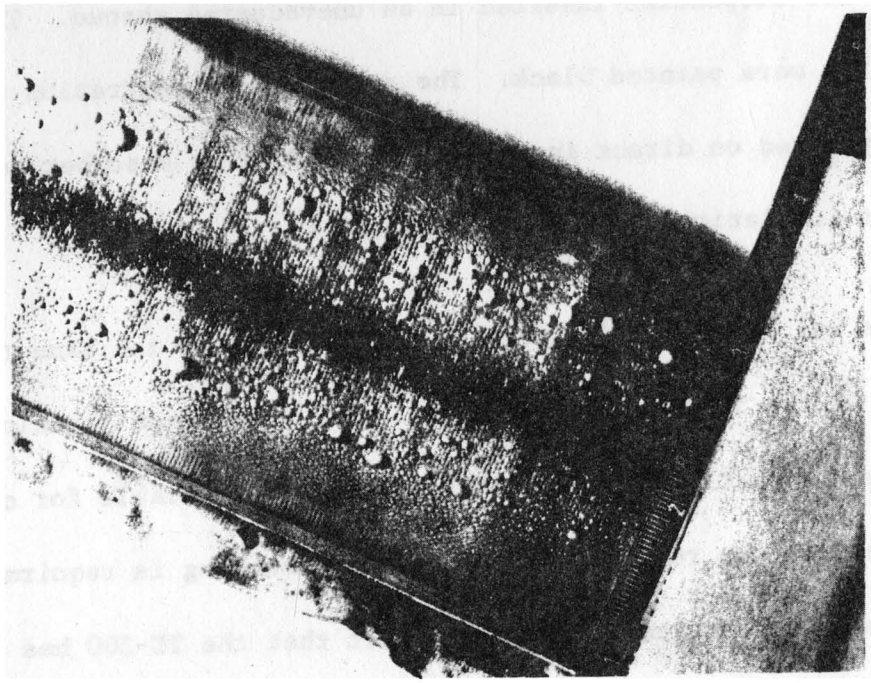

Figure 8-2. TC-400 Focal Width

SECTION 9

FLOW THROUGH EVAUCATED SHROUD

During the development of the TC-300 collector, it became apparent that a relatively complex piping system was required to remove useful heat from the shrouds. This is shown most dramatically in Figure 2-3. Complexity arises because the shrouds are open to heat removal hardware at only one end; see Figure 2-2. A shroud open at both ends would allow piping to run directly from one shroud to another. Such a scheme could reduce piping heat loss as well as material cost. The main design problem with shrouds open at both ends is one of thermal expansion - the inner tube is several hundred ^{o}F hotter than the outer tube. (The present domed design easily allows for this temperature differential since the inner tube can grow unimpeded.)

A flow through shroud which allows for thermal expansion was invented during the TC-300 development program. It is described in detail in Appendix D. A substantial increase in system efficiency could be realized with this shroud. Initial calculations indicate that system cost could be reduced as well.

R E F E R E N C E S

1. Bingmann, R.; Solar Energy Conversion - Solar Collectors, GE TIS Report 78-SDS-004, 17 February 1977.

2. Application of Compound Parabolic Concentrators, Prepared under NSF Grant AER-75-01065/PR/75/4. Report No. NSF/RANN/SE-AER/75-01065/PR/75/4.

3. Timoshenko, S. P., Goodier, J. N., Theory of Elasticity, 3rd Edition, McGraw-Hill Book Co., New York, 1970.

4. Nichols, J., Results for Initial Clamped Fin Testing, GE Document, PIR No. 1E30-3XCHMB-003, 1978.

5. Nichols, J., Additional Clamped Fin Test Results, GE Document, PIR No. 1E30-3XCHMB-007, 1978.

6. Product Specification, Urethane Insulation, Ground Systems, Space Division, General Electric Co., Drawing No. 63A130265, Rev. K, 28 March, 1978.

A P P E N D I X A

STRUCTURAL ANALYSIS OF

FOAM MODULE

GENERAL ELECTRIC
SPACE DIVISION
PHILADELPHIA

PROGRAM INFORMATION REQUEST / RELEASE

*CLASS. LTR.	OPERATION	PROGRAM	SEQUENCE NO.	REV. LTR.
PIR NO. U	— 1E30	— 3XIR&D —	009	

*USE "C" FOR CLASSIFIED AND "U" FOR UNCLASSIFIED

FROM	TO
J. Hatman	D. Wein

DATE SENT	DATE INFO. REQUIRED	PROJECT AND REQ. NO.	REFERENCE DIR. NO.
3/20/78			

SUBJECT: 2.9X COLLECTOR MODULE (MOD 0) STRUCTURAL ANALYSIS AND FOAM MODULE DEFINITION

INFORMATION REQUESTED/RELEASED

The attached structrual analysis was prepated by GE Thermal Systems, Tacoma, WA, for the 2.9X Solar Collector, Mod 0. The polyurethane foam module is capable of experiencing 100 mph wind and 20 psf snow loads.

Also included are reduced copies of the solar collector foam module, foam blank and associated molds and tooling. The following drawing breakdown provides the collector definition from Thermal Systems.

- 63D715246 Solar Collector (Foam Module)
  - 63D715245 Strongback - Solar Collector
  - 63D715247 Solar Collector (As molded)
    - 63D715231 Parabolic Core Pattern
    - 63D715237 Base Assembly Mold (4 sheets)

JJH:mb

Distribution:
D. Wein
J. Graf
E. Ernst
J. Hogan
J. Young

PAGE NO. 1 OF 17

RETENTION REQUIREMENTS

COPIES FOR	MASTERS FOR
1 MO.	3 MOS.
3 MOS.	6 MOS.
6 MOS.	12 MOS.
MOS.	MOS.
	DO NOT DESTROY

GENERAL ELECTRIC

REV. NO. | TITLE: 3X SOLAR COLLECTOR | CONT ON SHEET | SH NO. 1

CONT ON SHEET | SH NO. | FIRST MADE FOR

REVISIC

PARABOLIC COLLECTOR

LOADS

1. 100MPH WIND.
2. 20PSF SNOW LOAD.

DRAG COEFFICIENT OF COLLECTOR

$C_D = 1.35$ [1]

VELOCITY PRESSURE

$$q = 0.00256\, C_D V^2 = .00256 \times 1.35 \times (100)^2$$
$$= 34.56 \text{ PSF}$$

PROJECTED PANEL AREA

$$A = \frac{50 \times 102}{144} = 35.4 \text{ FT.}^2$$

TOTAL FORCE ON PANEL

$$P = 34.56 \times 35.4 = 1223.4 \text{ LB.}$$

[1] 7TH EDITION OF MARKS' HANDBOOK FOR MECHANICAL ENG. PAGE 11-89

PRINT

MADE BY J. M. Kell 3/9/78 | APPROVALS | DIV OR DEPT. | LOCATION | CONT ON SHEET | SH NO. 1

ISSUED

FF-803 WA 10-741 PRINTED IN U.S.A.

CODE IDENT

GENERAL ELECTRIC

REV. NO. | TITLE: 3X SOLAR COLLECTOR | CONT ON SHEET | SH NO. 2

CONT ON SHEET | SH NO. | FIRST MADE FOR

REVISI

PARABOLIC COLLECTOR

PHYSICAL DIMENSIONS OF STRONGBACK SANDWICH

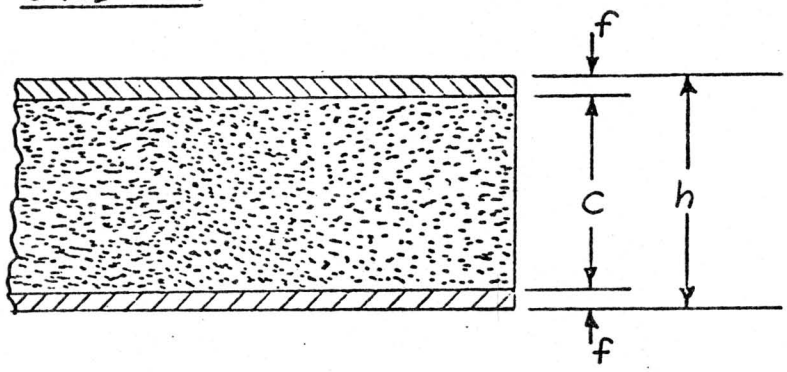

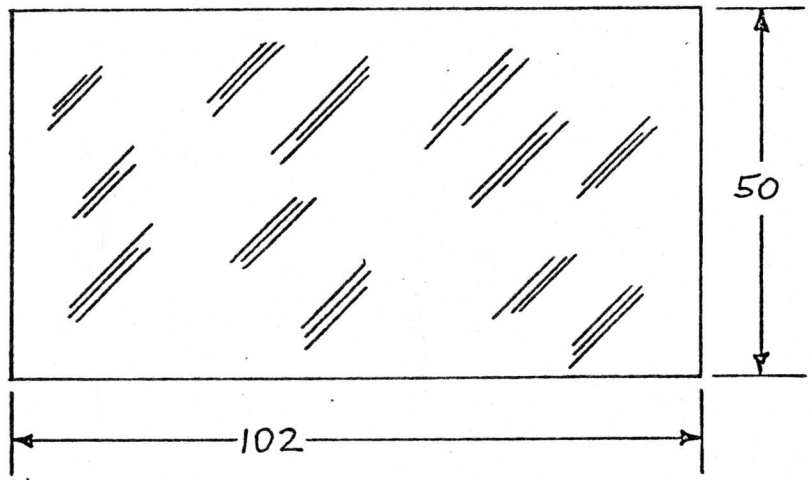

$a = 102$ IN. $\qquad f = 0.020$ IN.

$b = 50$ IN.

$C = 3.960$ IN.

$h = 4.0$ IN.

PF NO

MADE BY J. M. Kolb 3/9/78 | APPROVALS | DIV OR DEPT. | CONT ON SHEET | SH NO. 2

ISSUED | LOCATION | CODE

PF 803 W.A. (9-74)
PRINTED IN U.S.A.

GENERAL ELECTRIC

REV NO. | TITLE | CONT ON SHEET | SH NO. 3

CONT ON SHEET | SH NO. | FIRST MADE FOR

3X SOLAR COLLECTOR

REVISIO

PARABOLIC COLLECTOR

CORE MATERIAL

3 PCF RIGID POLYURETHANE FOAM

$G_c = 500$ PSI

$F_s = 30$ PSI

$F_c = 45$ PSI

FACE SHEETS

2024-T3 ALUMINUM

$F_y = 45{,}000$ PSI

$E_f = 10.6 \times 10^6$ PSI

THE DEFLECTION OF THE STRONGBACK IS CALCULATED FROM THE FOLLOWING EQUATION (FOR UNIFORM LOADING) LENGTHWISE DEFLECTION

$$\delta = \frac{5Pa^3}{384D} + \frac{Pa}{8N}$$

WHERE D AND N ARE THE FLEXURAL AND SHEAR STIFFNESS RESPECTIVELY.

$$D = \frac{E_f f (c+f)^2 b}{2(1-\mu^2)}$$

PRINTS

MADE BY J. M. Kohl 3/9/78 | APPROVALS | DIV OR DEPT. | 1

ISSUED | LOCATION | CONT ON SHEET | SH NO. 3

PP-803-WA (8-74)
PRINTED IN U.S.A.

CODE IDENT

PARABOLIC COLLECTOR

SUBSTITUTING VALUES WE HAVE

$$D = \frac{10.6\times10^{6}\times.020\times(3.96+.02)^{2}\times50}{2\times.91}$$

$$= 9.226\times10^{7}$$

$$N = G_c(c+f)b$$

$$= 500\,(3.96+.02)\times50$$

$$= 9.95\times10^{4}$$

AND FINALLY

$$S = \frac{5\times1223.4\times(102)^{3}}{384\times9.226\times10^{7}} + \frac{1223.4\times102}{8\times9.95\times10^{4}}$$

$$= 0.183 + 0.157 = 0.34 \text{ IN.}$$

$1/360^{*}$ OF SPAN $= 0.28$ IN. $\lesssim 0.34$

$\therefore$ THE STIFFNESS IS ADEQUATE.

LENGTHWISE BENDING MOMENT

$$M = \frac{wl^{2}}{8} = \frac{1223.4}{102}\times\frac{(102)^{2}}{8}$$

$$= 15{,}598.4 \text{ IN-LB.}$$

* STANDARD ALLOWABLE DEFLECTION OF STRUCTURE.

REVISIONS

PARABOLIC COLLECTOR

FACING STRESS

$$f_t = \frac{2M}{f(h+c)b}$$

$$= \frac{2 \times 15{,}598.4}{.02 \times (4.0+3.96) \times 50}$$

$$= 3919.2 \text{ PSI} \leftarrow$$

$F_t = 45{,}000 \text{ PSI}$ FOR 2024T3

CORE SHEAR STRESS

$$f_s = \frac{2V}{(h+c)b} = \frac{2 \times 611.7}{(4+3.96) \times 50}$$

$$= 3.1 \text{ PSI} < \frac{1}{5} \times 30 \text{ PSI} \leftarrow$$

HORIZONTAL SHEAR STRESS

$$I = 2 \times .02 \times 50 \times (1.99)^2 = 7.92 \text{ IN.}^4$$

$$f_{s_H} = \frac{VQ}{Ib} = \frac{611.7}{7.92 \times 50} \times .02 \times 50 \times 1.99$$

$= 3.1 \text{ PSI} < 19 \text{ PSI}$ MINIMUM FORM TO SKIN BOND SHEAR STRESS ←

PRINTS

3X SOLAR COLLECTOR

REVISIC

PARABOLIC REFLECTOR

STIFFNESS OF AND STRESSES IN, ASSEMBLY

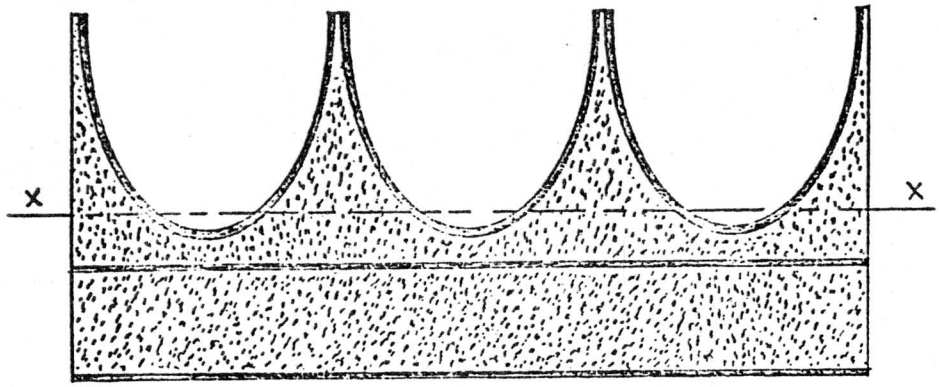

CENTROID OF SECTION

$A = 2 \times .02 \times 50 + 3 \times .025 \times 29.2$

$= 4.19 \text{ IN.}^2$

$4.19\,\bar{y} = .02 \times 50 \times .01 + .02 \times 50 \times 3.99$
$+ 3 \times .025 \times 2 [3 \times 15 + 3 \times 12.5 + 3 \times 9.45$
$+ 2 \times 7.36 + 2 \times 6.07 + 1.6 \times 5.43]$

$\bar{y} = 6.20 \text{ IN.}$ ←

THE AREA MOMENTS ARE TAKEN FROM A SCALE LAYOUT.

PRINT

REVISIC

PARABOLIC REFLECTOR

MOMENT OF INERTIA ABOUT CENTROID

$$I = .02\times50\times(6.19)^2 + .02\times50\times(2.21)^2 + 6\left\{\frac{.025}{12}\left[(2.9)^3+(2.8)^3+(2.6)^3+(1.52)^3+(1.08)^3+(.17)^3\right] + .025\times3\left[(8.8)^2+(5.95)^2+(3.25)^2+(1.16)^2+(.13)^2+(.77)^2\right]\right\}$$

$$= 100.5 \text{ IN.}^4$$

COMPRESSIVE STRESS IN PARABOLIC TIPS

$$f_b = \frac{15{,}598.4 \times 10.08}{100.5} = 1564.5 \text{ psi}$$

THE STRESS LEVEL IS LOW AND SINCE THE SURFACE IS RESTRAINED BY THE FOAM THERE IS NO POSSIBILITY OF LOCAL BUCKLING OF THE ALUMINUM REFLECTOR SKIN.

PRINT:

REVISIO

PARABOLIC REFLECTOR

DEFLECTION OF PANEL ASSEMBLY

$$\delta = \frac{5Pa^3(1-\mu^2)}{384E_fI}$$

$$= \frac{5 \times 1223.4 \times (102)^3 \times .91}{384 \times 10.6 \times 10^6 \times 100.5}$$

$$= 0.014 \text{ IN.}$$

THE DEFLECTION DUE TO SHEAR IS CALCULATED AS FOLLOWS

AN EQUIVALENT BEAM IS

$$r = \left[\frac{I}{A}\right]^{1/2} = \left(\frac{100.5}{4.19}\right)^{1/2} = 4.9$$

THEREFORE

$$h = 2 \times 4.9 = 9.8 \text{ IN.}$$

AND

$$N = 500 \times 9.8 \times 50 = 2.45 \times 10^5$$

$$\delta = \frac{1223.4 \times 102}{8 \times 2.45 \times 10^5} = .006 \text{ IN.}$$

AND FINALLY, THE TOTAL DEFLECTION

$$\delta_T = .014 + .006 = .020 \text{ IN.}$$

PRINTS

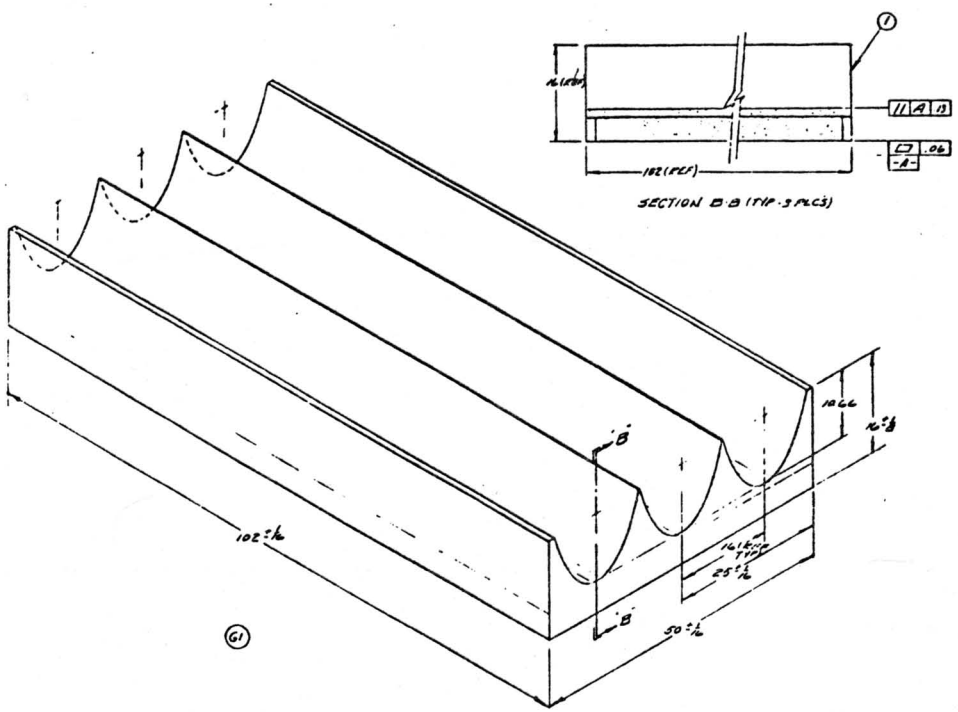

SECTION B-B (TYP-3 PLCS)

NOTES:
1. FILL ALL VOIDS WITH WHITE BODY PUTTY.
2. SMOOTH ALL ROUGH EDGES
3. FINISH-EPOXY SPRAY .003 MIN (COLOR WHITE)

MAR 16 1978

UNLESS OTHERWISE SPECIFIED
DIMENSIONS ARE IN INCHES
ROUNDNESS ON
2 PLACE DECIMALS ± .06
3 PLACE DECIMALS ± .06
ANGLES ±
FINISH ±
MATERIAL
ALL SURF. ✓
SEE SEPARATE PARTS LIST

GENERAL ELECTRIC
GROUND SYSTEMS OPERATION — VALLEY FORGE

SOLAR COLLECTOR

SIZE D | CAGE CODE NO | 83715246

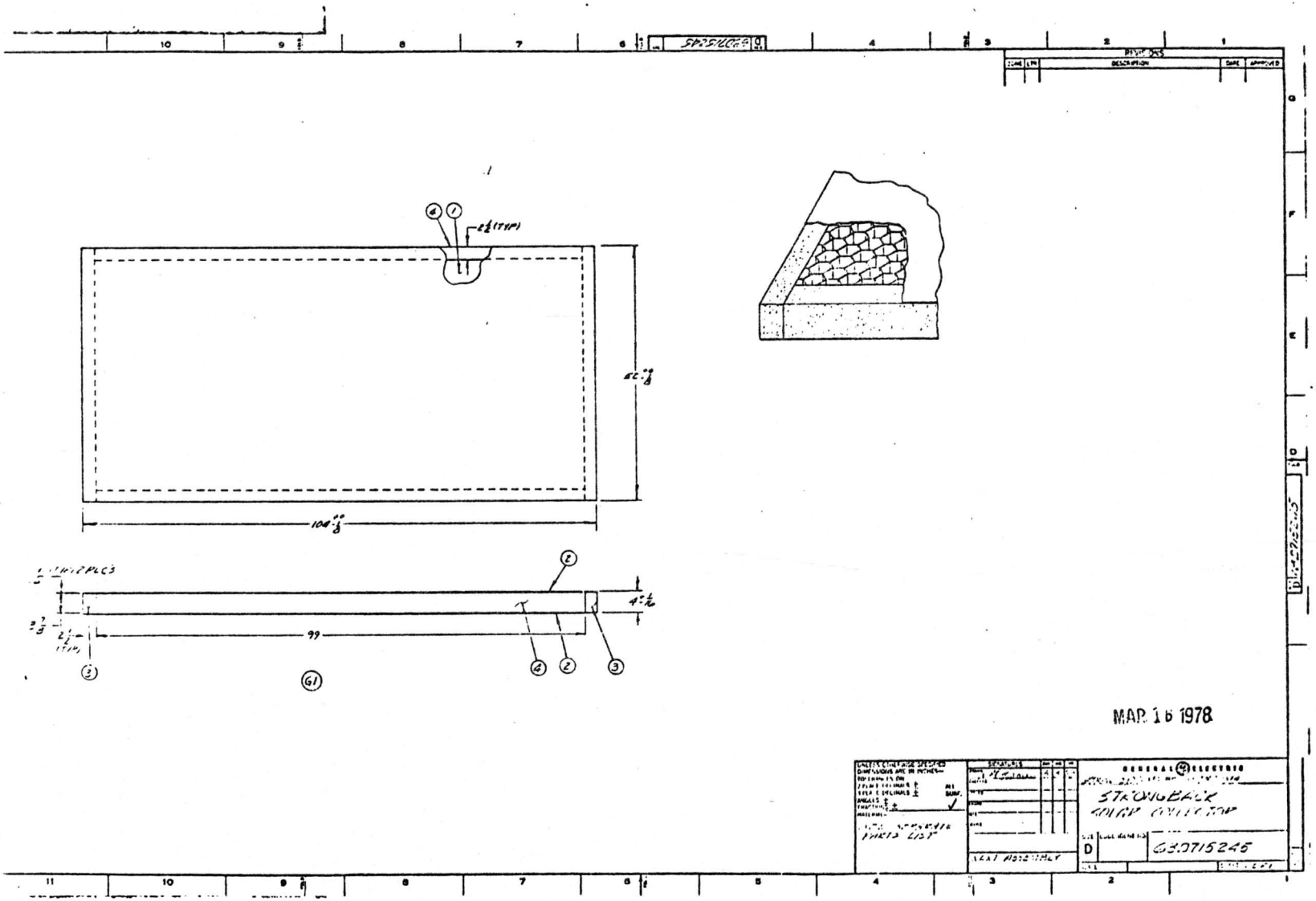
99
MAR 16 1978
STRONGBACK
GROUP ASSEMBLY
D
03.0715245

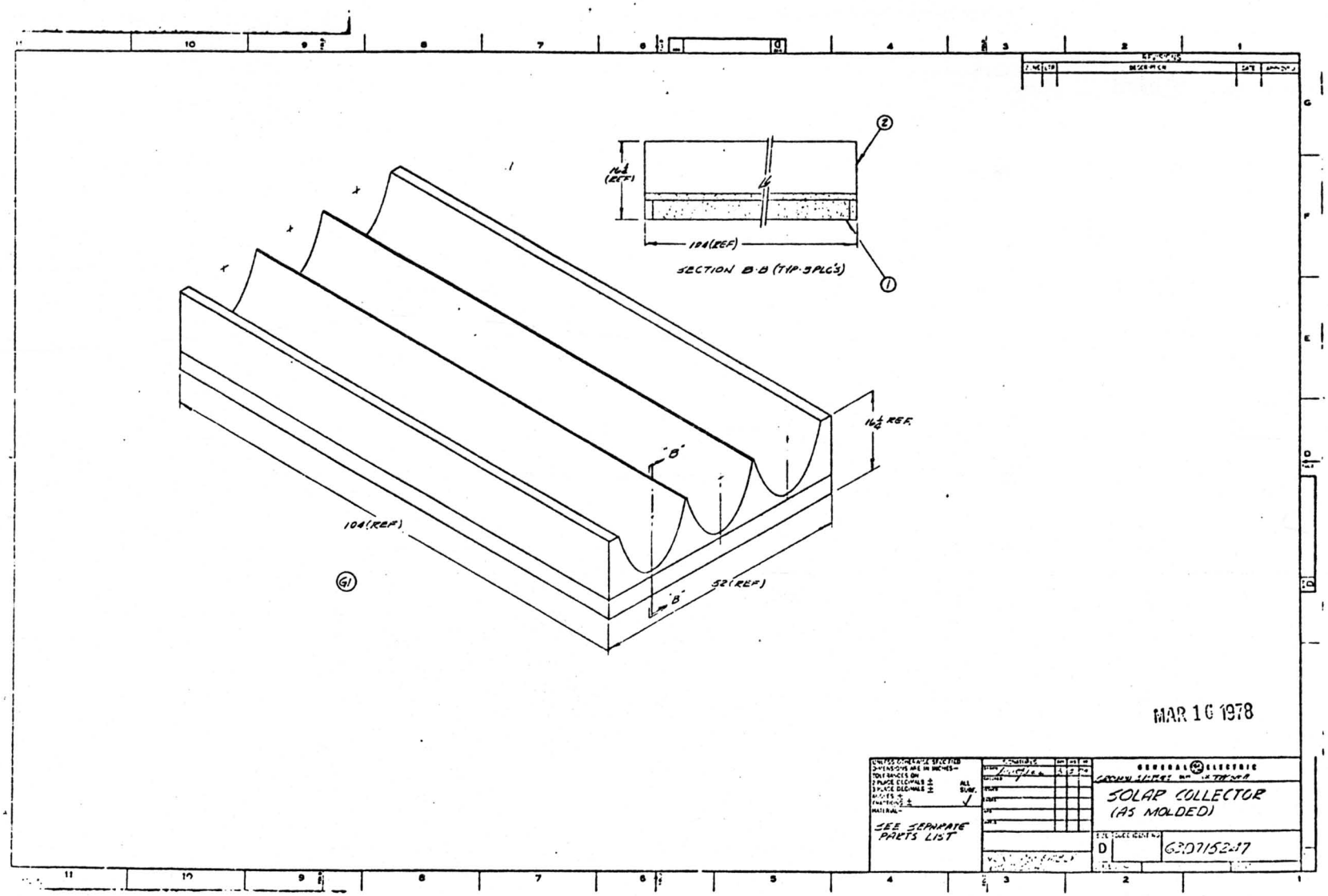
SECTION B-B (TYP. 3 PLC'S)
104 (REF)
104 (REF)
32 (REF)
B
B
SOLAR COLLECTOR
(AS MOLDED)
MAR 16 1978

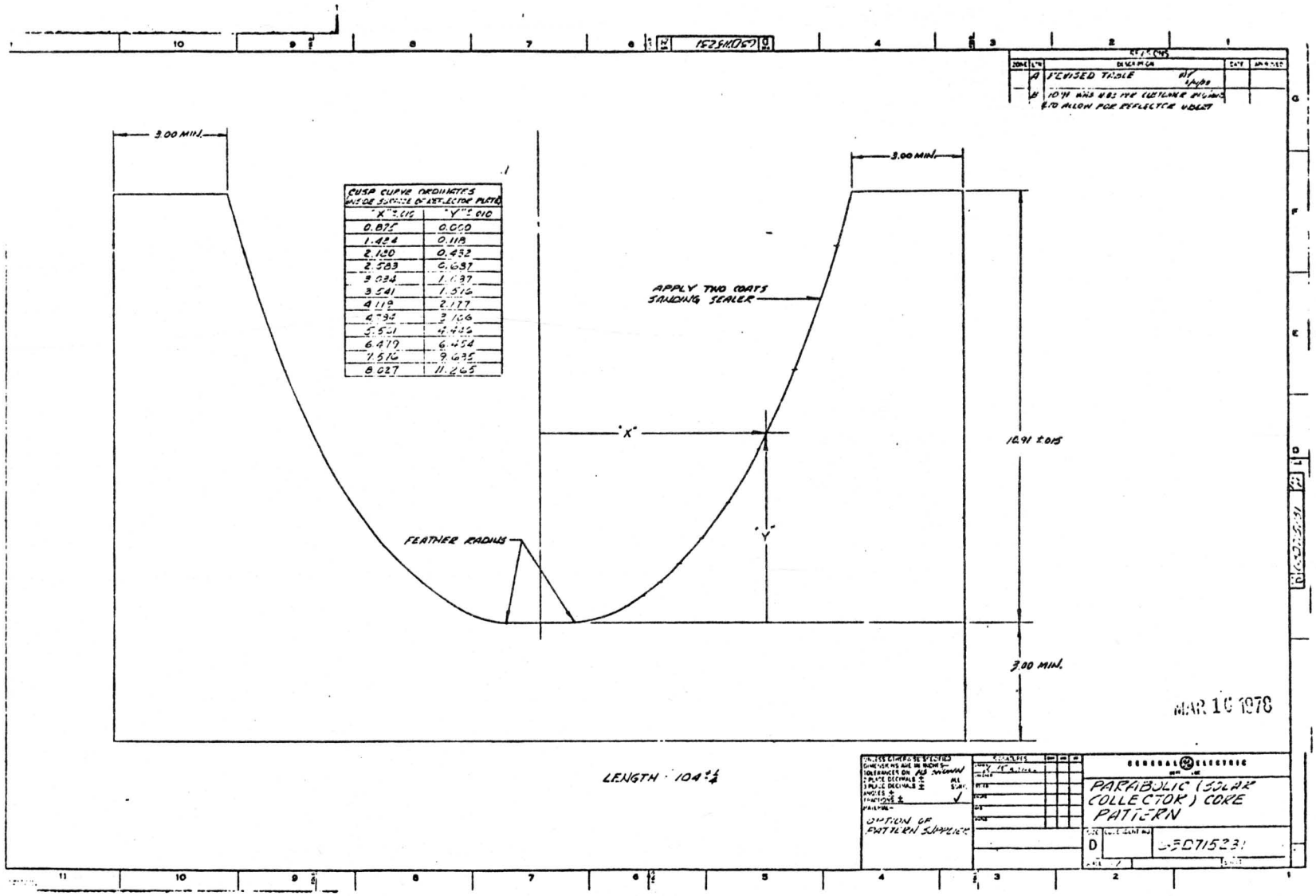

CUSP CURVE ORDINATES INSIDE SURFACE OF REFLECTOR PLATE

"X" ±.015	"Y" ±.010
0.875	0.050
1.424	0.118
2.120	0.432
2.583	0.687
3.034	1.037
3.541	1.516
4.119	2.177
4.732	3.106
5.501	4.442
6.419	6.458
7.516	9.635
8.027	11.265

ZONE	LTR	DESCRIPTION	DATE	APPROVED
	A	REVISED TABLE		
	B	10"W WAS #83 FOR CUSTOMER MARKING #10 MILON FOR REFLECTOR VALLEY		

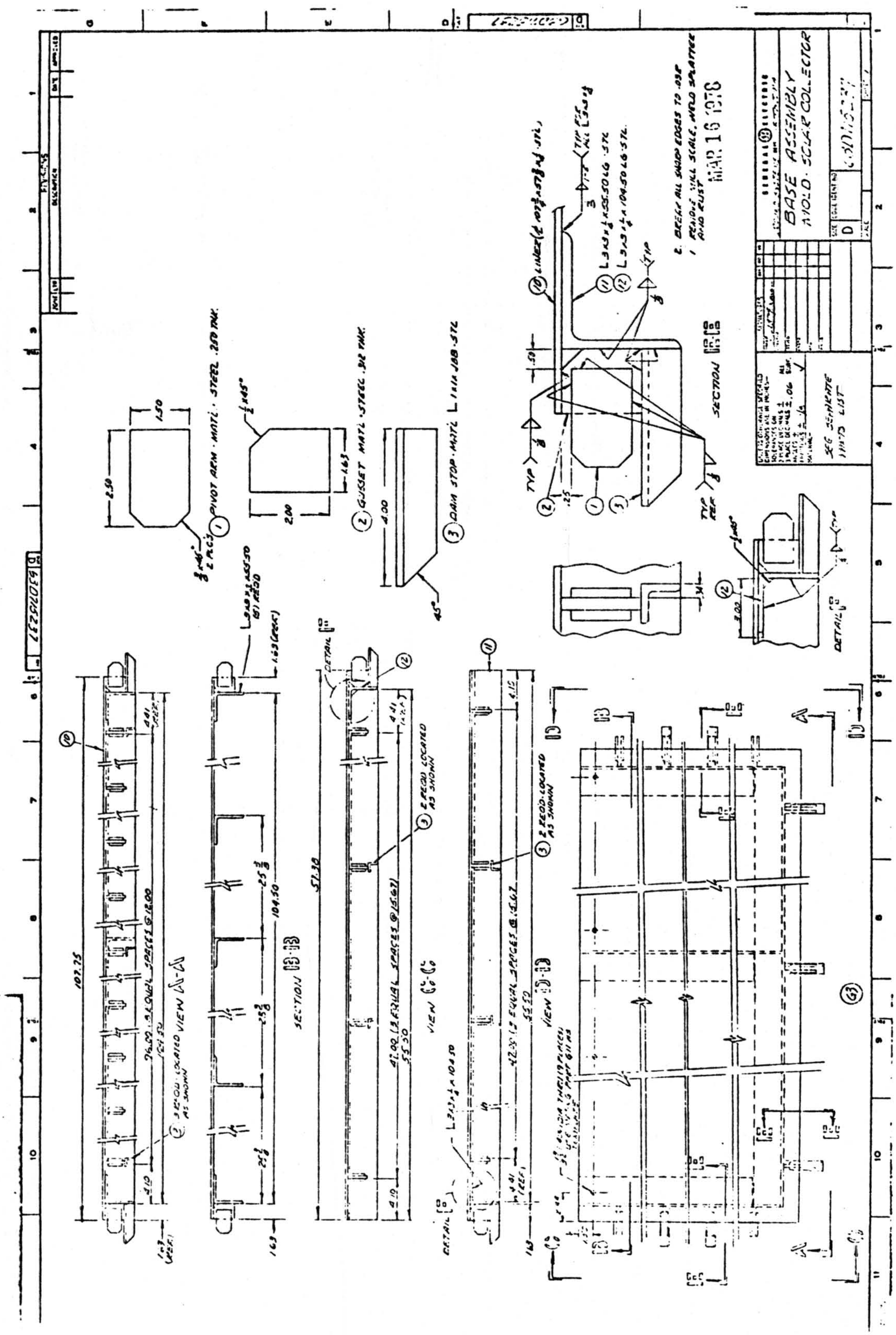
BASE ASSEMBLY
MOLD SCRAP COLLECTOR
MAR 16 1978
SECTION B-B
VIEW A-A
VIEW C-C
VIEW D-D
SEE SEPARATE PARTS LIST

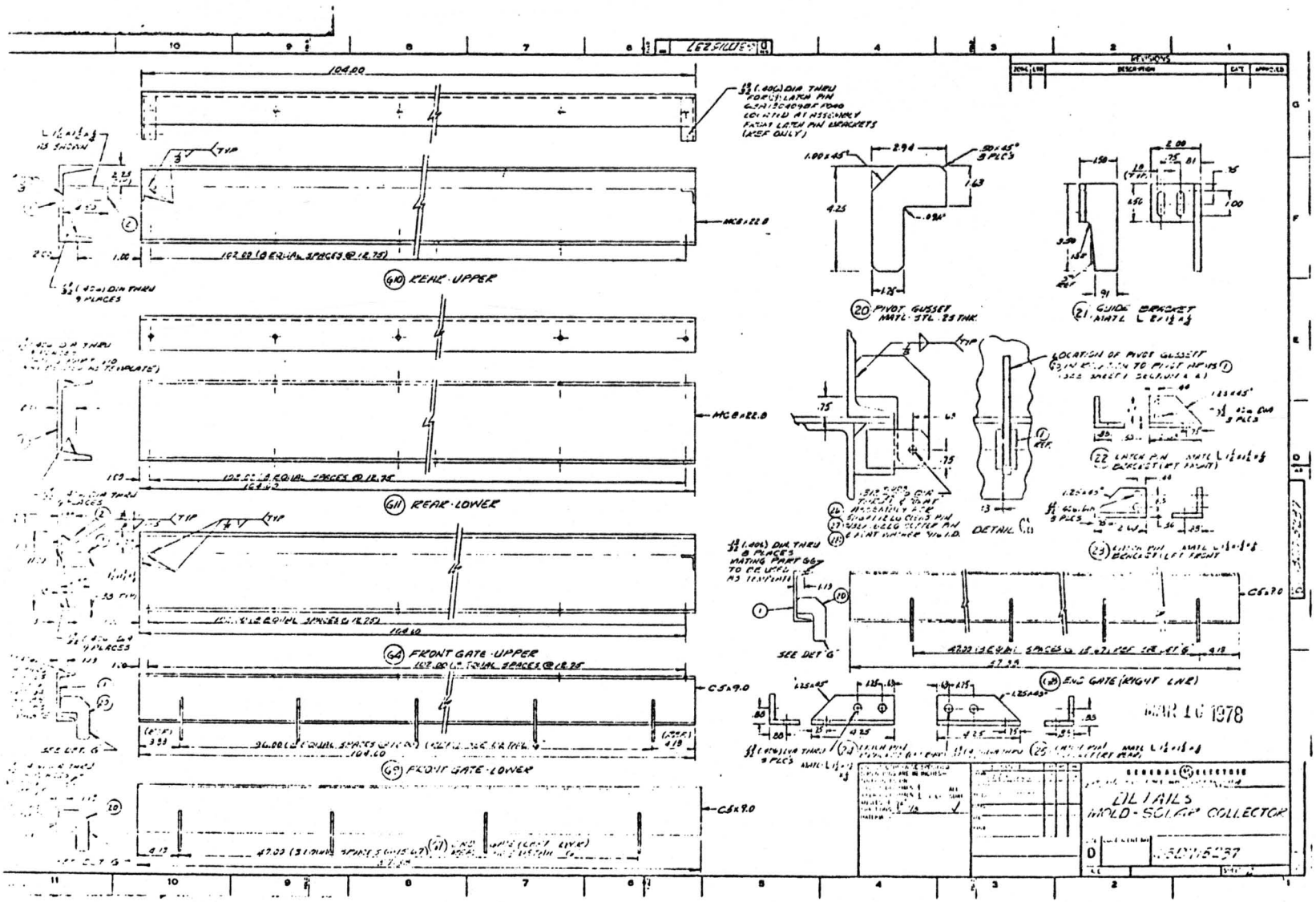
104.00
REAR UPPER
REAR LOWER
FRONT GATE UPPER
FRONT GATE LOWER
PIVOT GUSSET
GUIDE BRACKET
DETAIL C
END GATE (RIGHT END)
MAR 16 1978
DETAILS
MOLD-SCRAP COLLECTOR

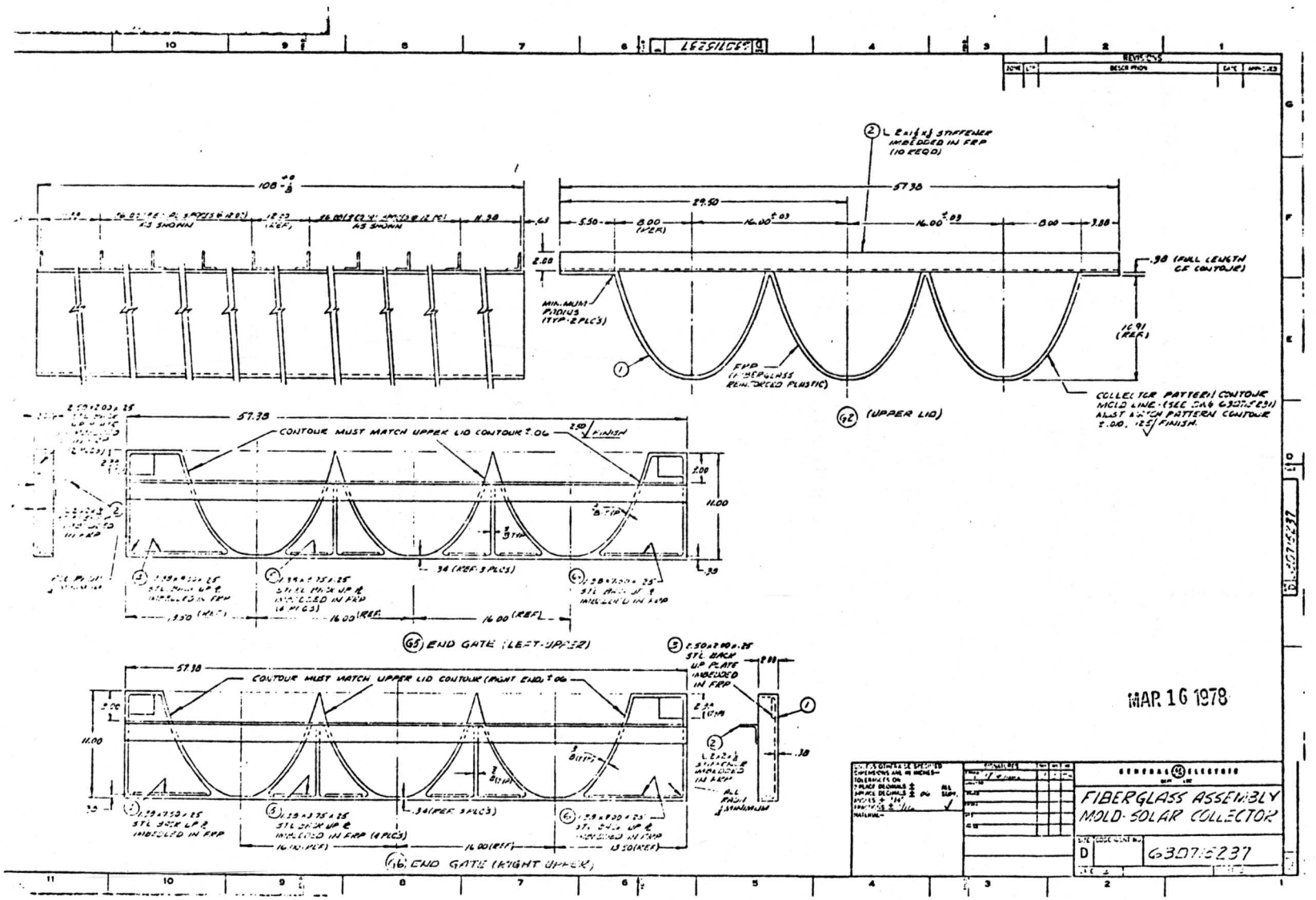
57.38
29.50
5.50
8.00 (TYP)
16.00 ± .03
16.00 ± .03
8.00
3.88
2.00
.98 (FULL LENGTH OF CONTOUR)
10.91 (REF)
MIN. MOLD RADIUS (TYP. 2 PLCS)
FRP (FIBERGLASS REINFORCED PLASTIC)
COLLECTOR PATTERN CONTOUR MOLD LINE - (SEE DWG 6307E231) ALIGN WITH PATTERN CONTOUR ± .010, 125 FINISH.
(2) L 2 x 1½ x ¼ STIFFENER IMBEDDED IN FRP (10 REQD)
(G2) (UPPER LID)
CONTOUR MUST MATCH UPPER LID CONTOUR ± .06
2.50 FINISH
11.00
34 (REF-3 PLCS)
16.00 (REF)
(G5) END GATE (LEFT-UPPER)
CONTOUR MUST MATCH UPPER LID CONTOUR (RIGHT END) ± .06
2.50 x 2.00 x .25 STL BACK UP PLATE IMBEDDED IN FRP
L 2 x 2 x ¼ STIFFENER IMBEDDED IN FRP
ALL RADII ¼ MINIMUM
.38
34 (REF-3 PLCS)
16.00 (REF)
13.50 (REF)
(G6) END GATE (RIGHT UPPER)
MAR 16 1978
GENERAL ELECTRIC
FIBERGLASS ASSEMBLY
MOLD-SOLAR COLLECTOR
SIZE D
CODE IDENT NO.
6307E237

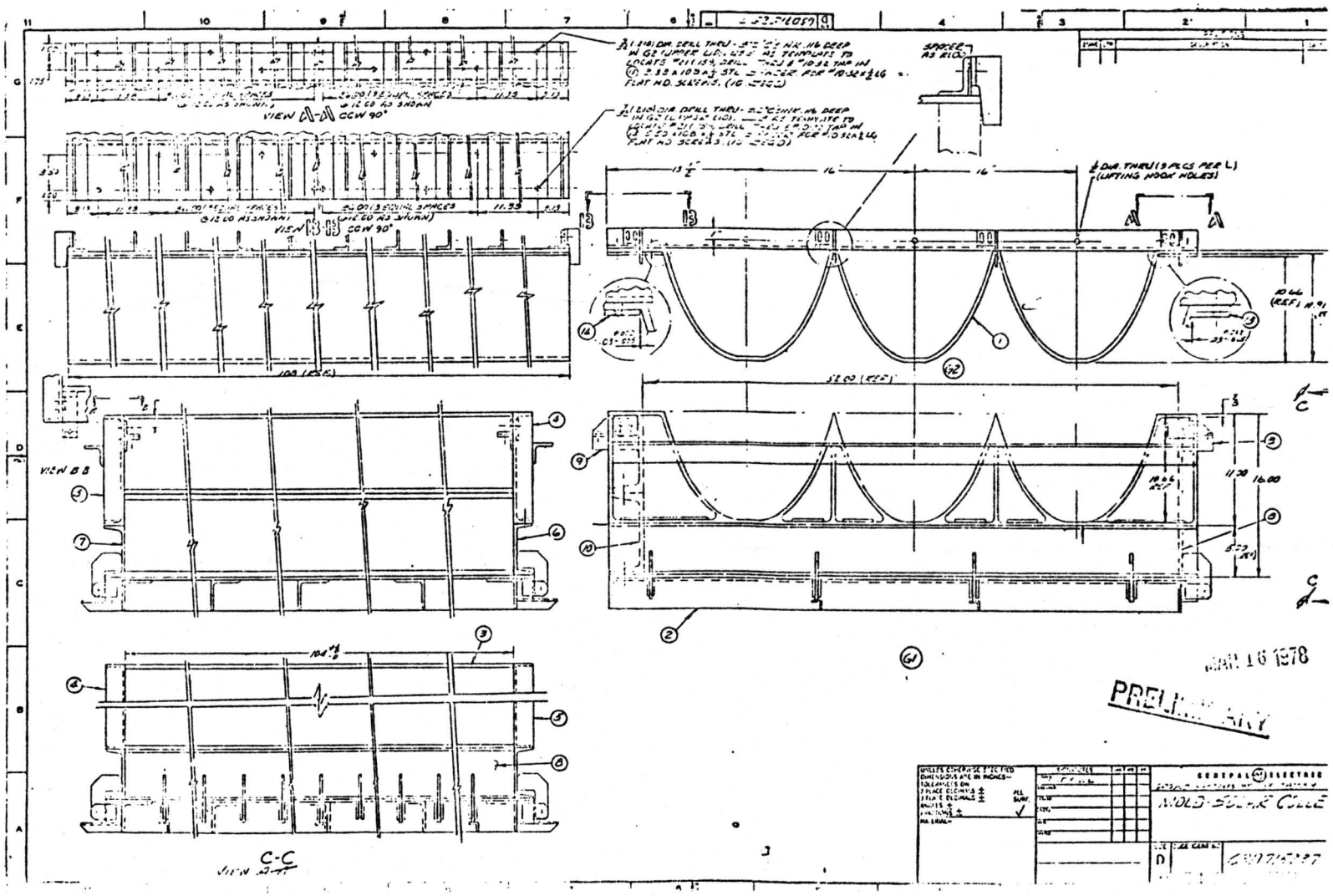
VIEW A-A CCW 90°
VIEW B-B CCW 90°
VIEW B-B
C-C
SPACER AS REQD
PRELIMINARY
MOLD-SOLAR CELL

A P P E N D I X B

TC-300

STRUCTURAL ANALYSIS

SHEET METAL DESIGN

APPENDIX B
TC-300 STRUCTURAL ANALYSIS - SHEET METAL DESIGN

3.1 SHEET METAL STRUCTURAL DESIGN

Structural design for the TC-300 solar collector unit, as defined in this section, begins at the 4.5 inch diameter U-bolt to mount pipe interface as shown in Figure B-1 and includes the following major components:

1. U-Bolt
2. Rib Doubler
3. Structural Rib
4. Side Rails
5. Reflector

Component stresses were calculated using a design wind loading of 40 lbs/ft^2 which can be derived from:

$$D = \tfrac{1}{2} \rho V^2 C_D$$

where: Air Density ρ = .0023 slugs/ft^3 (at sea level)
Wind Velocity V = 147 ft/sec (100 mph)
Coefficient of Drag C_D = 1.56
Drag D = lbs/ft^2

Additional consideration was given to gross weight loading of critical components during ground handling and buckling of thin members. For purposes of this analysis, it was assumed that 40 lbs/ft^2 wind loading could act in any direction. A material strength requirement placed on all components of this design was to show calculated stress levels less than or equal to material yield strengths at design loads.

B.2 U-BOLT

The U-Bolt attachment was designed for an unbalanced wind loading resulting in an overturning moment of 2326 in/lbs. at each U-Bolt. Material chosen for the U-Bolts was low cost SAE Grade 2 steel with a proof loading of 55,000 psi. Assuming a bolt torque loading of 70% proof load, the bolt stress is 38,500 psi. Since standard U-Bolts are available with 1/2-13 threads in the size range close to our application, a 1/2-13 thread was chosen.

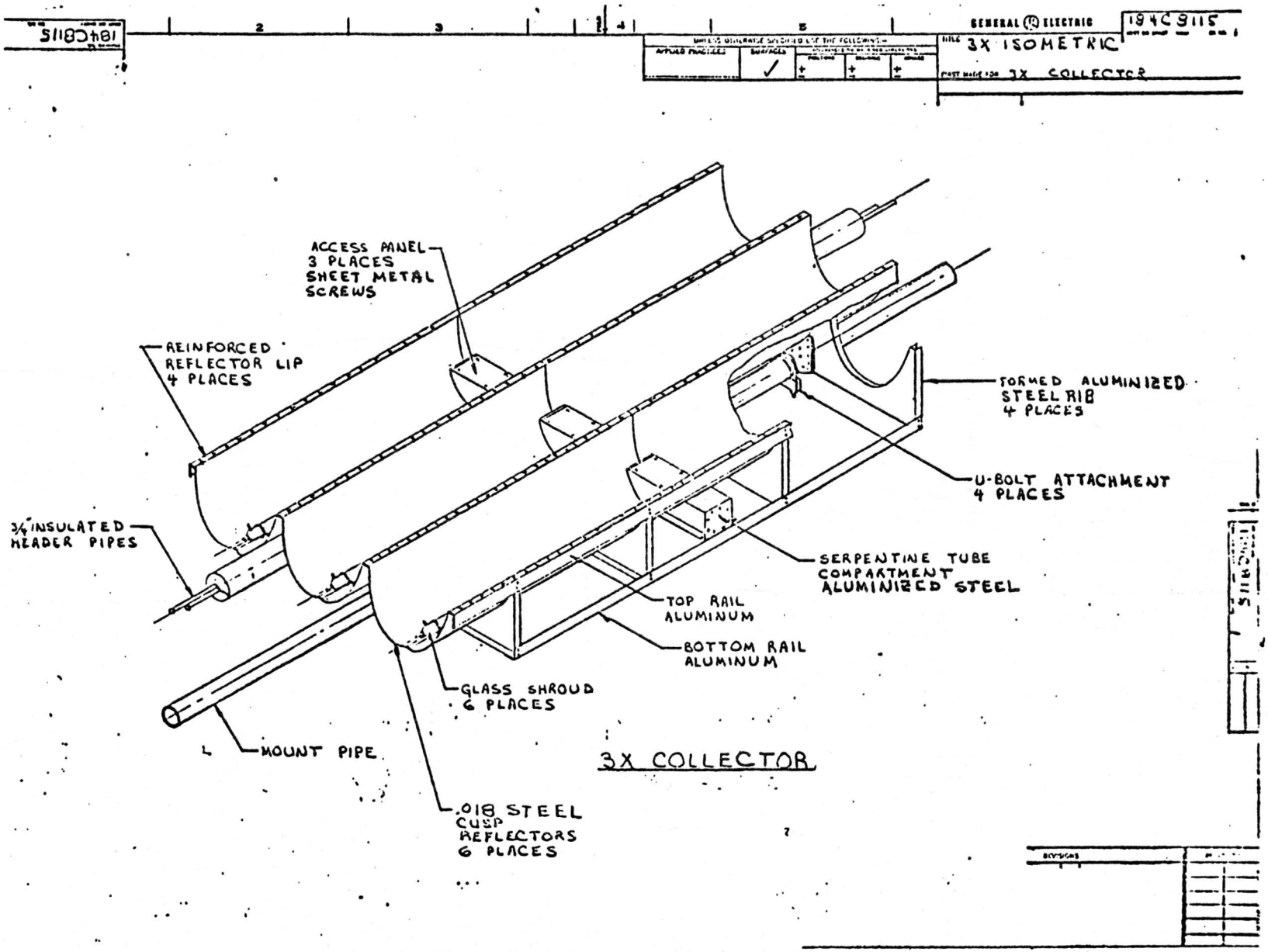

Figure B-1. 3 X Collector Assembly

Friction imparted on the mount pipe by one U-Bolt can be derived as follows:

$$F = 2 A S_t C_f$$

where: A = ½-13 tensile stress area

S_t = Bolt Stress

C_f = Coefficient of friction (metal to metal)

F = 2 X .1419 X 38,500 X .15

F = Coefficient of friction (metal to metal)

Friction force required to react wind load is simply $F' = \frac{M}{R}$ where M is the overturning moment at the pipe and R is the pipe radius.

$$F' = \frac{2326}{2.25} = 1034 \text{ lbs/U-Bolt}$$

when F' is less than F, the U-Bolt attachment will not slip.

$$1034 < 1639$$

Hoop stress in the mount pipe can be calculated as a uniform radial U-Bolt pressure around a pipe section resulting in a stress of:

$$S = \frac{PR \sqrt[4]{\frac{3(1-V^2)}{R_1^2 t^2}}}{2t}$$

where: P = Pressure from U-Bolt

R = Pipe outside Radius

V = Poisson's Ratio

t = Pipe Wall

R_1 = Mean Pipe Radius

Pressure on the pipe from the U-Bolt was found to be 2430 psi. Using standard wall schedule 40 pipe, the stress is calculated as:

$$S = \frac{2430 \times 2.25 \sqrt[4]{\frac{3(1-.27^2)}{2.12^2 \times .237^2}}}{2 \times .237}$$

S = 21,417 psi

Material minimum yield strength is 35,000 psi.

B.3 RIB DOUBLER

The rib doubler (see Figure B-2) is an .07 aluminized steel press formed part. The doubler was designed to react all the bending moments due reflector wind loading as well as overturning moment due to collector unbalanced wind load.

Bending stress at the doubler center line was calculated as $S = \frac{M}{Z}$, where M equals bending moment and Z is section modulus.

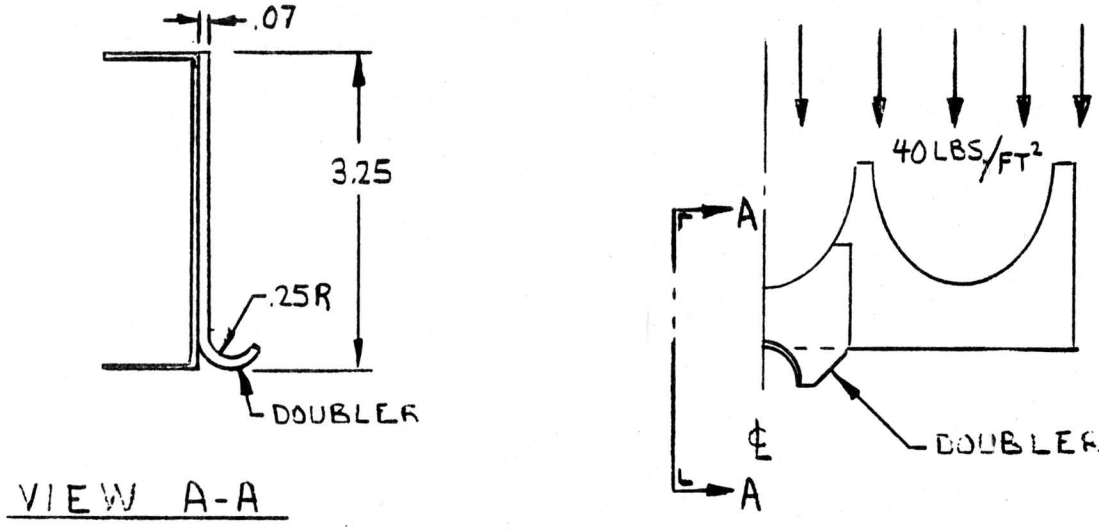

Figure B-2

Bending moment for the condition shown in Figure B-2 was found to be M=2326 in/lbs. per doubler and section modulus $Z_{min} = .1314$ in^3, $Z_{max} = .1423$. The stress is therefore:

$$S_{MAX} = \frac{2326}{.1314} = 17{,}702 \text{ PSI}$$

$$S_{MIN} = \frac{2326}{.1423} = 16{,}346 \text{ PSI}$$

Material Yield = 36,000 psi

The maximum loading for the rib doubler is one in which the wind is directed at an angle of about 30° to the bottom side of the collector as shown in Figure B-3. In this direction each doubler must react a component of flexural bending along its thin cross section as well as a component of bending at its center line as computed above.

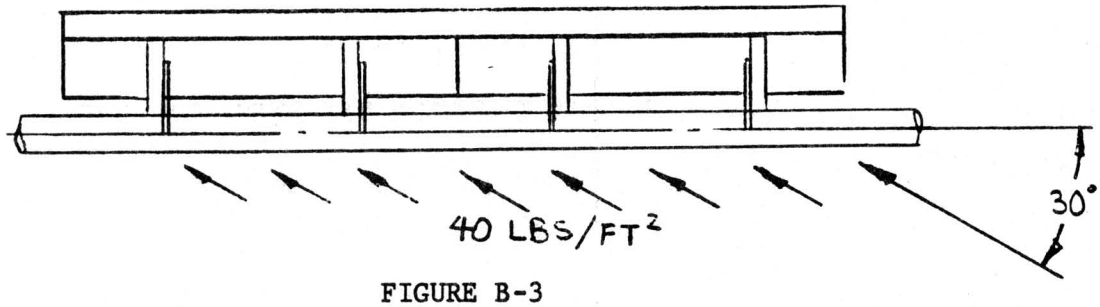

FIGURE B-3

Assuming the doubler reacts the flexural component of load in contraflex bending, the bending moment was found to be 251 in/lbs. per doubler. The section modulus for this direction is only .0084 in^3. The contraflex bending stress $\frac{M}{Z}$, therefore, is S_1 = 29,881 psi. The bending component at the doubler center line is:

$$S_2 = S_{MIN} \sin 30^\circ$$
$$= 16,346 \times .5$$
$$= 8,173 \text{ PSI}$$

The combined stress for this loading condition is the

$$S = \sqrt{S_1^2 + S_2^2}$$
$$S = \sqrt{29,881^2 + 8,173^2}$$
$$S = 30,979 \text{ PSI}$$

Material Yield = 36,000 psi

Since the flexural section modulus goes down dramatically with material thickness and since the flexural bending moment could be somewhat higher if the doubler does not react entirely in contraflex bending, .07 was considered minimum allowable material thickness.

In addition to the above analysis, stresses in the rib doubler due to an unbalanced wind load were also checked. The unbalanced load resulted in a 2326 in/lb. overturning moment reaction at each doubler collar. Since the applied load at the collar was close coupled to the main body of the doubler, the maximum stress was calculated as a combination of torsional bending stress and fiber tensile stress at the junction of the doubler collar to its main body. The maximum stress for this condition was calculated to be 10,186 psi.

The next critical area in the rib doubler is the rivet joint attaching it to the structural rib. Due to the thin materials being used, the rivet joint is most critical in rivet bearing stress. This joint was analyzed assuming that the load in each rivet is proportional to the individual distance of each rivet to the centroid of the rivet group.

The maximum load is defined as:

$$P_{MAX} = \frac{M R_{MAX}}{\sum R^2}$$

where M is the total moment reacted by the rivet group,
R_{Max} is centroidal distance of the furthest rivet, and $\sum R^2$ is the sum of the square of all the rivet centroidal distances. See Figure B-4.

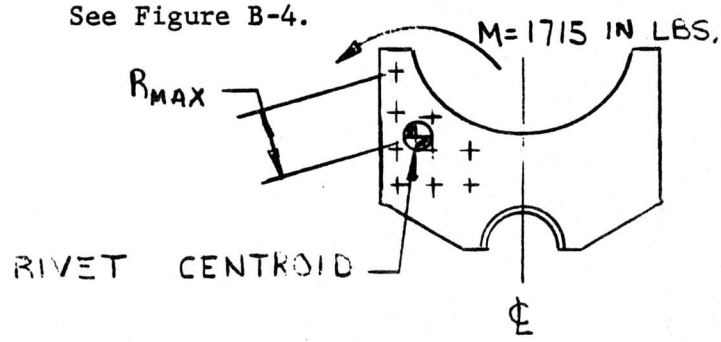

FIGURE B-4

The moment reacted by the rivets at their centroid was found to be 1715 in/lbs. per rivet group. R_{max} and R^2 are 3.48 in. and 39.49 in. respectively. Using the above expression, the maximum rivet load was calculated as:

$$P_{MAX} = \frac{1715 \times 3.48}{39.49}$$

$$P_{MAX} = 151 \text{ LBS.}$$

The allowable loads for a 304 stainless steel rivet with 2D edge distance are as follows:

Rivet Bearing = 154 lbs.
Rivet Shear = 477 lbs.
.025 Material Bearing = 185 lbs.

Since 151 < 154 and since the analysis was performed with the assumption that the rib doubler is receiving all the bending moment from the collector, the joint is acceptable even if the structural rib is manufactured in two halves with a separation of the rib at the doubler center line.

B.4 STRUCTURAL RIB

The structural rib is a press formed part which encounters relatively low stress levels in the TC-300 collector except at the rib doulber rivet joint. Sizing of the rib is governed primarily by reflector size and number and by rivet joint requirements. Aluminized steel .025 thick was chosen for the structural rib for the following reasons:

1. Availability of stock material
2. Compatibility with other collector components
3. Corrosion resistance
4. Formability
5. Economy

Stress was checked in the rib outer concave to the loading condition shown in Figure B-5.

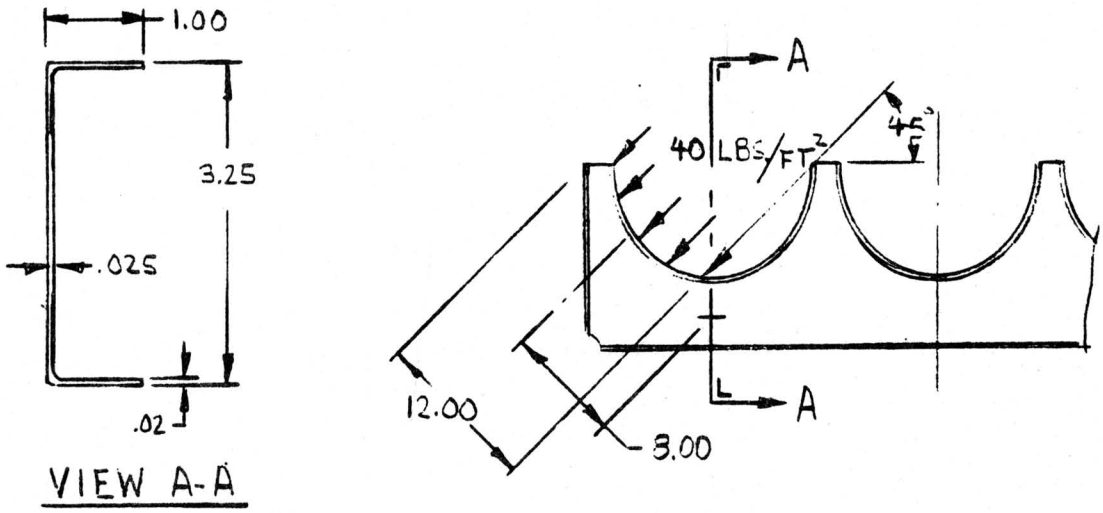

FIGURE B-5

Using a simple bending stress analysis, the stress was found to be 6895 psi - well below the 36,000 psi yield stress.

Critical buckling moment was also checked at the rib outer concave. The expression used for this was:

$$M' = \frac{\pi\sqrt{(EI_Y)(KG)}}{\ell}\sqrt{1+\pi^2\frac{I_f E d^2}{2KG\ell^2}}$$

where: E is modulus of elasticity,
I_Y is section moment of inertia about a vertical axis,
K is a constant of cross section geometry,
G is modulus of rigidity,
I_f is flange moment of inertia
d is vertical web thickness, and
ℓ is distance between flange supports

Since this relation is primarily for use on a constant section with supports at a distance ℓ, its use was intended only as a crude but conservative guide to determine if a problem could exist. Using the above expression, the critical moment was calculated as 11,298 in/lbs.

Operating moment was found to be only 681 in/lbs. Therefore, rib loading is well below any critical buckling problem.

An additional stress check was made on the structural rib at its junction with the rib doubler. See Figure B-6.

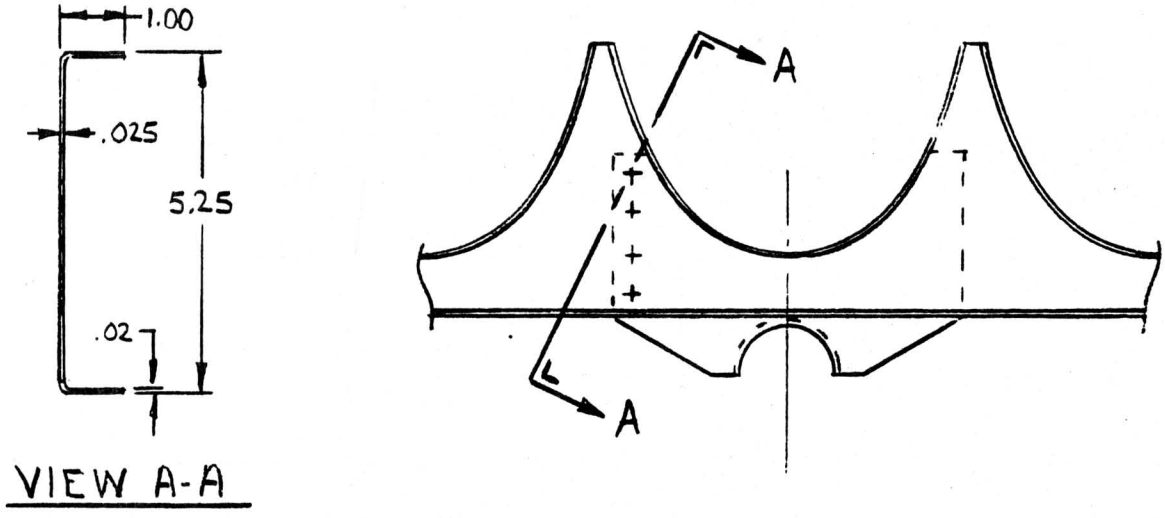

FIGURE B-6

The bending stress at view A-A shown above was calculated as 10,770 psi; well below the 36,000 psi allowable.

B.5 SIDE RAILS

Side rails are used at the top edge of the TC-300 collector to reinforce the reflector outer lips and also at the bottom edge to stabilize the structural ribs. See Figure B- . In addition, since the reflectors are parted midway along the collector length, the side rails must support the weight of the collector during ground handling. Aluminum extrusions were chosen for the side rails, since they are available in stock angles and because the stock sizes can withstand ground handling loads without buckling.

Since the side rails are not connected from top to bottom (as seen in Figure B-1) by a shear web, it was assumed for a worst case that the moment of inertia of these components as a structure was only the sum of the individual component moments of inertia.

To determine the critical buckling moment in an angle side rail which has a vertical web unsupported on its compression side, a buckling analysis for a single vertical web was used. To calculate the critical buckling moment in this manner, it was assumed that the portion of total moment reacted by the single web is equal to the ratio of the moment of inertia of the web to that of the entire structure, or:

$$\frac{M_w}{M_s} = \frac{I_w}{I_s}$$

The collector weight was calculated as 150 lbs. With this weight, the moment reacted by the side rails when the collector assembly is supported at its ends is Ms = 1912 in/lbs. The sum of the side rail moments of inertia was found to be Is = .596 in^4. The moment of inertia of a single vertical web is Is = .1 in^4. Therefore, the moment reacted by a single vertical web is:

$$M_w = \frac{I_w}{I_s} M_s$$

$$M_w = \frac{.1}{.596} (1912)$$

$$M_w = 321 \text{ IN. LBS.}$$

The critical buckling moment for a single vertical web was determined from the following relation:

$$M' = \frac{\pi b^3 d \sqrt{EG(1-.63\frac{b}{d})}}{6\ell}$$

where: b = Web thickness
d = Web height
E = Modulus of elasticity
G = Modulus of Rigidity
ℓ = Distance between supports

Using the above equation, the critical moment was found to be 426 in./lbs. The G loading to buckle a side rail is then:

$$G = \frac{426}{321}$$

$$G = 1.33$$

Since the collector will be handled on the ground at less than max. gross weight and since the upper side rails receive some support from reflectors, the G loading to buckle a side rail will be higher than calculated above.

B.6 REFLECTOR

Steel sheet .013 thick is used as a substrate material for the TC-300 reflector. A metalized polyester film will be thermally bonded to the steel for use as a reflective surface. Each reflector becomes a structural part which is 51 inches long when formed into a parabolic shape after installation in the structural rib. The longitudinal edges of each reflector are bent over and riveted to adjoining reflector edges for reinforcement. A hydrostatic test was performed on a single reflector to insure its structural integrity. Considerable deflection was noted at the unreinforced reflector edge midway between rib supports. A stress check was then performed on a reinforced reflector edge to insure its strength.

Maximum loading used to determine moment distribution along the reflector edge is the same as that used on the structural rib in Figure B-5. At 40 lbs./ft^2 wind load, the portion of load shared by the lip of a single reflector is:

$$P = \frac{\frac{12}{2} \times 51 \times 40}{144}$$

$$P = 85 \text{ LBS}$$

The total load, P, is the result of a uniform load distribution, $\bar{w}$, along the reflector edge which is:

$$\bar{w} = \frac{85}{51}$$

$$\bar{w} = 1.67 \text{ LBS/IN.}$$

Since the wind direction to produce the above loading is at 45° to the direction of maximum deflection in the reflector edge, the loading acting upon the edge to produce maximum stress is then:

$$w' = 1.67 \cos 45^\circ$$

$$w' = 1.18 \text{ LBS/IN}$$

The load and moment distribution are shown in Figure B-7.

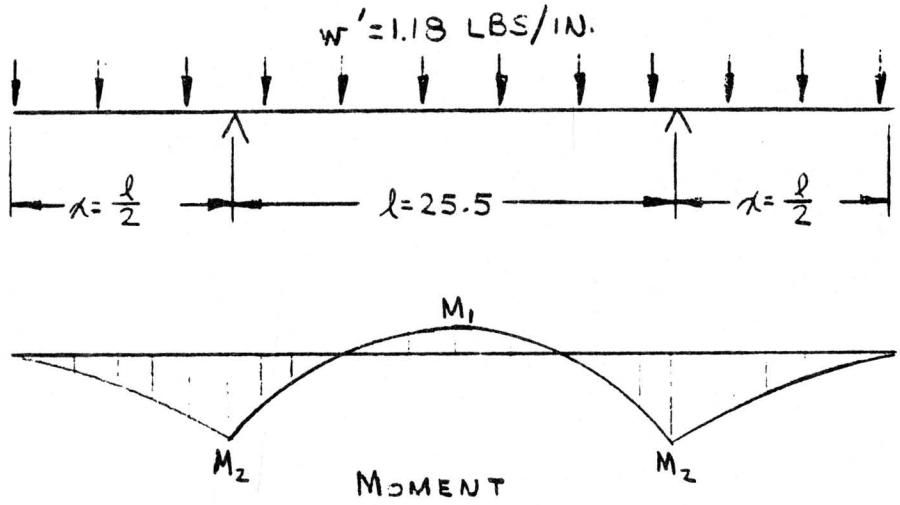

FIGURE B-7

For the distribution shown in Figure B-7, the maximum moments are as follows:

$$M_1 = \frac{\bar{w}}{8}(l^2 - 4x^2)$$

$$M_1 = 0$$

$$M_2 = \frac{\bar{w}x^2}{2}$$

$$M_2 = \frac{\bar{w}l^2}{8}$$

The maximum moment is then:

$$M_2 = \frac{1.18 \times 25.5^2}{8}$$

$$M_2 = 96 \text{ IN LBS.}$$

To find the reinforced edge section modulus in the direction of maximum deflection, it was assumed that the reinforced edge was a beam with proportions shown in Figure B-8:

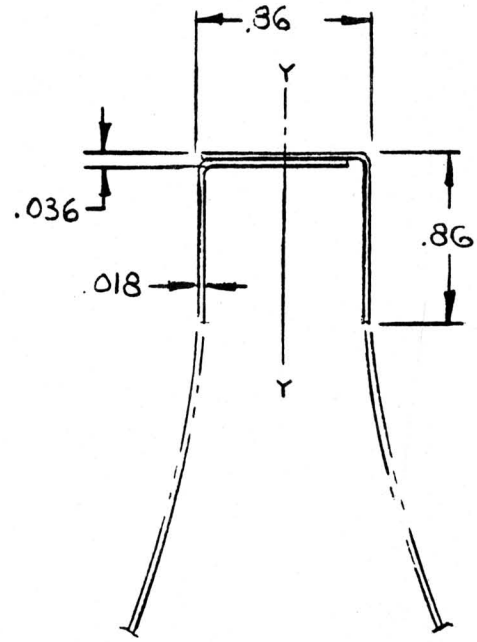

FIGURE B-8

The section modulus about the Y-Y axis was calculated as Z = .0167 in^3. The bending stress for a reinforced edge is therefore:

$$S_B = \frac{M}{Z}$$

$$S_B = \frac{96}{.0167}$$

$$S_B = 5,749 \text{ PSI}$$

Material yield stress is 36,000 psi.

Additional calculations to determine rivet spacing were also made. Rivets along each reinforced reflector edge must withstand bending shear flow so that two edges joined together with rivets will act as a unit. The beam

shear diagram for a reflector edge is shown in Figure B-9.

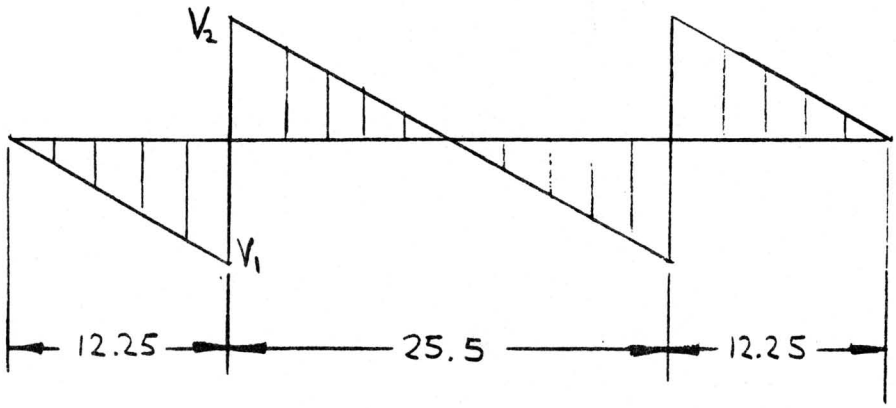

FIGURE B-9

The beam shear is then:

$$V_1 = V_2 = 118 \times 12.76$$
$$= 15.06 \text{ LBS/IN}$$

The average shear is:

$$\bar{V} = \frac{15.06}{2}$$
$$\bar{V} = 7.53 \text{ LBS/IN.}$$

To find the bending shear flow, the delta bending stress over a one inch beam segment must be found; see Figure B-10.

$$\text{MAX } \Delta S_B = \frac{\bar{V}}{Z}$$

$$\text{MAX } \Delta S_B = \frac{7.53}{.0167}$$

$$\text{MAX } \Delta S_B = 451 \text{ PSI}$$

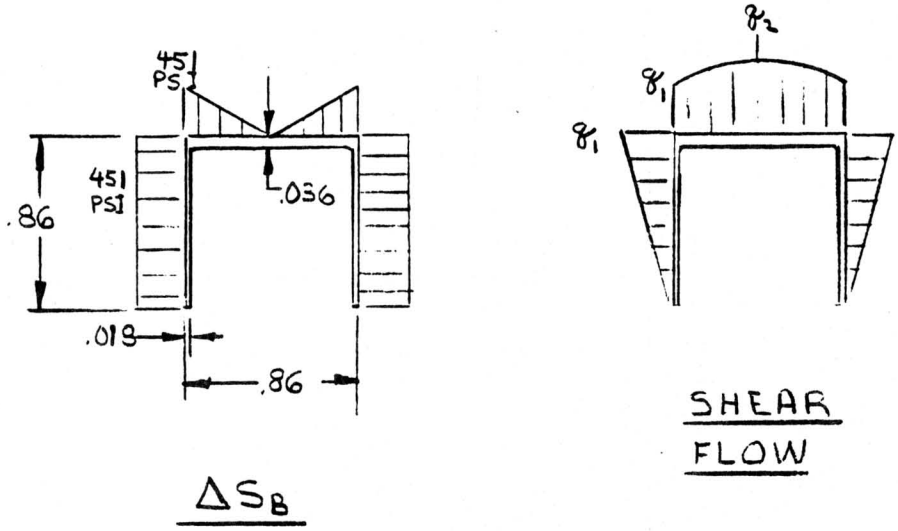

FIGURE B-10

The shear flow at any point in from the free edge of the beam cross section must balance ΔS_B as shown in Figure B-10. To find the shear flows q_1 and q_2, therefore, the equations are:

$$q_1 = 451 \times .018 \times .86$$
$$q_1 = 6.98 \text{ LBS/IN.}$$

$$q_2 = q_1 + \frac{451}{2} \times .036 \times .43$$
$$q_2 = 10.47 \text{ LBS/IN}$$

To find a rivet spacing in the reflector longitudinal edge, the rivet allowable load is divided by the shear flow q_2.

$$L = \frac{P_{LBS}}{q_2 \text{ LBS/IN}}$$

Since 1/8 dia. protruding head 304 stainless steel blind fasteners are used in most parts of the TC-300 collector, they were also chosen for the reflector edge joint. The allowable rivet loads used are as follows:

Rivet Shear = 365 lbs.
Rivet Bearing = 116 lbs.
Sheet Bearing = 134 lbs.

Rivet bearing is the lowest allowable load, therefore, the rivet spacing is:

$$L = \frac{116}{82}$$

$$L = \frac{116}{10.47}$$

$$L = 11.08 \text{ IN.}$$

For ease of design, the rivet spacing used is 8.00 inches.

B.7 MISCELLANEOUS COMPONENTS

All other components in the TC-300 collector not discussed above were considered to be non-structural and were designed with materials common to components analyzed above. The compartment which houses the serpentine tubes was made from .025 aluminized steel. All remaining rivet joints were made with 1/8 stainless steel blind rivets.

A P P E N D I X C

TC-300

FLUID LOOP STRESS

ANALYSIS

APPENDIX C
TC-300 FLUID LOOP STRESS ANALYSIS

C.1 FLUID LOOP CALCULATIONS

C.1.1 Header Pipe Welded Branch Connection

The header pipe branch weld, sized for strength purposes, must have a leg height at least equal to the branch pipe wall thickness. However, the header run pipe must also be reinforced at the branch pipe joint. The branch pipe weld can be used as reinforcement but must be sized accordingly; see Figure C-1.

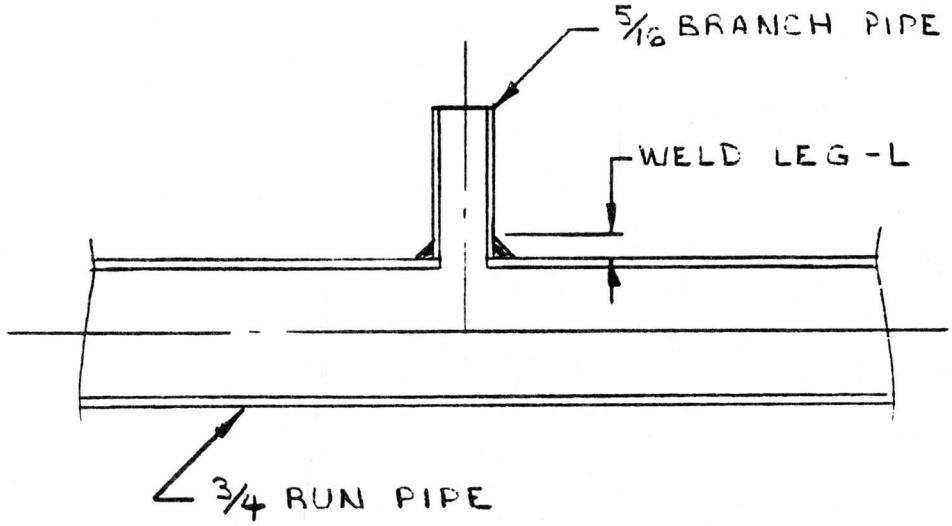

Figure C-1 Header Connection Cross Section

In this branch pipe design, the branch pipe wall thickness is .028. Therefore, for strength purposes, the fillet weld must have a minimum .028 leg. The run pipe reinforcement requirement is calculated as an area whose minimum value for a 90° branch is:

$$A = 1.07(t_{m_h})(d_1)$$

where: t_{m_h} = minimum allowable run pipe wall
d_1 = branch pipe I.D.

The minimum allowable run pipe wall is:

$$t_{m_h} = \frac{PD_c}{2(SE + PY)} + A$$

where: P = operating pressure
D_c = run pipe O.D.
SE = maximum allowable material stress at operating conditions
Y = a material temperature coefficient
A = additional thickness

Minimum wall thickness was calculated as = .006. Since = .25, the area, A, is:

$A = 1.07 \times .006 \times .25$
$A = .0016$

The minimum weld leg for reinforcement purposes is then:

$$L = \sqrt{2A}$$
$$L = .057$$

The minimum weld leg height must be the larger of the two values found above. In this design, the weld size requirement was placed at .06 to .12.

Stress due to sustained loads at the branch pipe connection, resulting from pipe and fluid weight loads and pressure/temperature loads must be checked so that:

$$S_1 = \frac{PD_c}{4t_n} + \frac{.75i\,M_A}{Z} \leq S_h$$

where: P = operating pressure
D_c = branch pipe O.D., .312 in.
t_n = branch pipe wall, .028 in.
i = weld stress intensification factor, 1.86
M_A = moment due to weight, .312 in./lbs.
Z = branch pipe section modulus, .00161 in^3
S_h = allowable material stress at operating temperature

The operating pressure used was 250 psi and the temperature was 400°F. Under these conditions S_1 was calculated as 3409 psi and S_h was found in a table to be 16,100. Therefore:

$$3409 < 16{,}100$$
$$\text{OR}$$
$$S_1 < S_h$$

Stress due to occasional peak loading conditions must also be checked. In this application, occasional loads would be those resulting from a stagnation condition. For this condition the pressure and temperature are 681 psi and 500°F. The following equation must be satisfied for occasional loads:

$$S_2 = \frac{P D_o}{4 t_n} + \frac{.75 i M_B}{Z} + \frac{.75 i M_A}{Z} \leq k S_h$$

where: M_B = moment loading due to occasional loads
k = a constant of loading frequency, 1.20

Stress, S_2, was calculated as 4,600 psi, K is 1.2 and S_h is 15,900 psi. Therefore:

$$4{,}600 < 1.2 \times 15{,}900$$
$$4{,}600 < 19{,}080$$
$$\text{OR}$$
$$S_2 < kS_h$$

The third loading condition required to be checked is additive stress, which is thermal expansion stress and thermal expansion plus sustained stress. The first equation which must be satisfied is:

$$S_E = \frac{i M_C}{Z}$$

where: M_C = range of moments due to thermal expansion, 9.72 in/lbs.
S_A = allowable stress range, 25,267
S_E = thermal expansion stress

The moment, M_c, was calculated from the movement of the run pipe, 1.5 inches, during thermal cycling; see Figure C-2.

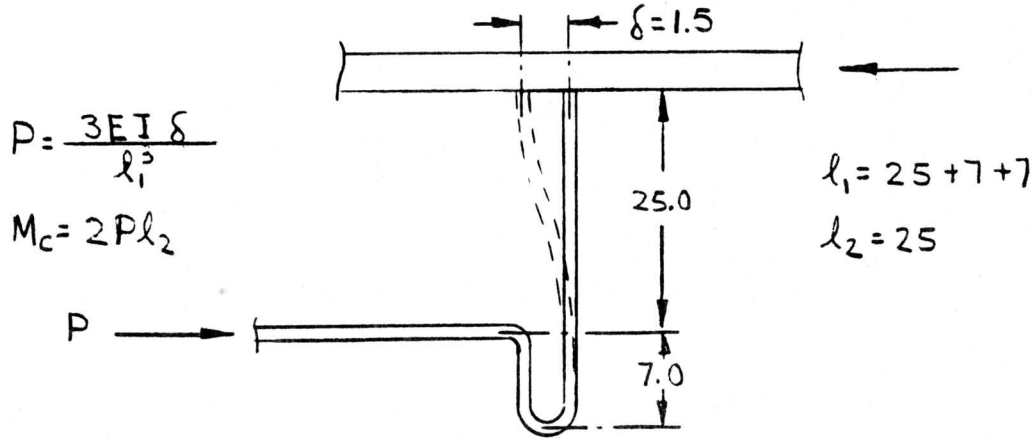

Figure C-2 Pipe Run Plan and Dimensions

The allowable stress, S_A, is found from:

$$S_A = f(1.25\,S_c + .25\,S_h)$$

where: S_c = material allowable at minimum cold temperature, 18,700 psi
S_h = material allowable at maximum hot temperature, 6,000 psi
f = stress range reduction factor, .9

Allowable stress, S_A, was calculated as 22,387. However, when the longitudinal pressure stress, S_{lp}, plus bending stress, $\frac{.75iM_A}{Z}$, is less than the allowable stress, S_h, at operating temperature, the difference can be added to the S_h term of the equation for S_A shown above. When this is done, S_A becomes 25,267 psi. The thermal expansion stress, S_E, was then calculated as 11,230 psi. Therefore:

$$11{,}230 < 25{,}267$$
OR
$$S_E < S_A$$

Sustained plus thermal expansion stress must now be satisfied by the relation:

$$\frac{PD_o}{4t_n} + \frac{.75iM_A}{Z} + \frac{iM_C}{Z} \leq (S_h + S_A)$$

The terms of the left hand side of this equation were calculated as 14,639 psi and those on the right side are 41,367. Therefore:

$$14{,}639 < 41{,}367$$

The requirement is satisfied.

As mentioned at the beginning of this section, the entire analysis outlined above was also performed for the .25 O.D. hairpin tube which connects to the welded branch pipe. Stresses for the hairpin tube are a higher percentage of the allowables than those for the branch pipe weld, but still well within acceptable limits.

A summary of the calculated stresses in the hairpin expansion pipe are listed below.

$$S_1 \leq S_h$$

$$4,732 < 13,700$$

$$S_2 \leq kSh$$

$$6,079 < 16,440$$

$$S_E \leq S_A$$

$$16,400 < 21,070$$

$$S_1 + S_E < S_h + S_A$$

$$21,142 < 34,720$$

A P P E N D I X D

FLOW-THROUGH EVACUATED SHROUD

GENERAL ELECTRIC
SPACE DIVISION
PHILADELPHIA

PROGRAM INFORMATION REQUEST / RELEASE

	*CLASS. LTR.	OPERATION	PROGRAM	SEQUENCE NO.	REV. LTR.
PIR NO.	U	-1E30	-JRF	- 390	

*USE "C" FOR CLASSIFIED AND "U" FOR UNCLASSIFIED

FROM	TO
John Hogan	Distribution

DATE SENT	DATE INFO. REQUIRED	PROJECT AND REQ. NO.	REFERENCE DIR. NO.
6/1/78			

SUBJECT

FLOW THROUGH EVACUATED SHROUD

INFORMATION REQUESTED/RELEASED

INTRODUCTION

A patent has been filed describing an evacuated shroud which allows coolant flow to enter one end of the shroud and leave the opposite end. Thermal expansion problems arising from the flow through feature are resolved by a bellows inserted in the outer tube with a glass to metal seal. A novel feature of the design is that this seal is never exposed to the working fluid temperature. The seal is exposed only to the ambient air temperature.

The patent docket is appended to this report. Patentability aside, however, the design should be evaluated for its ability to lower collector cost and increase efficiency. It is the purpose of this PIR to describe the design, discuss its cost advantage, outline the advantages in applying the design to the 3X collector and finally discuss the major development hurdle.

THERMAL EXPANSION

Thermal expansion is a major problem in the design of evacuated shrouds. The evacuation region is adjacent to the absorber surface in order to eliminate convective heat transfer. The absorber surface attains temperatures in excess of the working fluid temperature. The outer surface which defines the evacuated region however is essentially at ambient air temperature. Thus, the surface which encloses the vacuum has sections at substantially different temperatures and therefore, with substantially different expansion rates. This is the main thermal expansion problem of evacuated shrouds.

The GE evacuated shroud solves this problem by attaching a domed outer tube to a domed inner tube as shown in Figure 1. Differential thermal expansion between the two tubes is accounted for by the fact that the inner tube is free to expand (to the right in Figure 1), while imposing no stress on the shroud assembly. Heat must be transferred from the inner tube to the working fluid. A major disadvantage of the GE design is that the plumbing required to remove the heat must enter and leave the shroud from the same end. This imposes severe

DISTRIBUTION:

E. Ernst
J. Graf
J. Hatman
R. Heffelfinger
A. Laganelli
R. Laessig
W. Terrill
J. Trice
D. Wein
J. Young

PAGE NO. 1 OF 18

RETENTION REQUIREMENTS

COPIES FOR	MASTERS FOR
1 MO.	3 MOS.
3 MOS.	6 MOS.
6 MOS.	12 MOS.
MOS.	MOS.
	DO NOT DESTROY

FORM 1020B REV. (9-75)

fluid distribution requirements. This is especially true for east-west collectors which are rotated about an east-west axis -- a point to be discussed more fully in a separate section of this PIR.

Figure 2 sketches another concept which accounts for differential expansion between the absorber and outer surface of the evacuated region. This concept was pursued by a competitor of GE. The absorber can expand without imposing a stress on the assembly as in the GE design. Again fluid enters and leaves the same end of the shroud. An additional disadvantage of this design is the glass to metal seal. This seal is exposed to the working fluid temperature on a daily basis. This is a major drawback since cyclic exposure to a large ΔT is a common failure mode for glass to metal seals.

FLOW THROUGH TUBE

Figure 3 shows a recently designed absorber concept. It involves an inner and outer tube as does the GE evacuated shroud. The inner tube is coated and absorbs solar energy. The seals connecting inner tube to outer tube are the same as the seal on the left end of the GE shroud shown in Figure 1 (Dewar seal). Differential expansion between the inner and outer tubes is accounted for by the metal bellows inserted in the outer shroud. A glass to metal seal is therefore required. Such seals are not uncommon. Figures 4 and 5 present off-the-shelf items which contain this type of seal. In fact, the bellows of Figure 4 is similar to that required in the flow through shroud design. Figure 5 states that this seal is stronger than the parent glass. Temperature rating is 959°F. The novel feature of the flow through design however is that the glass to metal seal is only exposed to the ambient air temperature -- never to the working fluid temperature. Seal requirements are thus greatly reduced.

The advantages of the flow through shroud are realized in reduced heat transfer hardware and in a more efficient fluid distribution system. Heat flows from the inner tube to a working fluid tube across an air gap sized to allow radial expansion of the working fluid tube. This tube would nominally be a 3/4" copper or stainless steel tube with .049" wall. Shroud size could therefore be smaller than the current GE shroud. Note that the flow through design eliminates the need for clamps and fins. Furthermore, coolant can leave one shroud and flow directly into the next. As will be shown below, this substantially reduces header and insulation requirements.

Other advantages of the design are enumerated in the patent docket appended to this PIR.

APPLICATION OF FLOW THROUGH SHROUD TO 3X COLLECTOR

Changes to the design of the present GE shroud are only worthwhile if they decrease the net cost of collecting a given amount of energy. Thus, increasing the efficiency at the same cost or decreasing the cost at the same efficiency are the direction that new designs must pursue. This section will show that the flow through shroud has the potential to both increase efficiency and decrease cost when applied to the 3X collector. The shroud may well have application to other solar product lines, but only the 3X has been investigated at this time.

Figure 6 illustrates the driving motivation for having a shroud open at both ends. Figure 6 is the fluid distribution loop required to feed a row of eight 3X collectors. In each collector there are two tees, two flexible hoses, two 3/4 inch unions, two reducers, 17 feet of 3/4 inch stainless steel header tubing, 60 feet of 1/4 inch serpentine, heat transfer hardware including fins and clamps, and insulation for the 3/4 inch tubing and sections of the 1/4 inch tubing located outside the shrouds. This complex fluid distribution system results from the fact that the shrouds can only be fed from one end. Thus, coolant must be carried to the center of a collector, distributed to the shrouds, and then taken eight feet to the center of the next shroud. In this eight foot run roughly 20% of the energy collected in the shrouds is lost. Figure 7 shows how the same installation would appear if shrouds open at both ends were used. There are no headers, no tees, no flex hoses, no heat transfer hardware (clamps or fins), and no insulation. There is no heat loss between collectors. This substantially increases the heat collected for a given collector aperature area. The working fluid tube would be a 3/4 inch stainless steel tube. Twenty-four foot lengths appear practical. Such lengths are transportable and reduce the net number of 3/4 inch unions required. Because there are no headers to support or insulate, the frame could be substantially simplified. The above advantages are paid for with a more expensive shroud. The cost savings implied above must therefore be weighed against the increased shroud cost. The shroud costs are discussed first.

Figure 8 shows eight feet of the proposed shroud and two conventional shrouds (again eight feet of absorber length). Tube width on the flow through design may be chosen to optimize efficiency or reduce cost. Tube widths on the conventional design are fixed. The conventional shroud has two Dewar seals and four dome operations per eight foot of absorber. The flow through design has two Dewar seals and two glass to metal seals per eight foot of absorber. For the present we assume that a glass to metal seal can be made for the same cost as two dome operations. (The cost of the glass to metal seal is crucial; however, an accurate determination of this cost is outside the scope of this PIR. The above assumption seems reasonable if a glass solder technique can be used for the seal). With the above assumption, the cost difference between the two designs is the bellows cost. A quote of $14 (quantity of 5000) has been received for a 2 inch stainless steel bellows. Since a final flow through design would probably use an outer shroud which was less than two inches, this bellows cost can be expected to come down. However, to be conservative, a bellows cost of $14 will be used. A

conventional four foot shroud is presently costed at $9. Based on the above, four feet of flow through shroud would cost $16.

On the other side of the ledger are the cost advantages which result from the flow through shroud. Recently, the 3X was costed for the Columbia Gas proposal. The cost of the fluid distribution system for 30 ft^2 of aperature area appears on the left side of Table 1. On the right side appears the cost for a flow through system based around 3/4 inch stainless steel tubing. The comparison for the entire collector is shown in Table 2. Here it is assumed that the frame cost for the flow through design is 25% less than for the conventional design. This saving is likely to be greater. It results from the elimination of the header region of the frame. The costs of Table 2 do not include G&A or tooling and, aside from the serpentine and shrouds, are approximate in nature. The cost comparison is not yet complete. The flow through design collects roughly 20% more energy than does the conventional design. Therefore, fewer collectors are needed to collect the same amount of energy. The flow through design delivers the same energy with only 83% of the collector area of the conventional design. Accounting for this the ratio of the flow through cost to the conventional cost is:

$$\frac{\text{FLOW THROUGH COST}}{\text{CONVENTIONAL COST}} = (.83)\ \frac{(230.43)}{(373.12)} = .51$$

Again, G&A and tooling are not included.

The cost of tooling for any new design is of course a cost penalty for that design. However, it is dangerous to rigidly apply this penalty, especially near the beginning of a product cycle. Judging from other examples of product development the first design to appear in the marketplace rarely remains competitive or attractive to buyers for an extended period of time. In the early years of the solar age, we can expect competitors to improve on the evacuated shroud design. For GE to remain competitive new design ideas should not be bludgeoned by retooling costs.

CONCLUSION

A feasible flow through evacuated shroud design has been presented in this PIR. It appears to be extremely cost-effective. This statement rests on the ability to make a metal to glass seal for a reasonable cost. It is emphasized that this seal is never exposed to the working fluid temperature. This application suggests a glass solder seal. Such a seal is less expensive then fusing the metal into the glass while the glass is molten. It is recommended that a prototype flow through shroud with a glass solder seal be made and that the actual cost of making this seal in quantity be assessed.

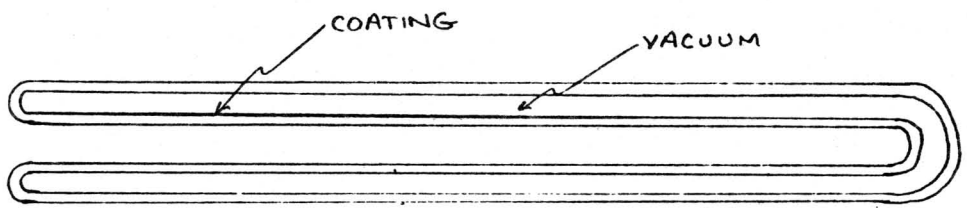

NOT TO SCALE

FIG 1

G.E. EVACUATED SHROUD

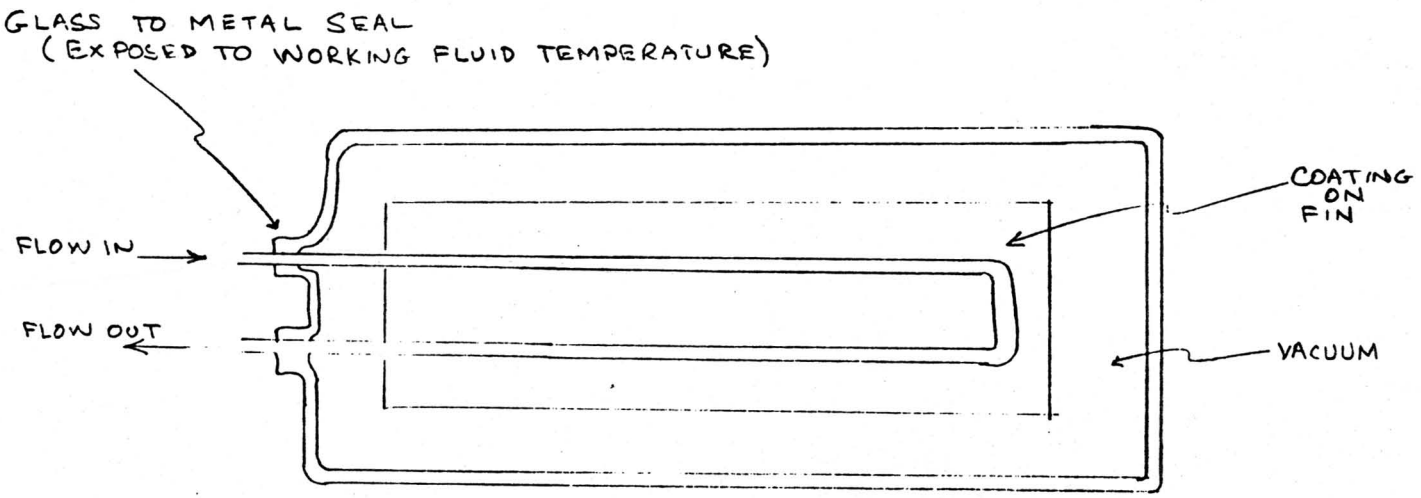

FIG 2
EVACUATED SHROUD

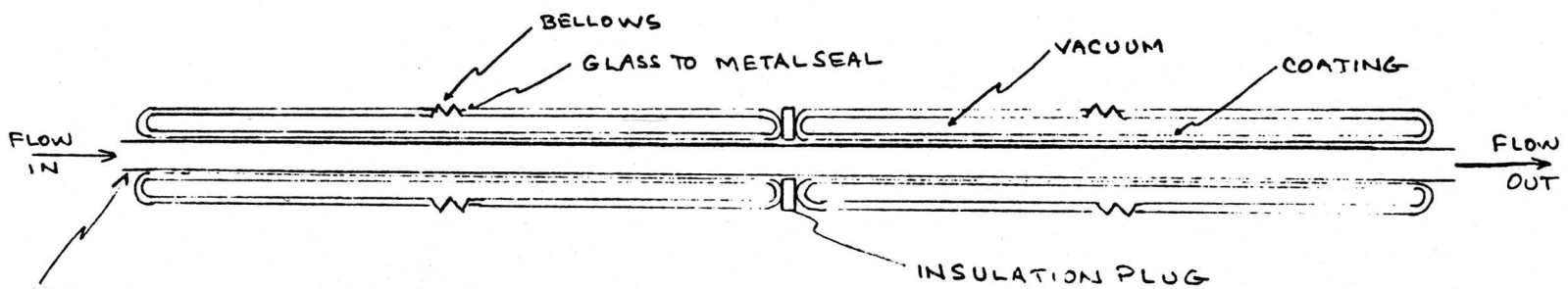

NOT TO SCALE

NOTE: GLASS TO METAL SEAL NOT EXPOSED TO WORKING FLUID TEMPERATURE

FIG 3

FLOW - THROUGH EVACUATED SHROUD

Flexible glass-end tubing

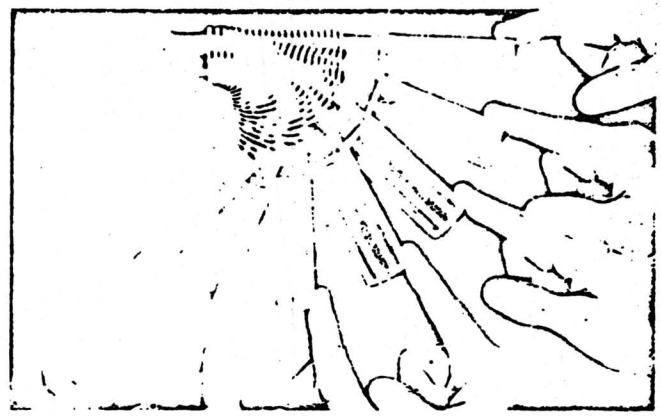

PURPOSE

CAJON Flexible Glass-end Tubing is designed to isolate vibration from glass systems.

APPLICATIONS

Vibration absorbers • Relief for thermal expansion • Low pressure, high purity systems • Industrial and research vacuum systems • Replace expensive vacuum fittings • Permits connection of misaligned components

FEATURES

CAJON Flexible Glass-end Tubing compensates for expansion, misalignment and vibration in glass systems. The one step glass-to-stainless transition utilizes only the parent materials. No overlapping seams to entrap gases. The nominal produced flexible length is compressible by at least 20% and extendable by 50% (see table of dimensions).

CAJON Flexible Tubing is available with glass on both ends or on one end for glass-to-metal transitions. The glass end is flame cut for smooth edges. Glass ends are stress relieved.

TECHNICAL DATA

MATERIAL:

321 stainless steel fused to type 7740 Pyrex glass tube.

TEMPERATURE RATING:

Operating temperature ratings are dependent on application and installation methods, cycle life required, O.D. and nominal length of tubing, angular displacement and other variables. Contact factory for additional information.

PRESSURE RATING:

Ultra-high vacuum to 25 psig.

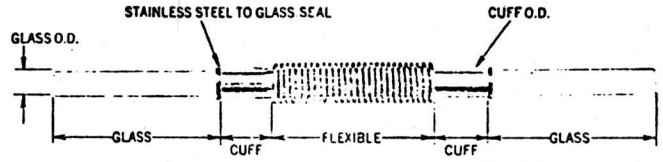

TABLE OF DIMENSIONS

	Glass O.D. (inches)	Tube O.D.	Nominal Flexible Length (inches)	Compressed Flexible Length (inches)	Extended Flexible Length (inches)	Glass Length (inches)	Cuff Length (inches)
Right Angle	¼	6mm	2	1½	3	3	¾
	⅜	9mm	3	2½	4½	3	¾
	½	12mm	3	2½	4½	3	1
	¾	19mm	3	2½	4½	3	1
	1	25mm	3	2½	4½	3	1
Straight	¼	6mm	2	1½	3	3	¾
	⅜	9mm	3	2½	4½	3	¾
	½	12mm	3	2½	4½	3	1
	¾	19mm	3	2½	4½	3	1
	1	25mm	3	2½	4½	3	1

All dimensions in inches. Dimensions for reference only – subject to change.

FIG 4

CAJON Glass/Metal Transition Tubes

PURPOSE

CAJON Glass/Metal Transition Tubes are designed for converting from a glass to a metal system through a transition which utilizes only the parent materials.

APPLICATIONS

Transition from a glass system to a metal system • Industrial and research vacuum systems • Corrosive fluid lines • Connect ionization gauges to stainless steel vacuum systems • Either end adaptable to CAJON Ultra-Torr Fittings • Stainless steel end adaptable to SWAGELOK Fittings • Connecting valves to glass systems • Sight gauges • Manometers • Low pressure, high purity systems • High temperature applications.

FEATURES

One step glass-to-stainless transition eliminates troublesome graded seals • Smooth internal surface for high conductance • Nonporous transition area to prevent absorption and outgassing • Transition structure stronger than parent glass • Transition area offers thermal compatibility with parent materials • Glass end is flame cut for smooth edges • Glass ends are stress relieved.

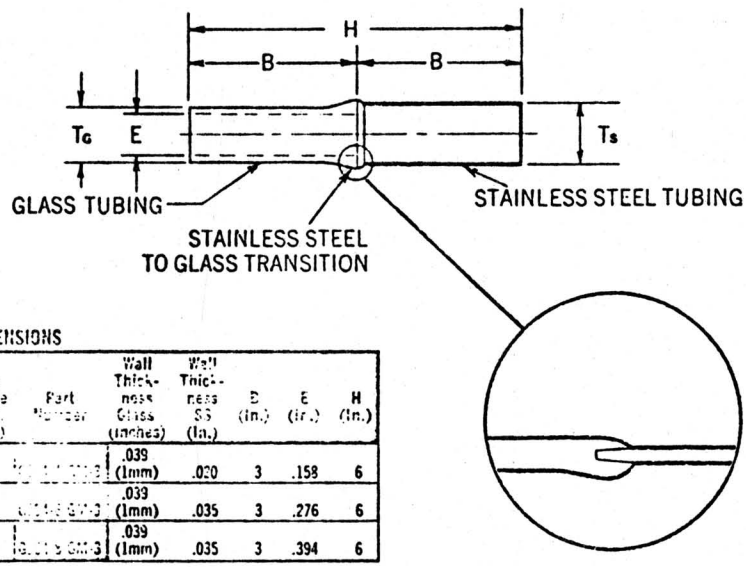

TABLE OF DIMENSIONS

TG Tube O.D. (Inches)	TS Tube I.D. (In.)	Part Number	Wall Thickness Glass (Inches)	Wall Thickness SS (In.)	B (In.)	E (In.)	H (In.)
.236 (6mm)	¼	[illegible]	.039 (1mm)	.020	3	.158	6
.354 (9mm)	⅜	[illegible]	.039 (1mm)	.035	3	.276	6
.472 (12mm)	½	[illegible]	.039 (1mm)	.035	3	.394	6

TECHNICAL DATA

MATERIAL

GLASS TUBE — 7740 Pyrex
METAL TUBE — 304 stainless steel

TEMPERATURE RATING

Temperatures are limited to the strain point of the glass end which is 515°C (959°F).

PRESSURE LIMITS

Ultra-high vacuum to 25 psig.

TESTING

All CAJON Glass/Metal Transition Tubes are 100% stress relieved and helium leak tested before leaving the factory.

All dimensions in inches. Dimensions for reference only — subject to change.

FIG 5

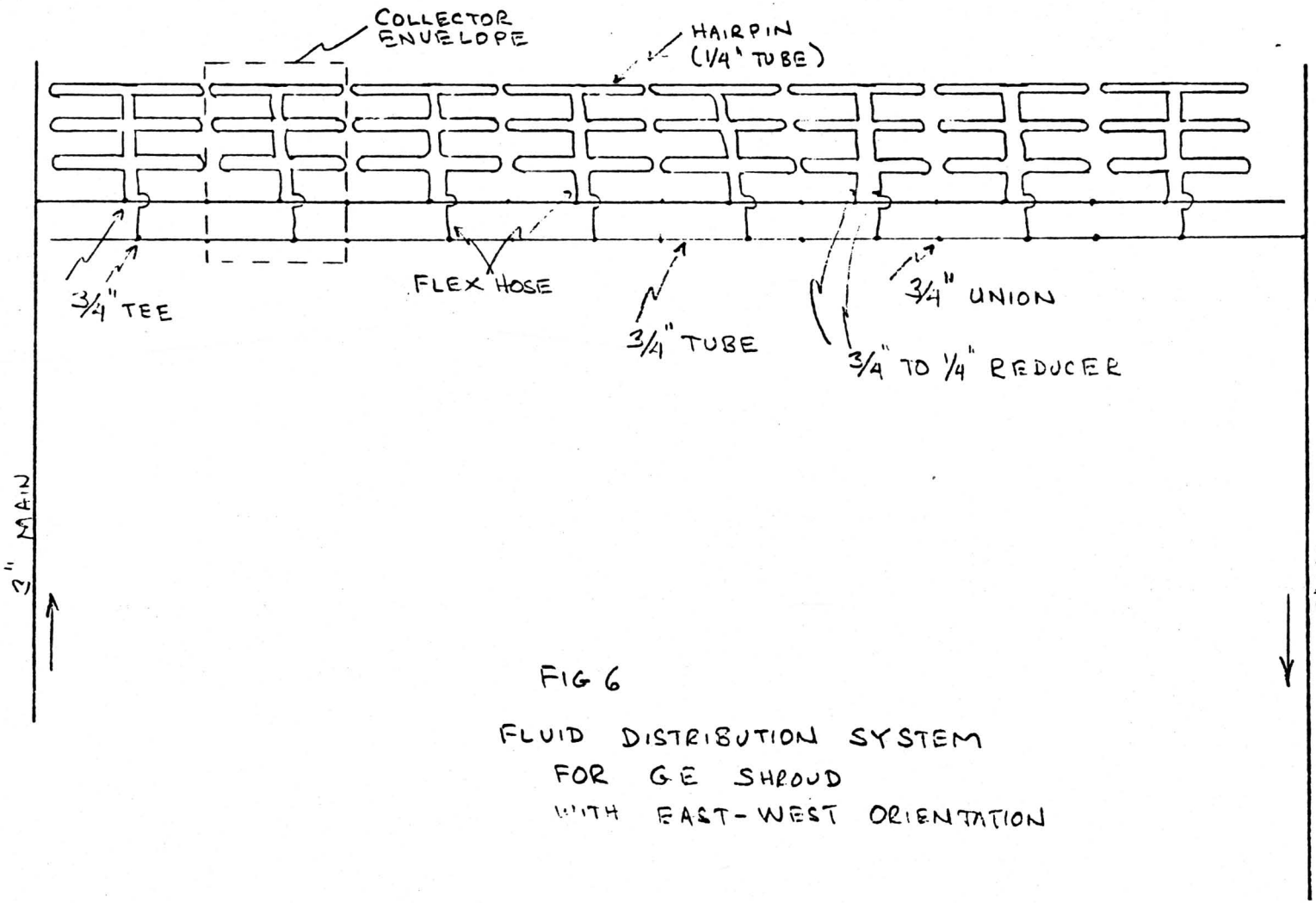

FIG 6

FLUID DISTRIBUTION SYSTEM
FOR GE SHROUD
WITH EAST-WEST ORIENTATION

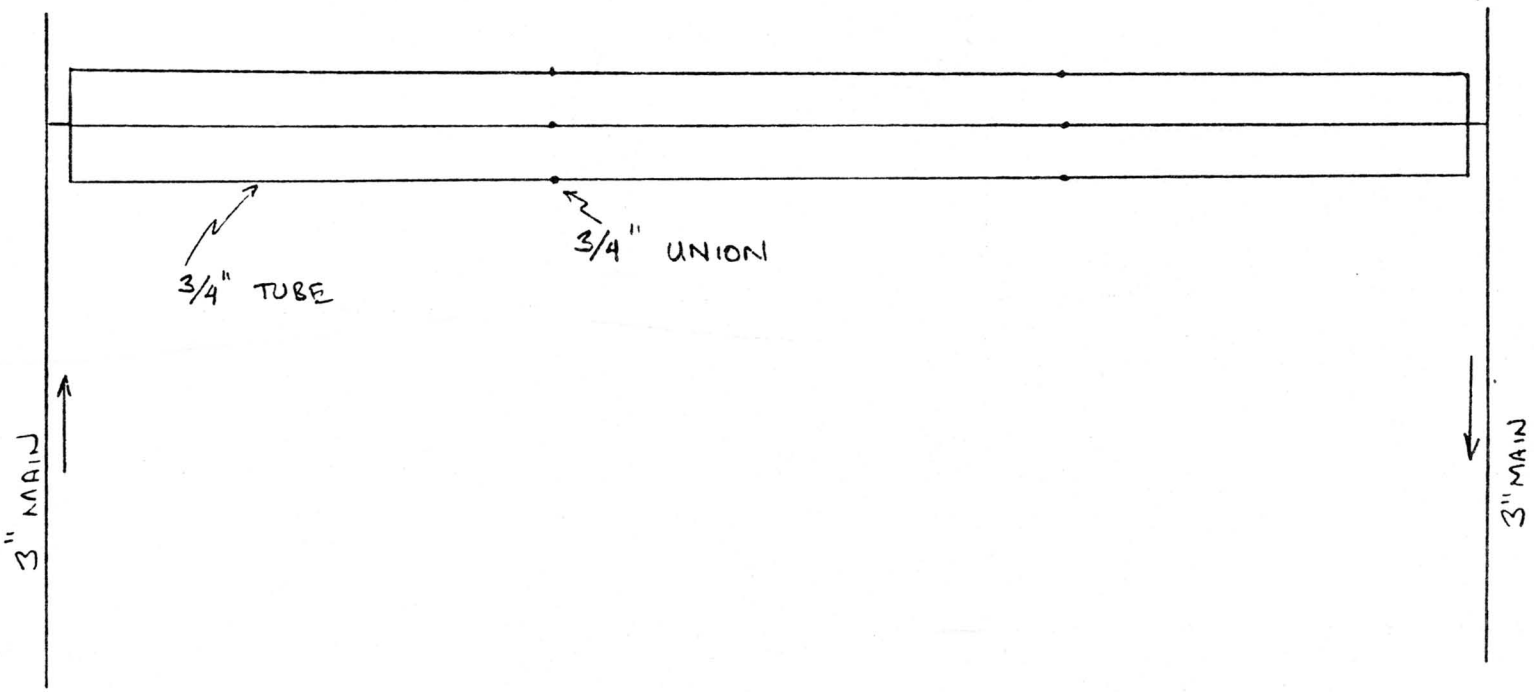

FIG 7

FLUID DISTRIBUTION SYSTEM

WITH FLOW THROUGH SHROUD

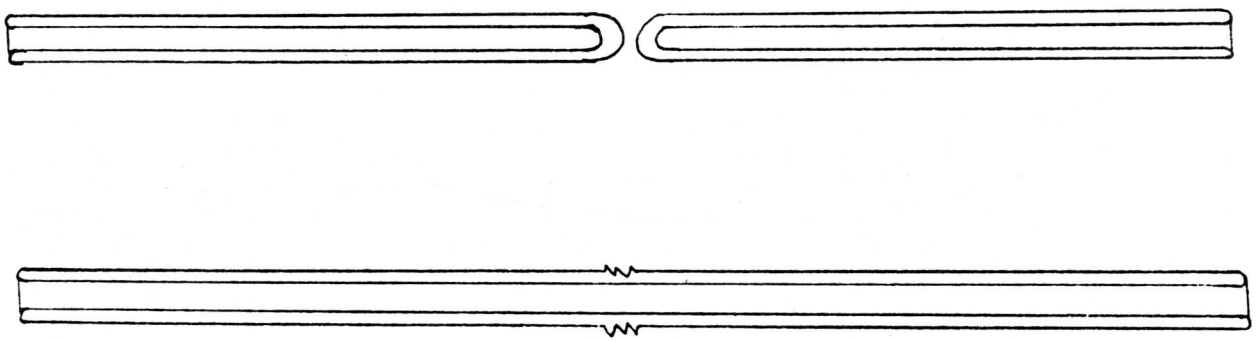

LINE THICKNESS
REPRESENTS
GLASS THICKNESS

FIG 8

COMPARISON OF EIGHT FEET OF CONVENTIONAL SHROUD TO EIGHT FEET OF FLOW THROUGH SHROUD

TABLE 1

COST OF FLUID DISTRIBUTION SYSTEM

FOR 30 FT² OF APERTURE
3X - EAST-WEST

CONVENTIONAL SHROUD	
1/4" STAINLESS TUBING	$ 20.50
FLEX HOSE	$ 25.00
3/4" STAINLESS TUBING	$ 14.40
CLAMPS	$ 32.40
FINS	$ 6.82
FITTINGS	$ 30.00
ASSEMBLY	$ 30.00
	$ 159.12

FLOW THROUGH SHROUD	
3/4" STAINLESS TUBING	$ 19.00
FITTINGS	$ 8.43
	$ 27.43

TABLE 2

COLLECTOR COST
30 FT²
3X

COMPONENT	CONVENTIONAL	FLOW THROUGH
REFLECTOR	$60	$60
STRUCTURE	$70	$52
INSULATION	$30	$1
FLUID DISTRIBUTION	$159.12	$27.43
SHROUDS	$54	$90
	$373.12	$230.43

NOTES

1. COSTS DO NOT INCLUDE G+A, COMPONENT ASSEMBLY, SHIPPING, OR HANDLING

2. FLOW THROUGH DESIGN COLLECTS 20% MORE ENERGY FOR GIVEN AREA

THUS COST RATIO FOR COLLECTION OF EQUAL AMOUNT OF ENERGY IS

$$\frac{\text{FLOW THROUGH COST}}{\text{CONVENTIONAL COST}} = \left(\frac{1}{1.2}\right)\left(\frac{230.43}{373.12}\right) = .51$$